Modeling Sand Wave Field Dynamics in the North Sea using Delft3D Flexible Mesh

Pauline Overes

May 2021

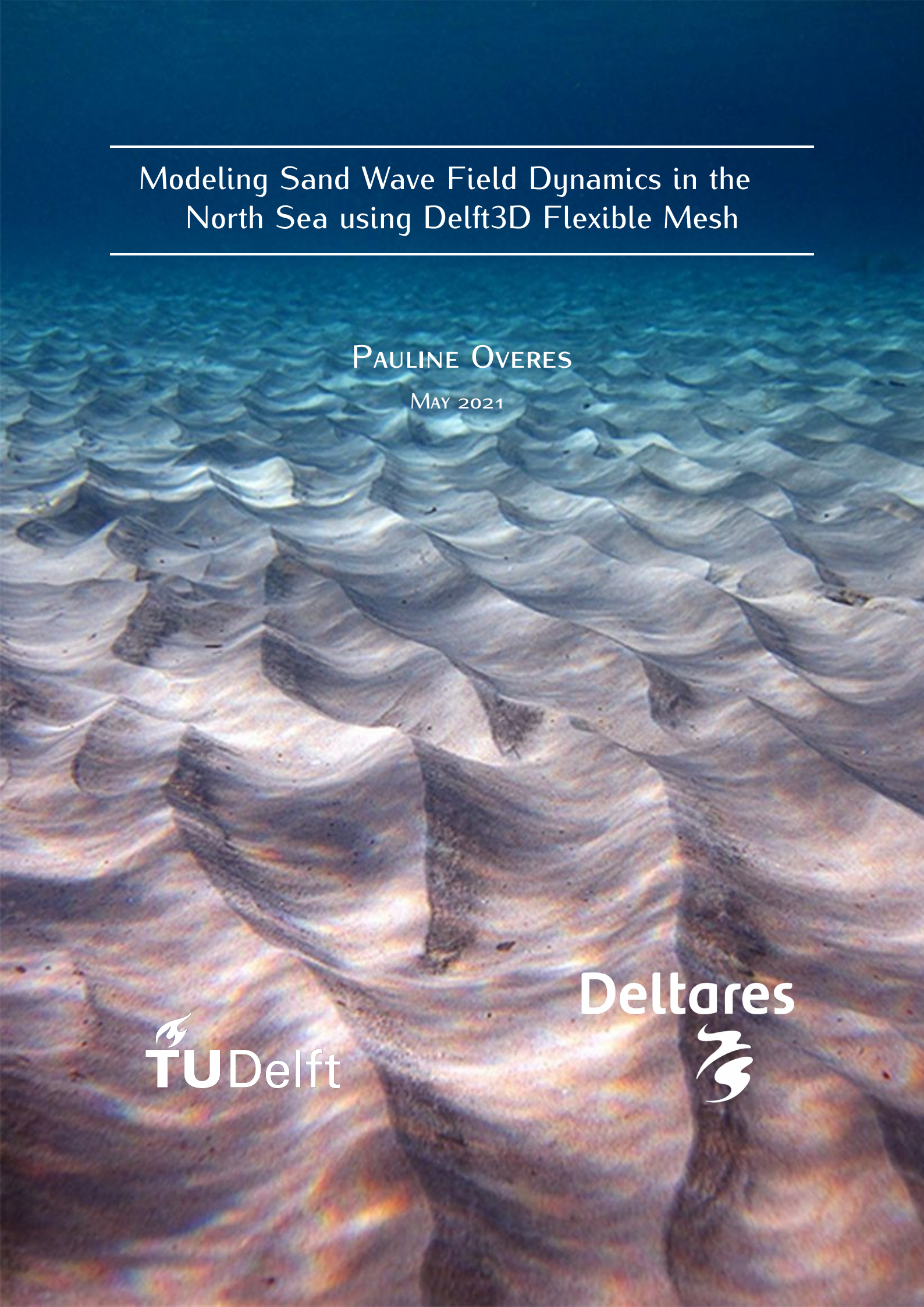

TU Delft

Deltares

Modeling Sand Wave Field Dynamics in the North Sea using Delft3D Flexible Mesh

by

Pauline Overes

To obtain the degree of

Master of Science
in Hydraulic Engineering

at the Delft University of Technology,
at the faculty of Civil Engineering and Geosciences,
to be publicly defended on the 19th of May 2021

Student number:	4380819	
Project duration	September 1st 2020 - May 19th 2021	
Thesis committee:	Prof. dr. ir. S.G.J. Aarninkhof	TU Delft, chair
	dr. ir. A.P. Luijendijk	TU Delft, Deltares
	Prof. dr. ir. A.J.H.M. Reniers	TU Delft
	dr. ir. B.W. Borsje	University of Twente
	ir. T. Roetert	Deltares

TU Delft

Deltares

Preface

Before you lies my final work to obtain the title Master of Science at the faculty of Civil Engineering and Geosciences at Delft University of Technology in the field of Hydraulic Engineering.

The past year has been remarkably different from what I envisioned when I started my Master studies 2.5 years ago. The corona virus and government measures to control the spread of the virus have largely constrained me to work from home. Although I was not able to see as much of Deltares during my graduation project, my daily supervisors have always been there for me through various online sources, for which I am eminently grateful. Through online meetings Arjen and Bas have been highly successful at spreading their enthusiasm about the topic of sand waves. I am thus thrilled to have been granted the opportunity to continue my research in this field in a PhD position at Deltares and the University of Twente. I am excited to continue working with Arjen and Bas and would like to express my gratitude for this opportunity and their guidance and support during the last year.

I would further like to thank Tom, who has granted me a view into the fields of sand wave data analysis and wind farm development. Both of those fields were new to me and your views have helped me to put my research into a bigger perspective. To Ad and Stefan I am grateful for their critical reviews and constructive feedback, which have helped me to get my work to a higher level. I would further like to thank Joao, who has always made time to help me. Your knowledge and support have enabled me to set up my own 3D models.

I am also grateful for the support of my friends and family. I would especially like to thank my (only) home-office colleague Stein, who has motivated and challenged me with his refreshing views. Your support and company have made this year a lot more enjoyable.

Pauline Overes
Delft, 2021

Summary

Offshore wind farms are being built at an unprecedented pace in the North Sea. The Dutch government is aiming for a CO2 neutral energy supply by 2050 and vast cost reductions have turned (offshore) wind energy into a worthy competitor for other (green) energy sources. Most of the planned wind farms in the Dutch North Sea are located in areas where the seabed is covered with sand waves. In the North Sea these sand waves have lengths of 100-1000 m, heights of 1-8 m and they migrate with rates of up to 10 m/year (Morelissen et al., 2003). Sand wave migration and changes in shape, may cause a significant rise or drop in local bed level. This bed level variation over time could decrease the stability of foundations or bed protections or cause exposure of cables and pipelines.
Various offshore infrastructural projects, like offshore wind farms, thus require long term (30-50 years) predictions of the seabed dynamics. Currently data-driven methods are used to determine the range of expected bed levels. However, the uncertainty in these predictions is significant, with sand waves being the largest source of uncertainty. Furthermore, no real understanding of the systems at hand forms the base of these predictions. Not many attempts have been made to accurately model sand wave dynamics in real-life situations using a process based model. Since sand waves often have steep slopes in migration direction, a need for small numerical grid sizes arises. On the other hand oceanic hydrodynamics are affected by large scale bed forms. To include (the influence of) these bed forms, large model domains are required. This makes numerical modelling of sand wave fields rather difficult due to the balance between grid sizes and computation time.
The newly developed Delft3D Flexible Mesh (FM) model may be able to overcome some of these problems. Through the use of unstructured grids, the desired level of detail can be reached in certain sand wave areas. In combination with the possibility to run simulations in parallel, on multiple cores, computation times can be reduced significantly. However, the Delft3D FM model has not yet been used for the prediction of sand wave dynamics. The aim of this research is to find the opportunities and challenges of the Delft3D FM model for quantitative modelling of sand wave dynamics in the North Sea.

First a model-model comparison is carried out between the Delft3D FM and the Delft3D-4 model. Delft3D-4, being the predecessor of Delft3D FM and established in the field of sand wave modelling, provides a benchmark upon which confidence in the Delft3D FM model can be built. This comparison is based on a widely used simplified sand wave model set-up. From this analysis it is concluded that the Delft3D FM model is capable of reproducing the key processes leading to sand wave growth and migration. The dependencies of the growth and migration rates on hydrodynamic forcing and sand wave length are similar between Delft3D-4 and Delft3D FM. Some inequalities in absolute growth rate are found in the short wave length range, but these can be attributed to a difference in implementation of the bed slope related transport. The strength of this transport mode can easily be tuned through the bed slope parameter (α_{bs}). Furthermore, the behaviour towards equilibrium is comparable for both models. Given this good agreement between the models, the remainder of the study is carried out using Delft3D FM.

Subsequently the performance of the Delft3D FM model is assessed through a 2DV (2 Dimensional Vertical) case study, with a model sand wave bathymetry based on measurements. This case study, situated in the North Sea, is used to study the importance of different tidal constituents as well as some model sensitivities. In all model cases the Delft3D FM model showed a quick reduction in slope steepness in the first part of the simulation period. This slope reduction is not found in the sand wave measurements and is possibly caused by a mismatch of the boundary conditions. In the remainder of the simulation the sand wave height increased steadily. From measurements no, or little sand wave growth is observed. This artificial growth is likely caused by excluded processes, such as suspended sediment transport. The M4 tidal component is identified as an important driving force for the local sand wave migration. Moreover, the addition of a residual current caused further migration of the sand waves. The differences in morphological results with the simulation including the

full tidal signal indicate that other tidal components might also be of importance. From the sensitivity analysis it is observed that both the bed slope parameter (α_{bs}) and the bed roughness (C) have a significant influence on both sand wave growth and the final slope steepness. Although the separate factors were unable to improve the morphological results, they are identified as important tuning parameters.

Lastly, a 3D case study is carried out. This case study gives insight into the viability of the widely used 2DV model set-up and is used to explore the importance of 3D effects. From this case study it is concluded that even in a fairly regular sand wave field, without much variation in sand wave migration direction, 3D effects in hydrodynamics can be of importance. In a 3D model the variations in flow velocity and direction over a sand wave field are better represented. Furthermore, the ellipsoidal character of the tide leads to 3D pattern of bed load transport directions. At the location of steep sand waves slopes the direction of sediment transport is significantly influenced by bed slope transport. This might cause deviations between the sediment transport direction and the flow direction at the bed. These factors make the inclusion of a third dimension in sand wave modelling important for a good representation of sediment transport. In areas where tidal sand banks are present, these 3D effects are expected to be even larger (Leenders, 2018).

Through the case studies various opportunities and challenges for predicting sand wave dynamics using Delft3D FM are discovered. The Delft3D FM model showed a significant reduction of computation times for a 2DV case using a single core compared to Delft3D-4. For parallel simulations, using multiple cores, an approximately linear further reduction of computation time is observed in a 2DV setting. Furthermore, the possibility of unstructured grids presents a solution for the small grid sizes needed in sand wave areas. Other computational gains are realized through a morphological scale factor (which is also incorporated in Delft3D-4), optimized time-step management and a new type of boundary conditions. This new boundary condition imposes both water level and flow velocity over depth in both horizontal directions. In this way the local flow conditions are accurately represented and the influence of bed forms outside the model domain can easily be incorporated. This potentially eliminates the need for buffer zones.
Challenges for the application of Delft3D FM on sand wave cases are found in amongst others the availability of data. When less data on local hydrodynamics is available the accurate representation of processes driving sand wave dynamics becomes more difficult. Furthermore the inclusion of sub-grid processes, like the growth and migration of megaripples, could be problematic. In the model case studies no calibration was carried out. This calibration could potentially increase the effort needed to apply Delft3D FM to real life sand wave cases. Furthermore, the Delft3D FM model is still in development and significant differences between the results of different versions of Delft3D FM were observed. Care should be taken when applying a new version of Delft3D FM. The model is however being developed in collaboration with users which ensures quick feedback and thus stimulates improvement of the results between versions.

Recommended research includes extended exploration of the 3D effects influencing sand wave dynamics. Furthermore, improvement of morphological results and optimization of the model set-up will increase the applicability of Delft3D FM in an engineering setting. A model run forced by two Riemann boundaries showed improved morphological results, although the hydrodynamics were not well represented. These results might indicate where differences with reality originate. Examples of such differences are overestimation of peak velocities, exclusion of wind-driven currents and exclusion of processes like suspended sediment transport, free surface waves and grain size sorting. Further exploration of these factors could enhance the predictive capacities of Delft3D FM. Applying the model at other locations in the North Sea will help determine the overall applicability of the model.
Through this extended research the full potential of the Delft3D FM model can be discovered and prepared for future engineering applications. Insights gained into the processes influencing sand waves dynamics, through the use of Delft3D FM, could pave the way for more nature based solutions, thus reducing the need for dredging. In this way Delft3D FM could contribute to reducing risks, costs and environmental impact of offshore construction projects in sand wave areas.

Contents

List of Figures

List of Tables

Acronyms

2DH	2 Dimensional Horizontal.
2DV	2 Dimensional Vertical.
ADI	Alternating Direction Implicit.
DCSM	Dutch Continental Shelf Model.
FGM	Fastest Growing Mode.
FM	Flexible Mesh.
HKZWF	Hollandse Kust (Zuid) Wind Farm.
M2	Lunar semi-diurnal.
M4	Lunar quarter-diurnal.
MF	Morphological scale factor.
S2	Solar semi-diurnal.
U0	Residual current.

List of symbols

A	amplitude
A	wave skewness
A_0	initial sand wave amplitude
C	Chezy roughness coefficient
c_μ	calibration constant
D_{50}	median sediment diameter
d	depth
F_x	radiation stress gradient in x-direction
F_y	radiation stress gradient in y-direction
f	Coriolis parameter
g	acceleration due to gravity
H	wave height
H	total water depth
k	wave number
k	turbulent kinetic energy
L	wave length
M	sediment mobility number
M_e	excess sediment mobility number
P_x	hydrostatic pressure gradient in x-direction
P_y	hydrostatic pressure gradient in y-direction
S_b	Sediment transport rate
T	period
t	time
$U0$	residual current velocity
u	flow velocity in the x-direction
u_b	near-bed flow velocity
u_{cr}	critical depth averaged velocity
u_r	equivalent depth averaged velocity
v	flow velocity in the y-direction

w_s	sediment settling velocity
x, y, z	Cartesian coordinates
z_b	bed level
α_{bs}	bed slope parameter
γ_R	growth rate
ϵ	dissipation of turbulent kinetic energy
ϵ_p	bed porosity
ζ	water level
ν_V	vertical eddy viscosity
ρ_w	density of water
ρ_0	reference density of water
σ	scaled vertical coordinate
$\tau_{b,x}$	bed shear stress in x-direction
$\tau_{b,y}$	bed shear stress in y-direction
τ_s	shear stress at surface
ϕ	internal angle of friction of bed material
ϕ	phase
ω	flow velocity in the σ-direction

1 Introduction

1.1 Motivation

In light of the Paris Climate Agreement, the Dutch government has set challenging goals for the transition to renewable energy sources. By 2050 the whole Dutch energy supply should be CO2 neutral. An effective solution for this demand for green energy sources, in a densely populated country like the Netherlands, is formed by offshore wind farms (Rijksoverheid, 2020). Likewise, the European Union is planning great efforts to reach self imposed green energy goals. By 2030 the European offshore wind capacity should be fivefold the current capacity. By 2050 this number of offshore wind turbines should again be five times higher, leading to a capacity increase from 12 to 300 gigawatts between 2020 and 2050 (Van Raaij, 2020). The timing of these plans is no coincidence and can partly be attributed to the vast cost reductions of offshore wind energy. One planned Dutch offshore wind farm was tendered in 2018 at only 30% of the price estimated in 2013. These cost reductions can be attributed to, amongst others innovation, expansion of scales, reduced costs of raw materials and improvement of financing possibilities (Algemene Rekenkamer, 2018).
The shallow North Sea makes a suitable place for offshore wind energy and new wind farms are built at an unprecedented pace. Much of the North Sea however, is covered with bed forms which may pose a threat to offshore activity (Nemeth et al., 2003). These bed forms can be categorized as shown in Table 1.1 and vary widely in size and migration rate. Megaripples, although the most dynamic of the bed forms, are usually too small to pose a threat to for example foundations or pipelines. At the other side of the spectrum tidal sand banks are (almost) static, which means that their effects on hydrodynamics is highly predictable and morphological changes due to these bed forms are non existent on a time scale of decades. Tidal sand waves may have a significant wave height and migration speed, which makes them troublesome for offshore activities (Matthieu et al., 2012).

Table 1.1: Bed form characteristics (Morelissen et al., 2003)

Bed form	Length [m]	Height [m]	Migration rate
Megaripples	1-10	0.01-0.1	100 m/year
Sand waves	100-1000	1-10	0-10 m/year
Tidal sand banks	5000-10000	10-30	0-1 m/year

A significant part of the North sea is covered with sand waves and most of the planned Dutch windfarms are located in areas with sand waves (see Figure 1.1). Sand waves in the North Sea can grow to over 7 m in height (Damen et al., 2018) and migrate with several meters per year. Over the lifespan of offshore structures such as wind turbines, cables and pipelines, this may cause a significant rise or drop in local bed level. This bed level variation over time may decrease the stability of the foundation or bed protection or cause exposure of cables and pipelines. Furthermore, the migration of sand waves can accelerate siltation of navigational channels. The prediction methods for sand wave growth and migration, and thus the associated bed level changes, are however still in their infancy. For the safety of these offshore structures and navigational routes located in the vicinity of sand waves, continuous monitoring and in some cases dredging is required (Nemeth et al., 2003). These monitoring and dredging activities make construction in these areas more expensive and the lack of knowledge about the prediction of sand wave dynamics poses safety risks. Furthermore, dredging activities can negatively affect marine life as it increases turbidity and demolishes the marine micro environments formed by the sand waves. These micro-environments are formed due to the effect of sand waves on local hydrodynamics and

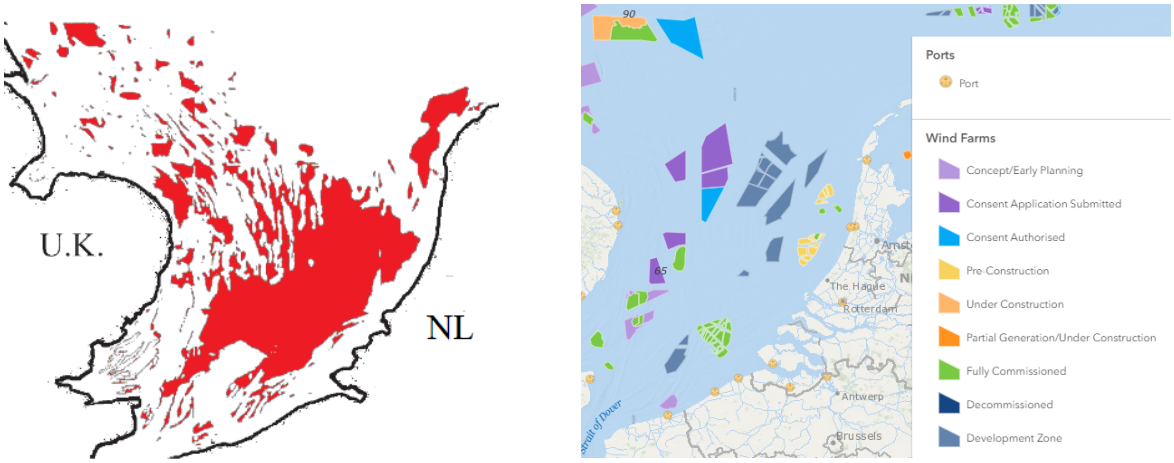

(a) Sand wave coverage of the North Sea (Nemeth, 2003)

(b) Built and planned wind farms in part of the North Sea, for full map see: 4coffshore.com/offshorewind (4COffshore, 2021)

Figure 1.1: Sand wave coverage (left) and planned wind farms (right) in the North Sea

function as a living environment for various organisms. This effect was emphasized by a study by Damveld et al. (2018) which showed differences in organism species and abundance between crest and trough areas of sand waves. Although dredging of sand waves has quite some disadvantages in some cases it is necessary to ensure the safety of offshore structures and navigational routes.
More insight into sand wave dynamics and the prediction thereof, may decrease the need for dredging and monitoring. This in turn will make the construction and maintenance of offshore wind farms, as well as other offshore constructions, less expensive, safer and more environmental friendly.

1.2 Problem definition

Various offshore infrastructural projects, like offshore wind farms, require long term (30-50 years) predictions of the seabed dynamics. These dynamics will determine the required depth of cables, pipelines and foundations as well as restrictions for other constructions like bed protections. Currently data-driven methods are used to determine the range of expected bed levels. The uncertainty in these predictions is however significant, with sand waves being the largest source of uncertainty. From studies conducted in sand wave areas in the North Sea it is observed that the width of the envelope of possible future seabed levels, over the lifetime of an offshore wind farm, is in the order of meters. In these studies the combined uncertainty due to sources other than sand waves only accounted for an uncertainty bandwidth in the order of decimeters (see Section 2.6). Examples of these other sources are survey inaccuracy, megaripples and the spatial resolution of the surveys. Moreover, these bed level predictions are not based on understanding of the systems at hand, but rather on historical data. Numerical models, which compute flow and sediment transport, could potentially increase the accuracy of these predictions. Furthermore, process-based models would allow for in-depth understanding of the processes behind sand wave dynamics.
Process-based models have been used to study sand wave behaviour (see Section 2.5). The set-up of most of these models is however idealized, describing a simplified tidal flow over a 2DV model area with sinusoidal sand waves. In reality the shape of the sand waves is often far from sinusoidal and tidal flows are more complicated than described in these models. Furthermore, the lion's share of these studies focuses on growing sand waves. Observations in the North Sea however indicate that the sand waves show only minor growth/decay and are in a quasi equilibrium with the changing conditions (Deltares, 2016a). Not many attempts have been made to predict sand wave behaviour in real-life situations using numerical models. Since sand waves may have very steep slopes in migration direction a need for small grid sizes arises. On the other hand oceanic hydrodynamics are affected by large scale bed forms, which may need to be included in the model. This makes numerical modelling of sand waves rather difficult due to the balance between grid sizes and computation time. Leenders (2018) were one of the first to use real bathymetry data in their model study using Delft3D-4. To achieve the right level of detail in the area of interest while keeping computation times reasonable, domain decomposition was used. In the results of this study effects of this decomposition were however visible near the edges of the domains. This resulted in errors with respect to sediment transport in the area of interest. Leenders (2018)

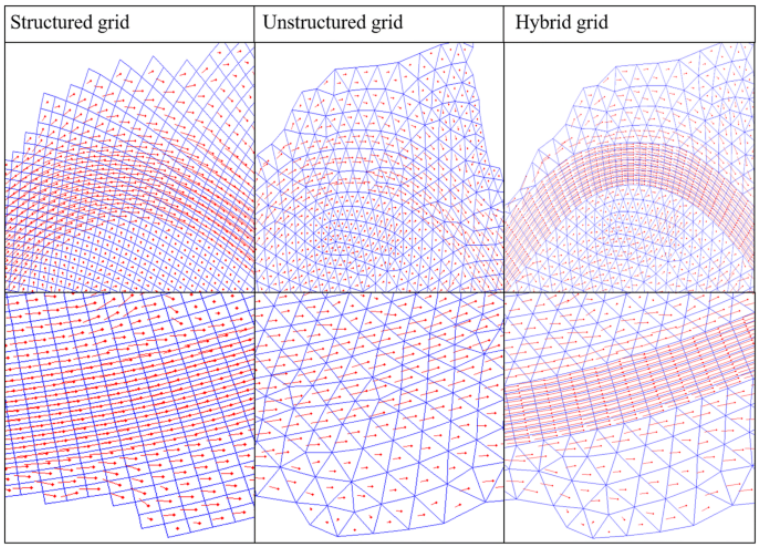

Figure 1.2: Example of structured, unstructured and hybrid grids (Bomers et al., 2019)

argued that these errors could be excluded by keeping the domain transitions well outside the area of interest, but that this would results in unreasonable computational efforts.
Using Delft3D Flexible Mesh (FM), a new numerical model developed by Deltares, it is possible to combine different grid sizes in different areas of the model without the use of domain decomposition. In contrast to Delft3D-4, which was used in several previous modelling studies, Flexible Mesh has the possibility to use unstructured and hybrid grids, which ensure a smooth transition between cells of different sizes and shapes. The difference between structured, unstructured and hybrid grids (which is a combination of the former two), can be seen in Figure 1.2. These kind of grids might therefore present a solution for sand wave modelling which due to the steepness of the of the sand waves (sometimes slopes of 1:4), needs relatively fine spatial discretization. Using unstructured grids, sand wave areas with a fine local grid are easily included in a larger model simulating the large scale hydrodynamics, as influenced by various bed forms and bed level variations, on a coarser grid. Another important distinction between the models is the possibility to run parallel simulations in Delft3D FM. When running in parallel the model area is divided into partitions which run simultaneously and communicate. This option has the potential for vast computation time reductions. Furthermore, through a new type of boundary condition which is implemented in Delft3D FM, the model is able to better impose realistic hydrodynamic conditions locally. This leads to a possible reduction of the model domain, by decreasing or eliminating buffer zones.
The Delft3D FM model has however not yet been used to predict sand wave dynamics. The applicability of the model to these phenomena is therefore unknown. Furthermore, due to the limited knowledge of modelling real sand wave fields in a semi-equilibrium state, the relative importance of different processes for sand wave dynamics is still to be explored.

1.3 Objective and research questions

The aim of this study is to model real-life sand wave field dynamics using Delft3D Flexible Mesh. The evaluation of the model performance will be based on accuracy, computation times and flexibility, as these are important factors for engineering applications. With the objective of this research in mind the main research question is defined as follows:

What are the opportunities and challenges in modelling sand wave dynamics by using Delft3D Flexible Mesh?

This main research question can be further elaborated into multiple sub questions. These sub-questions form the structure of the research to be carried out. The methods used for this study are elaborated upon in the next section. The following sub-questions are defined:

1. **To what level is the Delft3D FM model capable of reproducing the key processes leading to sand wave formation in comparison with Delft3D-4?**

Previous sand wave studies with complex numerical models were done using Delft3D-4, a predecessor of Delft3D FM. The results of these studies have been compared to field observations and it was concluded that the model is able to predict the overall key characteristics of sand waves reasonably well (i.e. wavelength, wave height and migration speed). If the Delft3D FM model yields similar results as the Delft3D-4 model in a simplified situation, the confidence in the Delft3D FM model for the sand wave application will increase. Furthermore, if similar results are observed, relations between environmental factors and sand wave dynamics found using Delft3D-4 can easily be applied to Delft3D FM.

2. **What tidal components should be included in the model boundary conditions to more accurately predict real-life sand wave dynamics in the North Sea?**
   The tide is identified as the main driving mechanism behind the existence of sand waves. Variations in tidal components are known to influence their growth and migration. Although these components have been thoroughly studied in simplified models their influence and importance in a more nature based situation is still to be further analyzed.

3. **What is the sensitivity of the model to changes in input values?**
   The sensitivity of the model will give insight into the uncertainty of the model predictions due to the uncertainty of input values. Furthermore the sensitivity analysis will shed light upon the possibilities of tuning the model to match local conditions.

4. **What is the importance of 3D effects for the local sand wave dynamics?**
   In sand wave fields changes in crest direction as well as bifurcations of sand wave crests are observed (Matthieu et al. (2013), Deltares (2016a)). In addition, research by Leenders (2018) showed that 3D effects caused by tidal sand banks can have a significant impact on sand wave dynamics. By studying the importance of these 3D hydrodynamics insight will be gained into the viability of 2DV models for morphological predictions.

1.4 Research approach

The research questions formulated above form the structure of the research to be carried out. The first question will be answered through a model-model comparison for an idealized model setting. For this model a 2DV set-up with sinusoidal sand waves is used which has widely been applied in previous research (e.g. Borsje et al. (2013)) to analyze different relations using Delft3D-4. The experience with this model set-up forms a knowledge base to which both the Delft3D-4 model and the Delft3D FM model results can be compared. This comparison shows whether the Delft3D FM model is capable of reproducing the key processes leading to sand wave growth and migration. Furthermore, this part of the study will give insight into the applicability of the results of research previously performed in Delft3D-4 to the Delft3D FM model.
Subsequently a 2DV case study is set up to test the Delft3D FM model in real life setting. This model is used to answer the second and third research question. The model for the 2DV case study is based upon the model used in the preceding comparison study. Some alterations are made to represent the local morphology and hydrodynamics at the chosen location in the North Sea. These alterations include a bed level based on measurements and forcing at the boundaries extracted from an overarching model. Several combinations of these boundary conditions are tested to determine the importance of the different tidal components. This same model is used in a sensitivity analysis in which some physical parameters are varied.
To answer the final sub-question a 3D case study is set up. To ensure a valid comparison of the results with the outcomes of the 2DV study, the 3D model is created to represent the same location in the North Sea as chosen for the 2DV model. For this 3D model an unstructured grid is used and the model is run in parallel. In this way some of the possibilities of Delft3D FM are explored. The 3D model is made to represent local hydrodynamics and morphology as well as possible. From the outcomes of the simulations 3D effects in hydrodynamics, sediment transport and morphology are studied.
The experience gained through modelling in both 2DV and 3D setting contributes to the overall testing of Delft3D FM for the sand wave application. This knowledge base will contribute to the development of sand wave models in Delft3D FM for engineering purposes.

1.5 Report outline

Chapter 2: Literature Study
In this chapter previous research on the topic of sand waves is discussed. The findings of these studies will give indications for the processes necessary to predict sand wave dynamics. Furthermore, previous modelling experience will be useful as a basis for modelling decisions. In Section 2.6 a current method for predicting sand wave dynamics is discussed. This provides a benchmark for the current level of accuracy of these predictions and the possibilities for improvement.

Chapter 3: Description of Delft3D FM
In this chapter the Delft3D FM model is discussed. In view of brevity only the formulations as used in this study are shown. Moreover the differences between the Delft3D-4 and Delft3D FM model are explained. These differences have to be accounted for when comparing the results of both models.

Chapter 4: Evaluation of Delft3D FM performance compared to Delft3D-4
In this chapter the set-up and results of the model-model comparison are shown. First a base case with a symmetrical tide is discussed. Subsequently the influences of wavelength and residual current are tested in both models. Furthermore the behaviour towards equilibrium is studied.

Chapter 5: 2DV case study
In this chapter the set-up and results of the 2DV case study are shown. The hydrodynamic and morphological results for various combinations of tidal forcing are shown. Subsequently the results of the sensitivity analysis are discussed.

Chapter 6: 3D case study
In this chapter the set-up and results of the 3D case study are shown. Indications of 3D effects in hydrodynamics, sediment transport and morphology are discussed.

Chapter 7: Discussion
This chapter contains a discussion of the limitations of the results.

Chapter 8: Conclusions
In this chapter the conclusions are presented. This includes the answers to the research question stated in Section 1.3.

Chapter 9: Recommendations
In this chapter recommendations for further research based on the results of this study are discussed.

2 | Literature study

In this chapter literature on the topic of (numerical modelling of) sand wave dynamics will be reviewed. First the formation of sand waves will be explained based on previous research. Subsequently processes that influence sand wave parameters and dynamics as found in literature are discussed. Furthermore the parameters of sand waves as found in the North sea through data analysis are reviewed and two methods for the prediction of sand waves used in previous research are shown: numerical models and data analysis.

2.1 Sand wave formation

The formation and dynamics of sand waves has been thoroughly studied in the past decades. For the explanation of these rhythmic bed forms first linear theory was used, which has been expanded to the use of (semi-) non-linear and complex numerical models in more recent years. Hulscher (1996) explained the occurrence of sand waves by the interaction of tidal currents and bed forms. Due to shadowing of the tidal current a residual average current is formed from the trough of the sand wave in the direction of the crest. This is shown in Figure 2.1 where the velocity profiles during the maximal tidal current and the tide-averaged residual currents are shown.

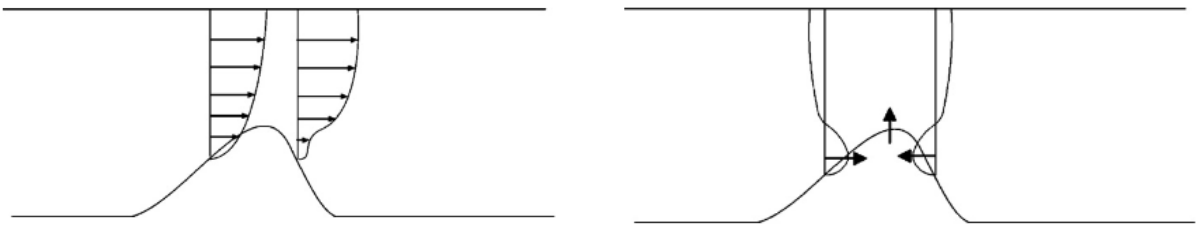

(a) During maximum flood flow

(b) Tide-averaged

Figure 2.1: Velocity profiles over a sand wave (Tonnon et al., 2007)

For a symmetrical tidal motion, the averaged flow over the vertical is zero. This means that these residual currents near the bottom are compensated in the vertical and a circulation cell is formed. These circulation cells are shown in Figure 2.2. The residual currents in these cells support the growth of these bed forms. Due to this circulation, grid refinement over the vertical is necessary to simulate sand wave formation.

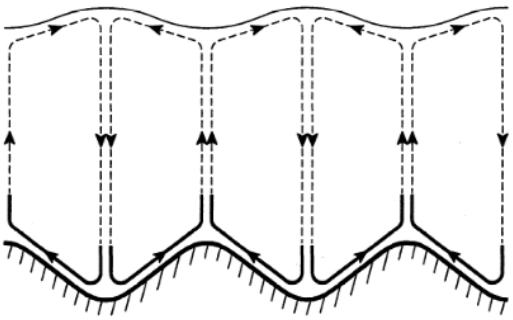

Figure 2.2: Tide-averaged circulation cells over a sand wave field (Hulscher, 1996)

Sand waves are observed to be very regular in wavelength and shape over certain areas. This degree of order is a result of the driving forces which act as a self-organizational mechanism (Matthieu et al., 2013). Looking at the dominant mechanisms for sand wave formation will give insight into which sand wave lengths are expected to grow and which will not grow (Borsje et al., 2014). Borsje identified the following three mechanisms: bed load transport, slope induced transport and suspended sediment transport. The first of these mechanisms causes sand wave growth, while the latter two cause decay of the sand waves as can be seen in Figure 2.3. The bed load transport instantly follows the currents. Under the influence of the flow circulation cells this transport mode moves sediment from the trough of the sand wave to the crest. In this way the bed load transport supports sand wave growth. Sediment is more easily transported downhill than uphill. This mechanism is called slope induced transport and causes the sediment transport rates to be higher when directed down a slope. Slope induced transport thus causes a net sediment transport from the crest towards the trough. The importance of this effect is however dependent on the steepness of the slope. This means that short waves will experience more decay than long waves, with the same wave height, due to slope induced transport. From the model study by Borsje et al. (2014) it is clear that suspended sediment have a damping effect on sand waves. Borsje et al. (2014) explained this with the phase lag between suspended sediment transport and sand waves. The extend of the damping is dependent on both sediment size and strength of the tidal current, which is supported by observations, showing no sand waves for certain Rouse numbers (Borsje et al., 2014).

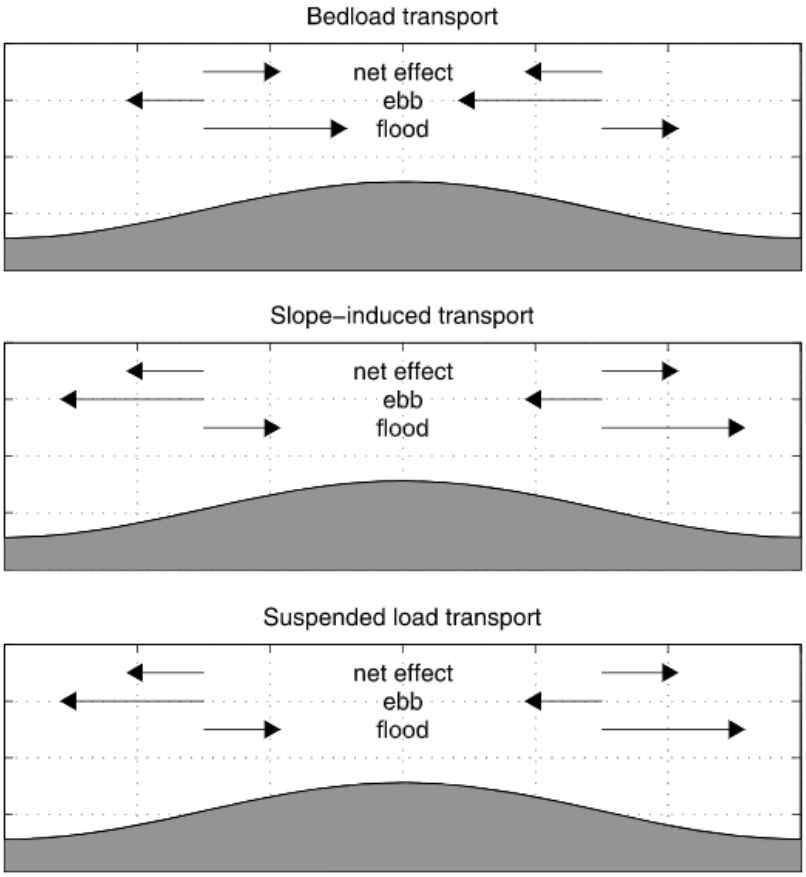

Figure 2.3: Schematic overview of the dominant processes in sand wave formation: bed load transport, slope induced transport and suspended load transport. Sand waves and fluxes not to scale (Borsje et al., 2014)

The three dominant mechanisms discussed above play a major role in determining which wave lengths will grow and which will not. At the short end of the spectrum sand waves are dampened by slope induced transport. At the long end on the other hand the suspended sediment transport dampens the sand waves. Furthermore, in regions where suspended sediment transport is dominant sand waves might not occur (Borsje et al., 2014).

2.2 Sand wave characteristics

The effect of environmental parameters on sand wave characteristics has been studied extensively. Four main measures are often used to characterise sand waves and their dynamics: wave length (L), wave height (H), migration and wave skewness (A). These and a few other measures are shown in Figure 2.4.

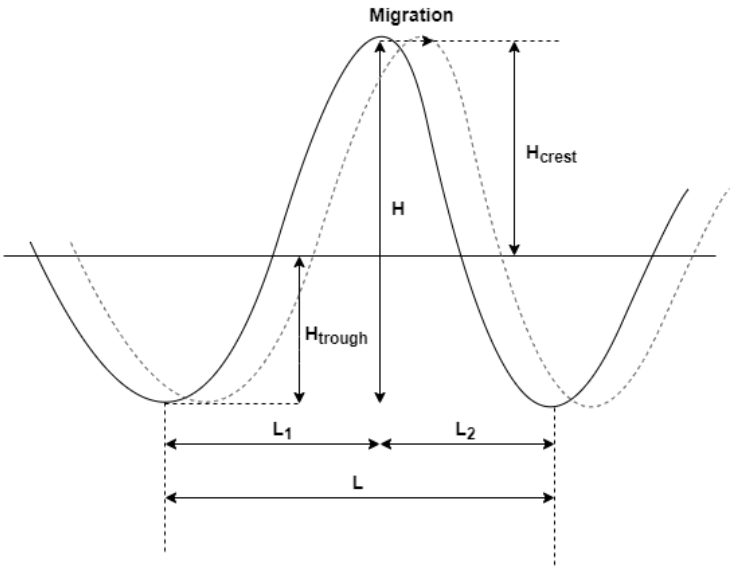

Figure 2.4: Schematic overview of sand wave characteristics

The wave skewness can be calculated as shown in equation 2.1 (Knaapen, 2005). A positive skewness means that the sand wave leans over in the chosen direction. A skewness of 0 indicates a symmetric wave. The wave skewness has been observed to be related to the migration speed and direction (Knaapen, 2005).

$$A = \frac{L_1 - L_2}{L} \tag{2.1}$$

2.3 Processes influencing wave characteristics

In previous studies a large range of processes which influence sand wave characteristics have been identified. In this section some of the important processes are highlighted and their influence on the sand wave characteristics is explained.

2.3.1 Tidal forcing

The tide has been identified as the main forcing mechanism for the formation of sand waves (Hulscher, 1996). When only taking into account the symmetrical M2 tidal constituent, sand wave growth was observed, but no sand wave migration. The growth rate of sand waves is dependent on the strength of the tidal current (Wang et al., 2019). Relatively strong tidal currents result in higher growth rates, when sand waves are present. Whether sand waves are formed is dependent on the strength of the tidal current relative to the grain size (Borsje et al., 2014). These findings are supported by data analysis on sand waves on the Dutch continental shelf. For low Rouse numbers, indicating strong tidal currents with respect to the grain size, and thus dominance of suspended sediment transport, no sand waves were found.
When on top of the M2 tide a residual current is present, the circulation cells, which cause sand wave formation, get distorted, leading to sand wave migration in the direction of the residual current (Besio et al., 2003). Sand wave migration can also be caused by an asymmetrical tidal forcing. Besio et al. (2004) explored the effect of forcing by the M4 tidal constituent in combination with the M2 tide. It was found that the M4 tide can

give rise to sand wave migration in positive and negative direction, dependent on the phase difference between the two tidal constituents. This also explained sand wave migration opposed to a residual current which was observed in the North Sea. For an increasing strength of the residual current Van Gerwen et al. (2018) found an increasing migration rate and a decreasing equilibrium wave height. Lastly the spring-neap tidal cycle can have a significant effect on sand wave formation (Blondeaux, Vittori, 2010). It was found that whether the modulation of the tide caused bed level stabilization or destabilization was dependent on the dominant sediment transport regime.

2.3.2 Storms and surface gravity waves

Campmans (2018) elaborately studied the effect of surface gravity waves on sand wave characteristics. With the use of linear and nonlinear modelling it was found that surface gravity waves can enhance the migration rate of sand waves when migration is already present. The surface gravity waves do not however cause migration themselves. When, for example during a storm, wind waves and a wind driven current are combined this can cause significant sand wave migration in the direction of the wind driven current. This migration can be in opposite direction of the long term migration direction of the sand waves. Furthermore, wind waves cause a decrease in equilibrium sand wave height (Campmans, 2018). These conclusions are supported by a study by Bao et al. (2020) who observed large sand wave migration and a significant decrease of sand wave height during a tropical storm on the Taiwan Shoal. Campmans (2018) also found that when comparing mild, intermediate and extreme storm conditions, the intermediate conditions had the largest absolute effect (when scaled to occurrence) on the sand wave migration, although they have a lower chance of occurrence than the mild conditions.

2.3.3 Underlying seabed topography

Underlying seabed topography can have a significant effect on sand wave characteristics. Several data-analysis and modelling studies have pointed to a maximum sand wave height with a linear dependence on water depth (Damen et al. (2018), Nemeth (2003)). Tonnon et al. (2007) pointed out that at smaller water depths surface gravity waves have a larger effect on sand waves and can significantly decrease sand wave height and increase

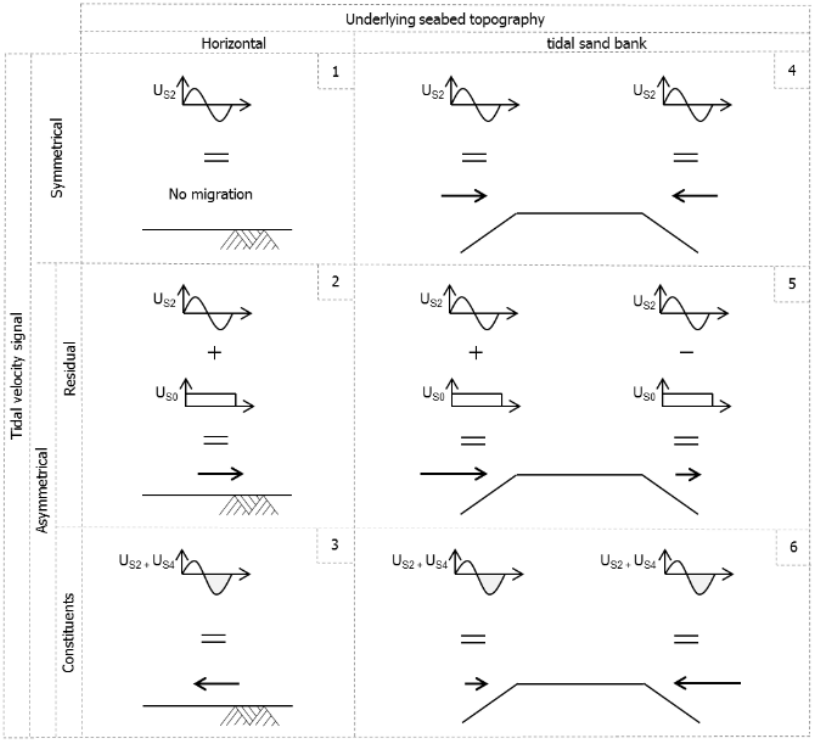

Figure 2.5: Schematic overview of sand wave migration direction on a flat bed (left) and on a tidal sand bank (right) (Leenders, 2018)

migration. Leenders (2018) showed that the diversion of currents by tidal sand banks, as explained by Roos (2003), can cause opposite migration directions of sand waves over a small area. These large scale bedforms deform the tidal flow which causes an opposite residual flow on both sides of the tidal sand bank averaged over the tidal cycle. This causes the sand waves to migrate towards the crest of the tidal sand bank for a symmetrical tide, see Figure 2.5. In case of residual flow or asymmetrical tide the migration rates and/or directions are also influenced by the underlying topography (Leenders, 2018).

2.3.4 Sediment transport modes and grain size sorting

As explained before the different sediment transport regimes have opposite effects on sand wave growth, see Figure 2.3. This means that a change in sediment size, which influences the dominant sediment transport regime can have a significant impact on sand wave characteristics. In several studies it was found that grain size sorting takes place over the length of a sand wave (Van Oyen and Blondeaux (2009), Damveld et al. (2020), Cheng et al. (2020)). Through modelling with graded sediment Van Oyen and Blondeaux (2009) found that whether coarse sediment piles up at the trough or crest regions depends on the relative strength of the tidal current. For weak tidal currents the coarser fractions pile up at the trough of the sand wave, while the finer fractions move towards the crest. In this case the graded sediment stabilizes the bottom relative to a uniform sediment of the mean grain size. On the other hand, in case of strong tidal currents the coarser sediment fractions are mostly found in the crest region, while fine fractions move towards the trough. The sediment grading then acts as a destabilizing factor (Van Oyen and Blondeaux, 2009). Damveld et al. (2020) studied the effect of graded sediment on sand wave growth and migration. While excluding hiding and exposure effects a higher standard deviation of the sediment diameter lead to decreased sand wave growth and increased migration.

2.4 Sand wave characteristics in the North Sea

Sand waves in the North Sea have been studied thoroughly since the North Sea is an attractive area for offshore activities and is quite well monitored. Damen et al. (2018) studied the spatial dispersion of sand wave characteristics by using a Fourier transform on 10 by 10 km blocks of North Sea bathymetry. The distribution of sand wave characteristics in the Dutch part of the North Sea from this analysis is shown in in Figure 2.6 for areas with over 80% sand wave coverage. It is clear that the shape and size of sand waves varies significantly throughout the North Sea. Sand wave heights vary from 1-8 m and sand wave lengths are in the order of 100-1000 m. In the South-Western area the sand waves are higher, shorter and less asymmetric. Close to shore no sand waves are observed and another clear edge of the sand wave domain is present starting from about halfway the straight part of the Dutch coastline. The lack of sand waves in the Northern areas can be explained by the dampening effect of suspended sediment. This relation was first found by Borsje et al. (2014) and states that in areas with low Rouse numbers, where suspended sediment transport is dominant, sand waves are dampened. In the data analysis by Damen et al. (2018) similar results were found, where the areas with low Rouse numbers and areas lacking sand waves largely coincided.

2.5 Numerical modelling of sand waves

Complex numerical models, such as Delft3D have been used to model sand wave dynamics. In most studies a simplified 2DV model with sinusoidal sand waves was used. Tonnon et al. (2007) was the first to use Delft3D for the purpose of sand wave modelling. In this 2DV model study the influences of various model parameters and model set-up on the growth and migration of an artificially made sand wave in the Dutch North Sea is analyzed. It was found that for this relatively sinusoidal sand wave the grid size should not be larger than around 10 m. Furthermore, using a roughness predictor which included the presence of ripples, but excluded megaripples, the results of a fifteen year hindcast model improved significantly. Other influences studied were: sediment size, bed slope parameter, different turbulence models and free surface waves. Over the years the sand wave changed shape to form a steep slope facing the ebb current, but the sand wave migration in this direction was minimal. None of the model variations formed such a steep slope without significant migration.
The exploration of Delft3D for sand wave cases was continued by Borsje et al. (2013), who showed that the Delft3D model is capable of growing sand waves with characteristics matching those found in observations. Using the k-ε turbulence model more realistic results for the sand wave length were found relative to the constant eddy viscosity turbulence model. In this study a simplified 2DV sand wave model set-up is used similar to the one used in this study. This set up was also adopted in various subsequent studies, such as: Matthieu et al.

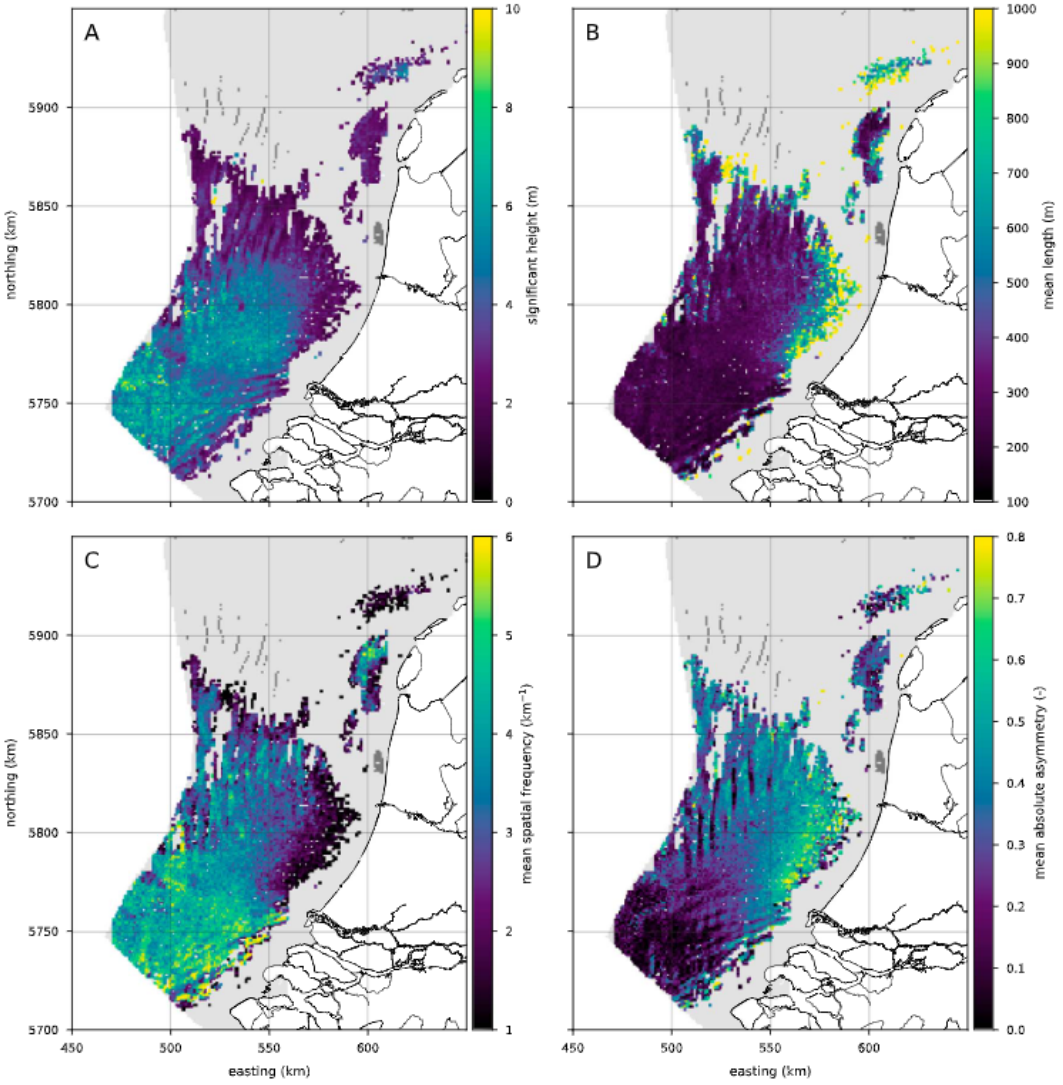

Figure 2.6: Sand wave characteristics (a) height, (b) length, (c) spatial frequency ($\xi = 1/L$), and (d) asymmetry aggregated per square km and for sand wave-coverage > 80% (Damen et al., 2018)

(2012), Matthieu et al. (2013), Borsje et al. (2014), Choy (2015), De Koning (2017), Van Gerwen et al. (2018), Wang et al. (2019) and Damveld et al. (2020).

Using Delft3D Matthieu et al. (2013) showed the self-organizational properties of sand waves. From this study it was concluded that sand waves do tend towards a preferred wavelength, although antecedent bathymetry does have a long-lasting influence on the precise sand wave characteristics. Borsje et al. (2014) used the Delft3D model to show the influence of suspended sediment transport on sand wave growth and migration. Choy (2015) found a significant effect of the bed slope parameter, which determines the the strength of slope related sediment transport, on sand wave growth and shape. Wang et al. (2019) also looked into the effects of varying the bed slope parameter and concluded that this parameter was an important calibration parameter. For finer sediments sizes, a larger bed slope parameter yielded more realistic results. Van Gerwen et al. (2018) used Delft3D to study the behaviour of sand waves on long timescales and found that both the inclusion of suspended sediment transport and tidal asymmetry significantly reduce the equilibrium wave height.

Leenders (2018) studied the effects of tidal sand banks on sand wave migration. To analyze sand wave migration in real-life, a 3D model of the North Sea was created. This was done using Delft3D-4 with domain decomposition. Through this domain decomposition the spatial discretization could be of more detail in the area of interest while keeping computation times acceptable. At the edges of the domains effects of the decomposition were

observed, which resulted in visible errors in terms of sediment transport within the area of interest. Leenders (2018) argued that these errors could be excluded by keeping the domain transitions well outside the area of interest, but that this resulted in unreasonable computational efforts. The sand wave migration directions did match reality in a qualitative sense. Damveld et al. (2020) used a Delft3D model with multiple sediment fractions to study the effect of graded sediment on sand wave dynamics and bed composition in sand wave areas. The Delft3D model has also been applied to engineering problems such as dredging and the burial depth of pipelines. This was done by amongst others Matthieu et al. (2012) and De Koning (2017).

2.6 Data-driven analysis

In preparation for future wind farms Deltares has carried out morphodynamic analyses for several planned wind farm locations in sand wave areas of the North Sea (Deltares (2015), Deltares (2016a), Deltares (2016b), Deltares (2019), Deltares (2020)). The main objective of these studies is to gain insight into the local seabed dynamics and classify areas as suitable or unsuitable for wind turbines, based on local seabed mobility. In these studies a data-driven analysis is carried out to characterise seabed features and historic seabed dynamics. This analysis is supplemented by numerical modelling of residual sediment transport patterns. This knowledge is then used to obtain an estimation of possible future seabed levels. At the moment this is the most important tool for seabed level predictions in sand wave areas. This type of analysis yields the highest quality with the availability of multiple historic bathymetry datasets measured over a period of several decades. Uncertainties in the future seabed levels increase significantly with lower spatial and temporal spread in available bathymetry data.
In these studies the bathymetry datasets are judged on extend and accuracy. The Royal Dutch Navy has done extensive bathymetry surveys in the Dutch North Sea over the past decades. The older datasets are usually of lesser accuracy and density. For the planned wind farm locations new measurement surveys are conducted with high accuracy. To identify non-erodible layers a geological study is carried out.
For the prediction of possible future bed levels the bathymetries and seabed dynamics are split into three classes of seabed features: megaripples, sand waves and large-scale bathymetry. All three classes are analyzed separately. Using Fourier transform spatial characteristics of the bed forms are extracted from the bathymetry measurements. The migration speed and direction of the bed forms are estimated between different bathymetry datasets using cross correlation methods.
To obtain more insight into the system behind bed level changes the Dutch Continental Shelf Model (DCSM) is used for hydrodynamic and sediment transport simulations in the area of interest, using the main tidal components in a 2DH setting. The results of this model are not used for predictions of seabed dynamics, but function as a tool to gain more understanding of the mechanisms behind the morphodynamics.
When no large discrepancies between the data-analysis and the modelling results of hydrodynamics and sediment transport are found, the bathymetry data is used to predict bed level changes. For this purpose different types of uncertainty are bundled to estimate the range of possible future bed levels. The identified uncertainties are amongst others: migration speed and direction of bed forms, survey inaccuracies, limited spatial resolution and the assumption of shape-retaining sand waves. For the study of the Hollandse Kust (Zuid) Wind Farm (HKZWF) location the estimated uncertainty bands, excluding sand wave dynamics, were 0.5 m upwards and 0.4 m downwards (Deltares, 2016a). From data-analysis in combination with the identified uncertainties a Best Estimate Bathymetry (BEB) as well as the lowest and highest seabed levels can be determined for some time in the future. The duration of bed level changes is based on a typical wind farm lifetime of a few decades (in the HKZWF case 35 years). As can be seen in Figure 2.7 in the HKZWF case the total uncertainty of the bed levels amounts to up to 4.5 m locally, of which only 0.9 m can be ascribed to sources other than sand waves. From this band of possible seabed levels the maximum lowering and rising at a certain location during this period can be determined. Areas are classified based on this estimation of the local maximum lowering and rising. Such a classification is shown in Figure 2.7, where first a minimum and maximum seabed level due to sand wave migration was determined and subsequently the uncertainty bands in downwards and upwards direction due to other factors were added to obtain the Lowest SeaBed Level (LSBL) and Highest SeaBed Level (HSBL) respectively. In the sand wave fields considered the majority of the area is deemed suitable for the construction of wind turbines, based on the expected change in bed level over the lifetime of the structure. Close to the crest of the sand wave fast lowering or rising of the seabed can take place. This makes the location less suitable for wind turbines, cables and pipelines.

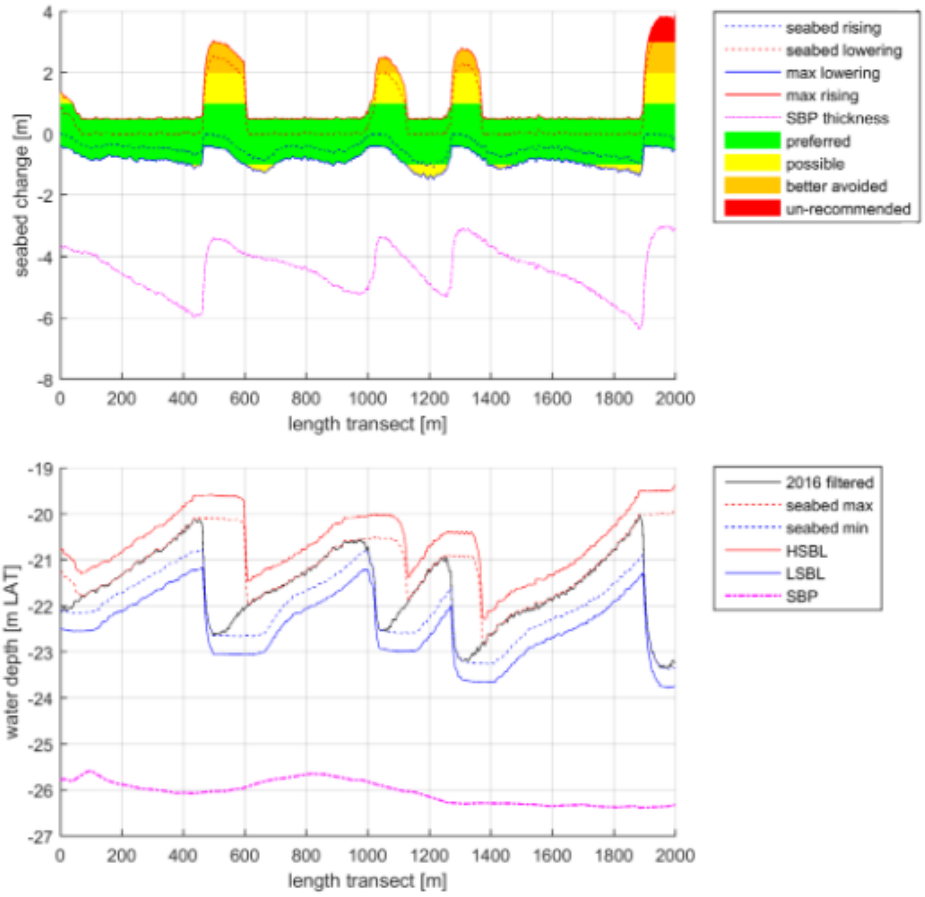

Figure 2.7: Upper plot: estimation of maximum lowering an rising of the seabed including uncertainty bands. Lower plot: 2016 measured bathymetr (black), lower and upper bed level due to sand wave migration (dashed blue and red line respectively) and the LSBL and HSBL (solid blue and red line) which include the mentioned uncertainty bands. Both plots represent a transect at Hollandse Kust (Zuid) Wind Farm (HKZWF) and a duration of bed level change of 35 years (Deltares, 2016a)

3 Basic description of Delft3D

In this chapter the basics of Delft3D and the most important differences between Delft3D-4 and Delft3D FM are described. Since these are two complex numerical models not all details will be discussed here. For further information about the Delft3D-4 and Delft3D FM models reference is made to the user manuals, (Deltares, 2020b) and (Deltares, 2020a) respectively. In Section 3.1 the Delft3D model is described briefly. The main differences between Delft3D-4 and Delft3D FM are discussed in Section 3.2. In the remainder of this chapter the formulations of hydrodynamics, sediment transport and morphology as used in this study in both the Delft3D-4 and Delft3D FM model are shown.

3.1 Delft3D model description

Delft3D is a process based model developed by Deltares. The model can be used for both 2D and 3D modelling of coastal, river and estuarine areas. The model is able to simulate flows, sediment transports, waves, water quality, morphological developments and ecology (Deltares, 2020b). Through online coupling, the main (flow) module is able to interact with other modules for simulations of for example waves or sediment. With Delft3D as base, Delft3D Flexible Mesh (FM) is developed to include differently shaped, unstructured, grids as shown in Section 1.2. These unstructured grids allow for smooth transition to finer or coarser grid cells in certain areas. This difference in grid shapes has extensive implications for the numerical computations that need to be carried out.

3.2 Main differences between Delft3D-4 and Delft3D FM

In this section some of the main differences between Delft3D-4 and Delft3D FM, as indicated in Deltares (2020a), are discussed. These differences are summarized in Table 3.1. For the specifics in terms of numerics reference is made to the manual: Deltares (2020a). The most important difference between the models is the possibility to use unstructured grids in Delft3D FM. Where in Delft3D-4 only (deformed) square grid cells could be used, the Delft3D FM model also allows for triangles, pentagons and hexagons. This increased freedom makes coupling between coarser and finer grids much easier and smoother. Furthermore the strict definitions of rows and columns used in Delft3D-4 are removed. This also means that grid points can no longer be indicated with indices (indicating row and column) and thus cartesian or spherical coordinates are used.
These differences in grid have a significant impact on the computational side of the model. Due to the regularity of the grid, Delft3D-4 is able to solve the hydrodynamic equations using Finite Differences Methods. In Delft3D FM Finite Volume Methods are used, as they are better capable of dealing with complex geometries. In Delft3D-4 the time integration of the shallow water equations is solved using an Alternating Direction Implicit (ADI) method, which alternates explicit and implicit solving methods between the both directions (of the rows and columns). Because this concept of rows and columns is not implemented in Delft3D FM this solver cannot be used in this model. Instead the continuity equation is solved in a single combined implicit system for both directions. The advection term uses an explicit time integration method and the resulting dynamic time step limitation, based on the Courant number, is set automatically, where Delft3D-4 uses a user defined time step. Lastly the Delft3D FM model has the possibility of parallel model runs, where the domain is divided into partitions which are run simultaneously.
All above differences impact the computational performance of the models. The Finite Volume Method is less efficient than the Finite Differences Method. Combined with the time step limitation this increases the computation times in Delft3D FM relative to Delft3D-4. It is however believed that this is compensated for due to the smooth refinement of models in Delft3D FM using unstructured grids, which allows for increased accuracy

in areas of interest and coarsening in other areas. This coarsening outside of the area of interest will decrease computational effort and thus computation time. Moreover further computational gains are reached through other means such as parallel running. In addition, the code efficiency of Delft3D FM is improved relative to Delft3D-4.

Table 3.1: Main differences between Delft3D-4 and Delft3D FM

Description	Delft3D-4	Delft3D FM
Grid types	Structured	Structured, unstructured & hybrid
Grid shapes	Rectangular or curvilinear	Rectangular, curvilinear, triangles, pentagons & hexagons
Cell definition	Based on rows and columns	Based on coordinates
Spatial derivative	Finite differences[1]	Finite volumes
Time integration	Implicit, explicit (ADI)	Implicit, explicit advection term
Time-step implementation	User defined	Automatic
Time-step limitation	No strict Courant limitation	Courant limited

3.3 Definitions

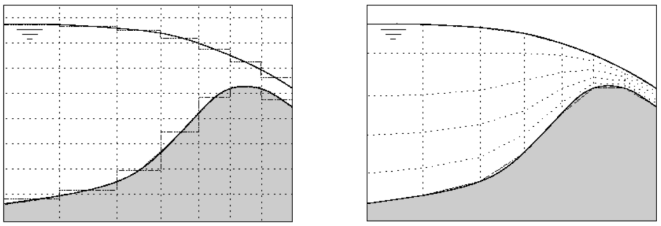

Figure 3.1: Vertical grid definitions Delft3D: Z coordinates (left) and σ coordinates (right) (Bijvelds, 2001)

For the vertical schematization two options are available in both models: Z or σ coordinates. For this study the σ coordinates are chosen, as they give a better representation of the actual bed level. This means that hydrodynamic equations of Section 3.4 are converted to the σ grid. The σ and z grid are illustrated in Figure 3.1. The definition of water level and depth are shown in Figure 3.2.

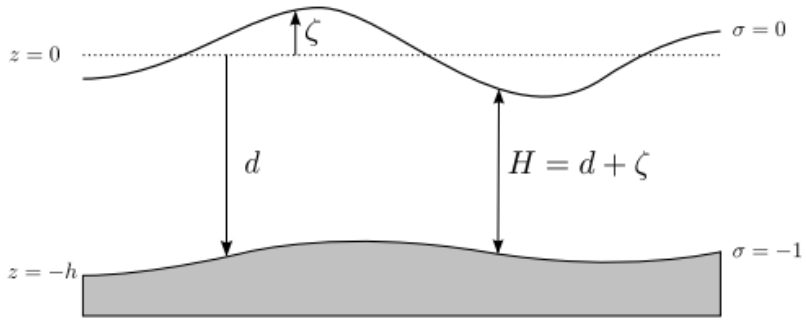

Figure 3.2: Definitions of water level (ζ), water depth (d) and total water depth (H) in Delft3D (Deltares, 2020b)

[1] Transport equation uses finite volumes

3.4 Hydrodynamics

In the flow computations Delft3D uses a staggered grid, meaning that the flow velocity and water levels are computed at different positions in space. The water levels are computed at the cell centres and flow velocities are computed at the grid cell faces. The models solve the shallow water equations. The vertical accelerations of the flow are assumed to be small, relative to the gravitational acceleration, which reduces the vertical momentum balance to the hydrostatic pressure relation. A turbulence model is used and represented by the spatio-temporally varying vertical eddy viscosity (ν_V). The 3D shallow water equations, in terms of sigma coordinates, reduce to:

$$\frac{\delta u}{\delta t} + u\frac{\delta u}{\delta x} + v\frac{\delta u}{\delta y} + \frac{\omega}{d+\zeta}\frac{\delta u}{\delta \sigma} - fv = -\frac{1}{\rho_w}P_x + F_x + \frac{1}{(d+\zeta)^2}\frac{\delta}{\delta \sigma}(\nu_V\frac{\delta u}{\delta \sigma}) \tag{3.1}$$

$$\frac{\delta v}{\delta t} + u\frac{\delta v}{\delta x} + v\frac{\delta v}{\delta y} + \frac{\omega}{d+\zeta}\frac{\delta v}{\delta \sigma} + fu = -\frac{1}{\rho_w}P_y + F_y + \frac{1}{(d+\zeta)^2}\frac{\delta}{\delta \sigma}(\nu_V\frac{\delta v}{\delta \sigma}) \tag{3.2}$$

$$\frac{\delta \omega}{\delta \sigma} = -\frac{\delta \zeta}{\delta t} - \frac{\delta (d+\zeta)u}{\delta x} - \frac{\delta (d+\zeta)v}{\delta y} \tag{3.3}$$

In these equations u and v represent the horizontal velocity in the x and y direction respectively. ω is the vertical velocity in the σ direction (with respect to the moving sigma plane). ρ_w is the density of water, P_x and P_y are the hydrostatic pressure gradient in x and y direction and F_x and F_y represent the horizontal Reynold's stresses. ν_V is the vertical eddy viscosity which is computed using a turbulence closure model. The above equations are solved using boundary conditions at the free surface and bed level. Assuming an impermeable bed and free surface, the kinematic vertical boundary conditions are found as shown in equation 3.4. The dynamic boundary conditions, representing the stresses at bed level and at the free surface are shown in equation 3.5 and equation 3.6. Where τ_b and τ_s represent the shear stress at the bed and free surface level respectively.

$$\omega|_{\sigma=-1} = 0 \quad \text{and} \quad \omega|_{\sigma=0} = 0 \tag{3.4}$$

$$\frac{\nu_V}{H}\frac{\partial u}{\partial \sigma}\bigg|_{\sigma=-1} = \frac{1}{\rho_0}\tau_{b,x} \quad \text{and} \quad \frac{\nu_V}{H}\frac{\partial v}{\partial \sigma}\bigg|_{\sigma=-1} = \frac{1}{\rho_0}\tau_{b,y} \tag{3.5}$$

$$\frac{\nu_V}{H}\frac{\partial u}{\partial \sigma}\bigg|_{\sigma=0} = \frac{1}{\rho_0}|\vec{\tau}_s|\cos(\theta), \quad \text{and} \quad \frac{\nu_V}{H}\frac{\partial v}{\partial \sigma}\bigg|_{\sigma=0} = \frac{1}{\rho_0}|\vec{\tau}_s|\sin(\theta), \tag{3.6}$$

3.4.1 Turbulence formulation

Delft3D offers multiple options for turbulence closure models. In the modelling studies below the $k-\epsilon$ turbulence model is used. In this (more advanced) turbulence model transport equations for turbulent kinetic energy (k) and energy dissipation (ϵ) are solved to determine the vertical eddy viscosity. The resulting vertical eddy viscosity is variable in space and time and is computed as follows:

$$\nu_V = c_\mu \frac{k^2}{\epsilon} \tag{3.7}$$

c_μ is a calibration coefficient which is taken as 0.09 (Deltares, 2020b).

3.4.2 Roughness formulation

To calculate the bed shear stress a formulation for the bed roughness is required. In the modelling study below the Chézy roughness formulation is used. The bed shear stress can then be computed as shown in equation 3.8.

$$\vec{\tau}_b = \frac{\rho_0 g \vec{u}_b |\vec{u}_b|}{C^2} \tag{3.8}$$

Where u_b is the magnitude of the horizontal flow velocity in the first layer above the bed and C is the user defined Chezy coefficient.

3.5 Sediment transport

As mentioned in the literature study there are two distinct modes of sediment transport. The bed load transport takes place close to the bed, where sediment grains roll or jump from one place to another. This mode of sediment transport responds instantaneously to changes in this flow velocity. Sediment grains are transported as bed load when they have a high settling velocity relative to the flow velocity. This mode of sediment transport has been linked to the growth of sand waves as mentioned in Chapter 2. When grains are too small or flow velocities are too high, sediment is transported in the upper part of the water column. This mode is called suspended sediment transport and shows a lagging effect with respect to flow velocities. Since this sediment transport mode is, at the time of this study, not yet fully implemented in Delft3D FM, suspended sediment transport will not be included in the simulations (even those using Delft3D-4).

3.5.1 Sediment transport formulation

Following previous studies the Van Rijn (1993) sediment transport formulation for bed load transport is used. The magnitude of sediment transport, corrected for the bed slope, is calculated using equation 3.9.

$$|S_b| = 0.006 \alpha_s \rho_s w_s D_{50} M^{0.5} M_e^{0.7} \tag{3.9}$$

In this formulation α_s is a correction factor for the bed slope (see below). ρ_s is the density of the sediment, w_s is the particle settling velocity and D_{50} is the median diameter of the sediment. M represents the sediment mobility number and M_e the excess sediment mobility number. These can be calculated as shown in equation 3.10.

$$M = \frac{u_r^2}{(\rho_s/\rho_w - 1)\, g D_{50}}, \quad M_e = \frac{(u_r - u_{cr})^2}{(\rho_s/\rho_w - 1)\, g D_{50}} \tag{3.10}$$

In this formulation u_{cr} represents the critical depth averaged velocity for initiation of motion, which is based on the Shield's curve. The velocity u_r is the magnitude of the equivalent depth averaged velocity, computed using the velocity in the bottom computational layer and assuming a logarithmic velocity profile. If u_r is lower than the critical velocity u_{cr}, the bed load sediment transport is set to zero.

3.5.2 Bed slope effect

The sediment transport is corrected for the bed slope using the factor α_s. To calculate this factor a formulation by Bagnold is used, which is shown in equation 3.11.

$$\alpha_s = 1 + \alpha_{bs} \left(\frac{\tan(\phi)}{\cos\left(\tan^{-1}\left(\frac{\partial z}{\partial s}\right)\right)\left(\tan(\phi) + \frac{\partial z}{\partial s}\right)} - 1 \right) \tag{3.11}$$

Where α_{bs} is a tuning parameter, ϕ is the internal angle of friction of the bed material and $\frac{\partial z}{\partial s}$ is the bed slope in the direction of the flow.

3.5.3 Bed level update and morphological scale factor

Using the calculated sediment transport the bed level can be updated using the formulation by Exner for continuity of sediment, shown in equation 3.12.

$$\left(1 - \varepsilon_p\right) \frac{\partial z_b}{\partial t} + \frac{\partial S_{b,x}}{\partial x} + \frac{\partial S_{b,y}}{\partial y} = 0 \tag{3.12}$$

In this formulation ε_p represents the bed porosity, which is taken as 0.4. The formulation states that the change in bed level (z_b) over time is a result of spatial differences in sediment transport rate. When a morphological scale factor (MF) is used, the bed level change is multiplied with this factor at every time step to speed up the calculation.

4 Evaluation of Delft3D FM performance compared to Delft3D-4

In this chapter the new Delft3D FM model will be tested for an idealized sand wave situation, with and without residual current. The results will then be compared with a Delft3D-4 model with the same set-up and parameters. Since Delft3D-4 has been used for modelling sand waves in numerous studies (see Section 2.5), similarities between the results of both models will increase the confidence in Delft3D FM for this purpose.

4.1 Model set-up

The 2DV model set-up used in this study is based on the set-up used in several previous studies, like Borsje et al. (2013) (see Section 2.5). The parameters used here show most resemblance with the model used by Damveld et al. (2020). The model set-up is identical for both models with the exception of a minor difference in boundary conditions. The modelling domain spans 50 km. In the middle of the domain, over a length of around 5 km, sand waves are present. The grid is coarser near the boundaries, with a maximum cell size of 1550 m and becomes finer near the sand wave area. At the area of the sand waves the cell size is reduced to 2 m. The vertical grid consists of 60 sigma layers with decreasing size towards the bed. The near bed layer has a thickness of 0.05% of the water depth (~25 m), which comes down to on average 0.0125 m. The horizontal and vertical grid are shown in Figure 4.1

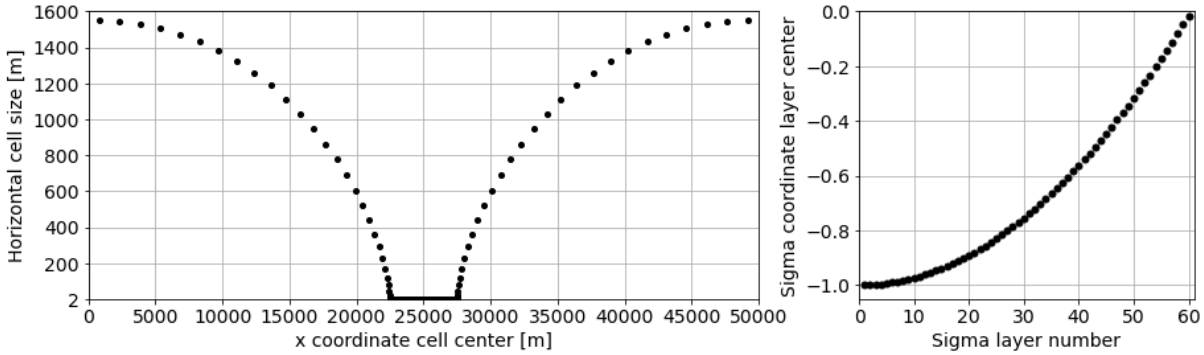

Figure 4.1: Horizontal (left) and vertical (right) grid of Delft3D-4 and Delft3D FM model

The initial bed level is shown in Figure 4.2. Towards the edges of the sand wave area the sand waves gradually decrease in height. In the flat area the grid coarsens causing the boundaries to be sufficiently far away to avoid interference with the model results in the sand wave area. At the two open boundaries Riemann boundary conditions are imposed. These boundary conditions ensure that waves can leave the domain without being reflected back. At these boundaries a tidal velocity is imposed in the Delft3D-4 model. In the Delft3D FM model the Riemann boundary condition could not (yet) be combined with a velocity perpendicular to the boundary. A tidal water level was thus imposed. The amplitude of the water level motion was chosen such that similar velocity amplitudes were found in the centre of the domain. To study migrating waves a constant residual current of 0.05 m/s was added to the symmetrical S2 tide in one of the simulations. The $k-\epsilon$ turbulence model is used as recommended by Borsje et al. (2013).
During the first tidal cycle the bed level change is set to zero, creating a spin-up period for hydrodynamics.

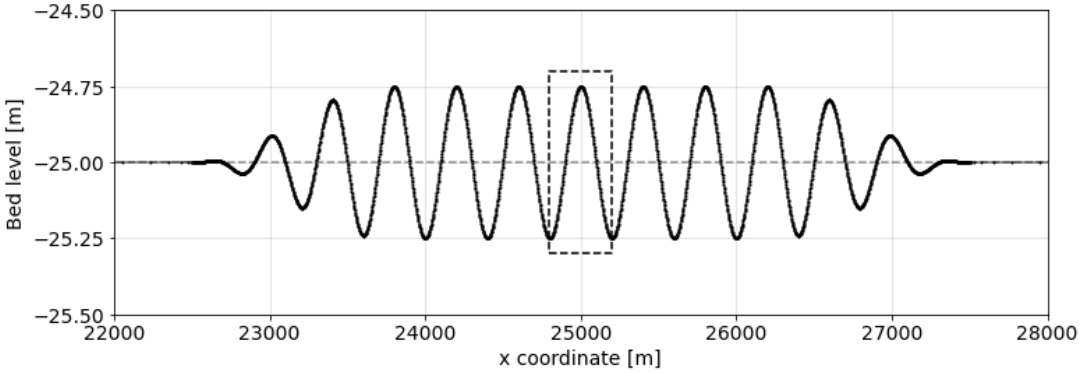

Figure 4.2: Initial bed level with L = 400 m(k = 0.016) and A = 0.25 m, box indicates location of Figure 4.5

Afterwards bed load transport (and slope-induced transport) is able to cause bed level changes. In all models the suspended load transport is set to zero, as this is not fully implemented in Delft3D FM at the time of this research. The bed load transport is calculated using Van Rijn 1993 (see Section 3.5). To speed up the simulation a morphological scale factor is used. Other model parameters are shown in Table 4.1. Three cases are studied: A) symmetrical boundary conditions, B) asymmetrical boundary conditions (addition of residual current) and C) modelling a symmetrical case to equilibrium. The Case A and Case B models were also used for a 1 year morphological prediction, with a morphological scale factor of 52, but otherwise identical settings. These results are included in Appendix A.1. A validation of the different values for the morphological scale factor used in these models is included in Appendix A.2.

Table 4.1: Parameters and settings used in both Delft3D-4 and Delft3D FM models

Description	Symbol	Value			Dimension
Tidal period	-	12			h
Tidal velocity amplitude[1]	-	0.65			ms^{-1}
Mean water depth	H_0	25			m
Initial sand wave amplitude	A_0	0.25			m
Sand wave length	L	400			m
Sediment grain size	D_{50}	0.35			mm
Bed slope correction parameter	α_{bs}	3			-
Grid spacing (fine part)	dx	2			m
Number of σ layers	-	60			-
Chezy roughness	C	75			$m^{1/2}s^{-1}$
Cases		**A**	**B**	**C**	
Morphological duration	-	10	10	300	$year$
Morphological scale factor	MF	520	520	2000	-
Residual velocity[1]	$U0$	0	0.05	0	ms^{-1}

[1]Velocity implemented in Delft3D-4, Delft3D FM water levels changed to match velocity in centre of the domain

4.2 Results

In this section the results of the above described simulations are shown. First the results in terms of hydrodynamics, bed load transport and morphology for a specific wave length are shown. Subsequently the growth and migration for various wave lengths and environmental conditions are reviewed. In the final section long term results of the model are presented.

4.2.1 Hydrodynamics and morphology

In this section the hydrodynamics and morphological change from the Delft3D-4 and Delft3D FM models are compared for Case A and Case B: with and without residual current. The hydrodynamics were obtained through a simulation with a duration of 36 hours (including 12 hours spin up), without morphological change.

Case A: Symmetrical Tide

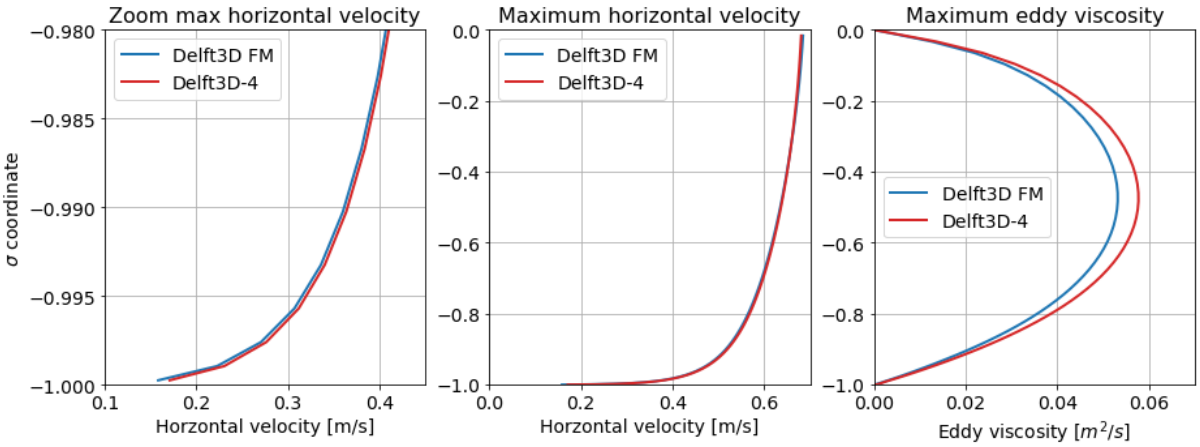

Figure 4.3: Maximum horizontal velocity and eddy viscosity during flood at center sand wave crest, (x = 25000), Case A: symmetrical S2 tide (L = 400 m)

To match the flood and ebb velocities at the centre of the domain appropriate boundary conditions were prescribed taking into account the deviating boundary types. The resulting flow velocities are shown in Figure 4.3. In the Delft3D-4 model the flow velocities are slightly more evenly spread over the height of the water column due to the higher eddy viscosity in this model. This difference in eddy viscosity could be caused by a small mismatch in the boundary conditions. Other possible causes are found in multiple slight computational differences between the models. In the cell closest to the bed, which is used to determine a depth averaged velocity for bed load transport computations, the horizontal flow velocity at the sand wave crest is about 8% higher in the Delft3D-4 model than in the Delft3D FM model as can be seen in the zoom in Figure 4.3. This relative difference quickly decreases further from the bed. Due to the interaction of the reversing tidal current with the sand wave bathymetry, residual circulation cells are formed (see Chapter 2). These residual currents are clearly visible in Figure 4.5, where the tide-averaged velocity magnitude and direction is shown over the area indicated in Figure 4.2 in the middle of the sand wave domain. At the crest of the sand wave (x = 25000 m) the residual flow is directed towards the surface and at both troughs in the Figure (x = 24800 m and x = 25200 m) the flow is directed towards the bed. Close to the bed the highest tide-averaged velocities are found, which are in the order of mm/s and

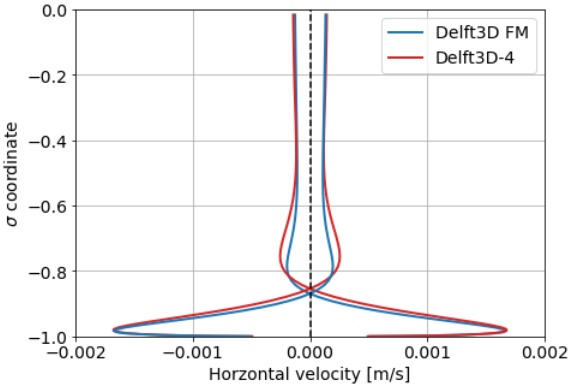

Figure 4.4: Tide-averaged velocity at the middle of the sand wave flanks (x = 24900 m and x = 25100 m), Case A (L = 400 m)

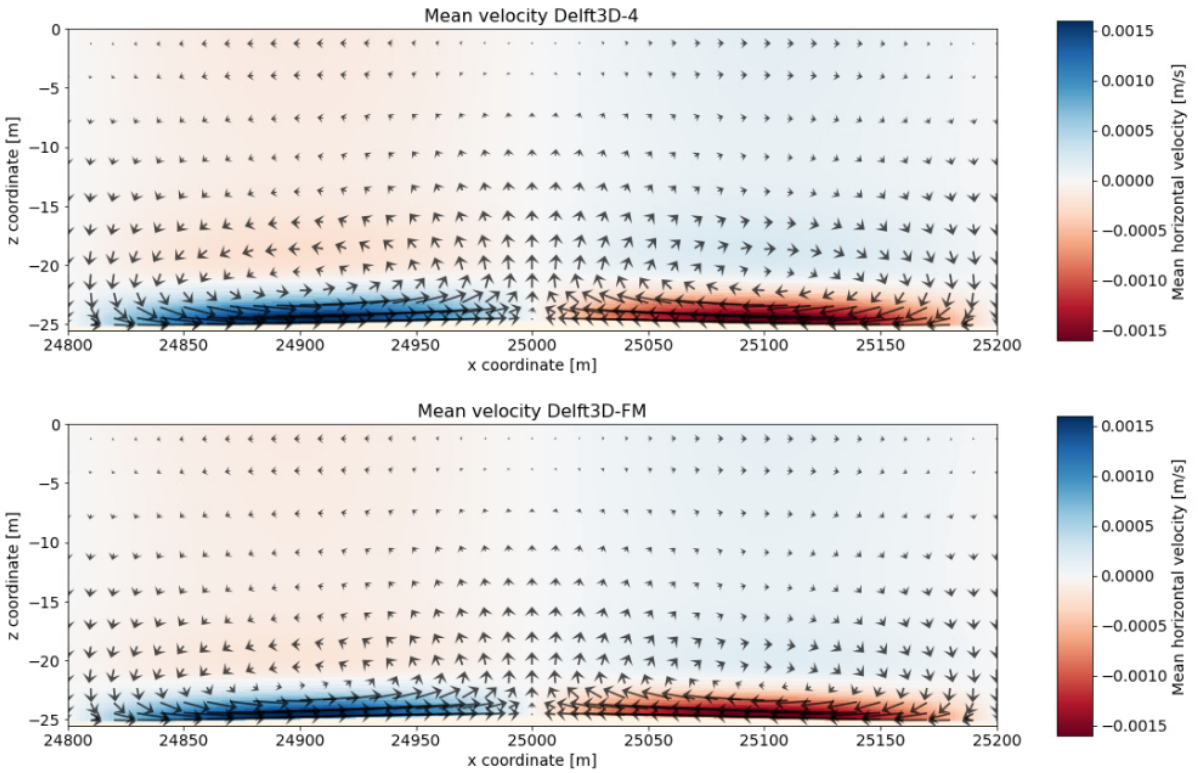

Figure 4.5: Tide-averaged velocity, Case A: symmetrical S2 tide (L = 400 m). For location see Figure 4.2. Vertical velocities not to scale

directed towards the crest of the sand wave on both flanks. These residual flows cause the sand wave to grow in height. In this case the boundary conditions are symmetric (S2 tide), which leads to symmetric residual circulation cells. The point of (horizontal) mean flow reversal is slightly lower in the water column for the Delft3D FM model. In this model the maximum tide-averaged return current at a few meters above the bed is also smaller. These slight differences are clearly visible in Figure 4.4 which shows the tide-averaged velocities at the center of both flanks. Near the bed both models are in good agreement, with a mean tide-averaged velocity offset of 1.5% in the lower 10 layers. The Delft3D FM model has a slightly higher mean flow velocity in the cell closest to the bed. At center of the flank this difference is around 3%. The mean velocities in both direction should balance over the vertical, which is visible in both models. Since the hydrodynamics, which form the basis of sand wave growth and migration, are in good agreement this increases the confidence in Delft3D FM for the purpose of sand wave modelling.
These residual flow patterns result in sediment transport towards the crest of the sand wave, which is shown

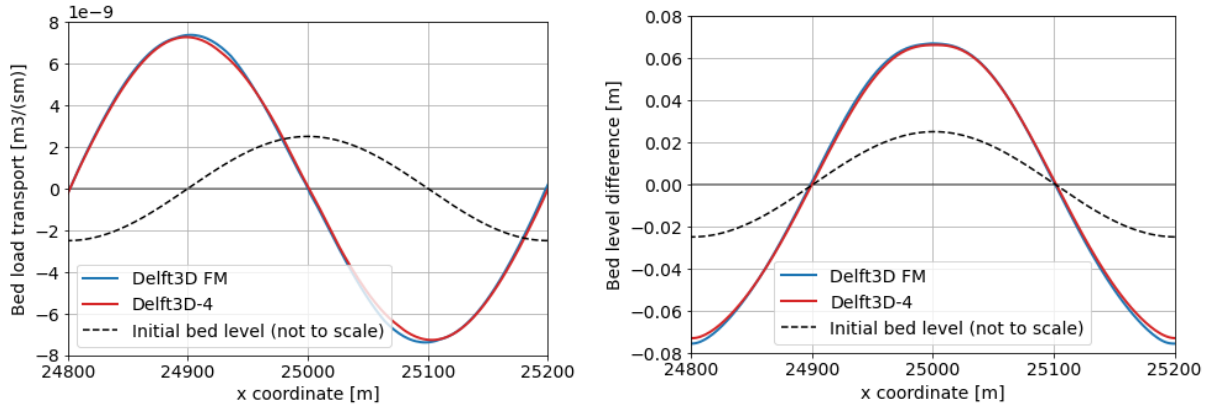

(a) Tide-averaged bed load transport, first tidal cycle

(b) Bed level change in 10 morphological years

Figure 4.6: Average bed load transport and resulting bed level change, including scaled initial bathymetry, for Case A: symmetrical S2 tide (L = 400 m)

in Figure 4.6a. The tidal flow causes bed load transport in both directions and the difference in transport rate between the flood and ebb flow leads to an average transport towards the crest of the sand wave on both sides. Although the observed difference in flow velocities close to the bed causes an inequality of instantaneous sediment transport rates between the models, this difference cancels out due to the returning current in this case. The observed bed load and erosion-sedimentation patterns are thus very similar. This bed level change is shown in Figure 4.6b for a period of 10 years. The Delft3D FM model shows slightly more lowering of the trough of the sand waves, but otherwise the results are nearly identical.

Case B: Residual Current

When a residual current is added, the previously symmetrical patterns are disturbed. The flow velocity and eddy viscosity are higher for one tidal direction than the other. The mean flow velocities no longer balance over the vertical, but are directed towards the residual current direction. More sediment is transported in one direction than the other and the sand waves start to migrate. The flank of the sand wave facing the residual current direction starts to erode and sand is deposited on the lee-side flank. The mean velocity on the left flank of the sand wave is shown in Figure 4.7a. Again the Delft3D-4 model shows slightly higher mean velocities. On the right flank the mean velocities near the bed are slightly lower than on the left flank. The difference between the models is however similar on both flanks.
Looking at the bed development as shown in Figure 4.7b, the sand wave is clearly migrating over time, as expected. There is erosion on the exposed (left) flank and sedimentation of the shadowed (right) flank. The Delft3D-4 model shows an almost negligible increase in migration rate, but otherwise results are identical. Both models also show growth of the sand wave over time. The absolute sedimentation and erosion volumes are larger than for the symmetrical boundary conditions due to an increase in (mean) flow velocities.

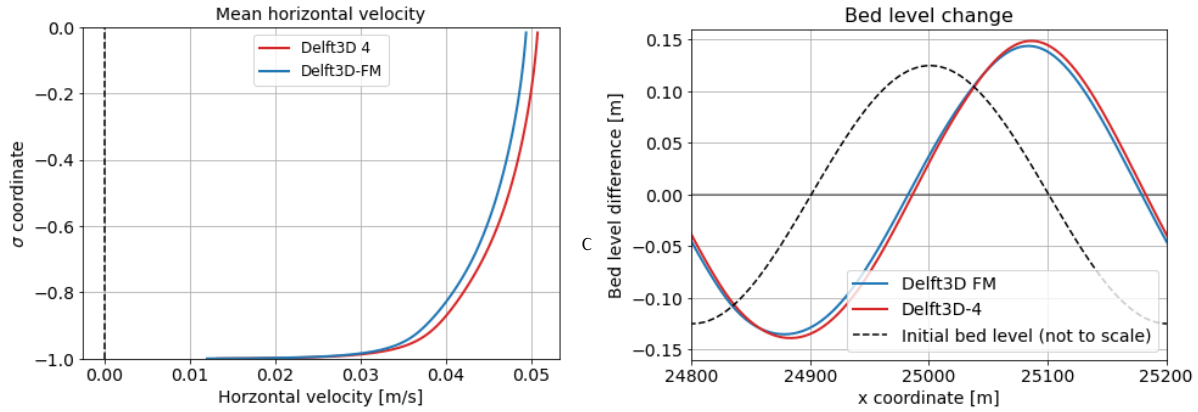

(a) Tide-averaged velocity at the middle of the left flank

(b) Bed level change after 10 morphological years including scaled initial bathymetry

Figure 4.7: Tide-averaged velocity and resulting bed level change for Case B: S2 tide with residual current of 0.05 m/s (L = 400 m)

4.2.2 Growth and migration rates

As mentioned these residual current patterns cause the sand wave to grow in height. This growth can be characterised by the growth rate. By comparing the growth rates for different situations, information about the occurrence and expected characteristics of sand waves can be obtained. By simulating initial bathymetries with different sand wave lengths, the wave length with largest growth rate or Fastest Growing Mode (FGM) can be found. This wave length can be used as an approximation for the wave length found in-situ for these environmental conditions, since it will overtake sand waves of other lengths (Matthieu et al., 2013). In this way modelling results can be compared to sand wave data to check whether the same sand wave lengths are found in nature. Furthermore, when the growth rate for all wave lengths is negative under certain environmental conditions, the seabed is stable.
For small amplitude waves (far from their equilibrium) the growth is assumed to be exponential (Besio et al., 2008) and the growth rate (γ_R) can be calculated as follows:

$$\gamma_R = \frac{1}{T} \mathrm{Re}\left\{ \ln\left(\frac{A_1}{A_0} \right) \right\} \tag{4.1}$$

Where A_1 is the complex amplitude of the sand wave at the end of the simulation and A_0 is the initial complex amplitude. These amplitudes are determined through a Fast Fourier Transform in the middle of the domain. T represents the duration between the initial and final amplitude. In the cases below a simulation of one tidal cycle is used (excluding one tidal cycle spin-up). A positive value for γ_R represents growth of the sand wave, where negative values represent decay (and thus returning to a flat bed). Whether a sand wave grows or decays is dependent on the interaction of the different phenomena described in Section 2.1. With the phase of the sand wave found using the Fast Fourier Transform the migration of the sand wave can be determined.

Case A: Symmetrical Tide

From the previous section it is clear that both models are able to grow sand waves. The growth rate for a sand wave with a length of 400 m is thus positive. For more insight into the growth of sand waves, the simulation is repeated for sand waves with nine different wave lengths, between 100 and 1000 m. The growth rates with respect to the wave number ($k = 2\pi/L$) are shown in Figure 4.8 (left, solid line), where a wave length of 100 and 1000 m are converted to wavenumbers of 0.063 and 0.0063 respectively. Both models are able to grow sand waves and for the longer sand waves the results are much alike. For shorter wave lengths (higher wave number) the Delft3D-4 model shows smaller growth rates and in some cases decay where the Delft3D FM model has positive growth rates. This divergence is caused by differences in implementation of the bed slope related transport. This can be demonstrated by neglecting bed slope transport in both models (by defining α_{bs} as 0). For a wavelength of 160 m (k = 0.39) the Delft3D-4 model shows a higher growth rate in that case and the difference in growth rate between the models is reduced to 9% (from 51%). This remaining difference could be attributed to the minor discrepancies in boundary conditions and model computations. Due to the increased importance of bed slope transport in the smaller wavelength regime (larger wave number) the difference in growth rate between the models is amplified there. The bed slope parameter is however often used as a calibration parameter, which makes it easy to tune the Delft3D FM model to match the results from the Delft3D-4 model. In the Delft3D FM model a wave length for the FGM of around 193 m is found, where the Delft3D-4 model has a FGM wave length of approximately 231 m. In the very long wave length regime (small wavenumber) the growth rates are extrapolated and show negative values. Although the sand waves are expected to decay in this range, in this case this negative part of the curve is not a result of simulated sand waves, but due to extrapolation. Since the boundary conditions are symmetrical the sand waves do not migrate.

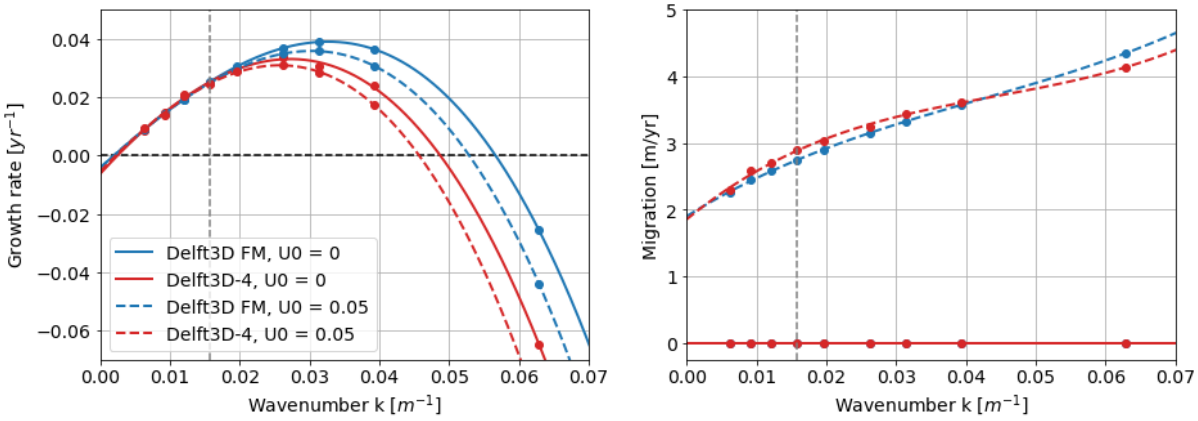

Figure 4.8: Growth rate (left) and migration rate (right) for Case A: symmetrical tide (solid line) and Case B: including a residual current of 0.05 m/s (dashed line) for a varying sand wave length. Dots indicate individual model results. Dashed vertical line indicates wave length used in detailed analysis above (L = 400 m, k = 0.016)

Case B: Residual Current

To study the effects of a residual current the models are again used for simulations with different wavelengths (varying from 100 to 1000 m) for two tidal cycles (one spin-up, one including bed level changes). Due to the inclusion of a residual current of 0.05 m/s the sand waves also migrate. The growth and migration rates are shown in Figure 4.8. As expected, the growth rates are slightly lower than in Case A. This decrease in growth rate for migrating waves was observed in previous model studies such as (Borsje et al., 2013). They also found that the FGM wave length did not change significantly due to the addition of a residual current of 0.05 m/s. This behaviour is observed in the results of both models. The migration rates for both models follow the same relation with the wave length. Shorter sand waves tend to migrate faster, which can be explained by the higher transport rates due to the steeper slopes of the sand waves. This relation was also found by (Besio et al., 2003). The results of a model study with similar set-up are shown in Figure 4.10. In this research (Damveld et al., 2020) varied the standard deviation of the sediment included in the model to study the effects of sediment sorting on sand waves. There are some differences with the set-up of this research, such as a bigger initial amplitude of the sand wave, which lead to higher growth and migration rate. In a qualitative sense the results are in agreement and the relations found between environmental factors and parameters such as the FGM wavelength and growth rate are similar.

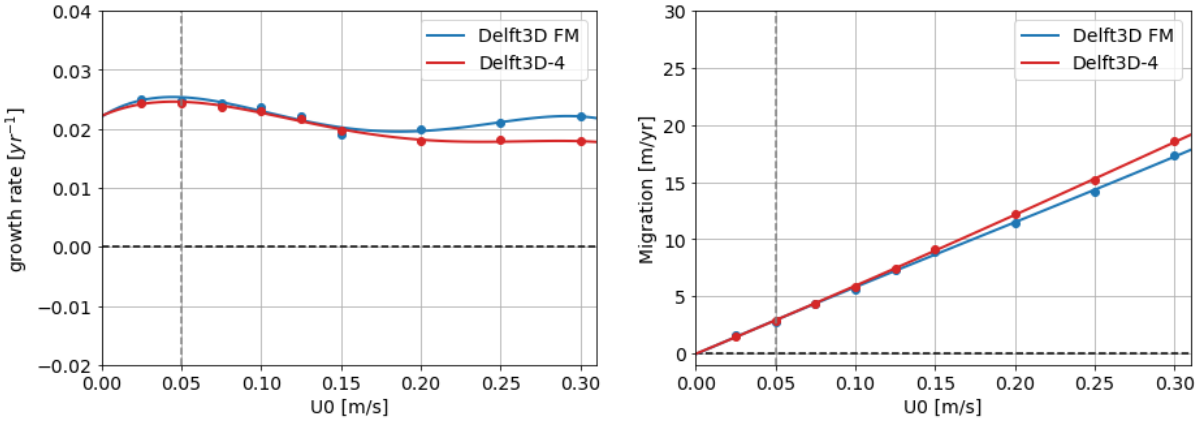

Figure 4.9: Growth and migration rate for Case B for varying residual currents (L = 400 m, k = 0.016). Dots indicate individual model results. Dashed vertical line indicates residual current used in detailed analysis above (U = 0.05 m/s)

When the magnitude of the residual current is varied the growth and migration rate change in a manner shown in Figure 4.9. Both models show similar relations. A larger residual flow velocity (at first) slightly decreases the growth rate. In reality there is a current velocity for which sand waves are unable to occur. This is caused by the dampening effect of suspended sediment load and the increasing importance of this sediment transport mode for higher flow velocities (Borsje et al., 2014). However, these models do not include suspended sediment and the slightly lower growth rates, for a stronger residual current, are the effect of an increased slope induced sediment transport. Negative growth rates, indicating decay of the sand waves, are not observed in either of the models. It could be that the growth rates will become negative for larger currents, but due to the exclusion of suspended sediment transport they may not become negative. The migration rates increase with the residual current strength in both models. The relation is slightly different, with a bigger influence of the current on the migration rates in the Delft3D-4 model, but both show an approximately linear relation. This relation between residual current strength and migration rate was also found by among others (Wang et al., 2019).

4.2.3 Modelling to equilibrium

To study the differences between the two models on the long term and to asses the behaviour of sand waves in (semi) equilibrium in both models, the same model set-up as used in Case A is simulated for a period of 300 years. As a result of the exclusion of suspended sediment transport a dampening mechanism found in nature is missing in the model. Due to this difference the sand waves are not expected to reach an absolute equilibrium wave height within the 300 year period included in the model, but rather that the growth rate decreases for bigger wave heights and the sand waves keep growing. This effect was seen in a study by Van

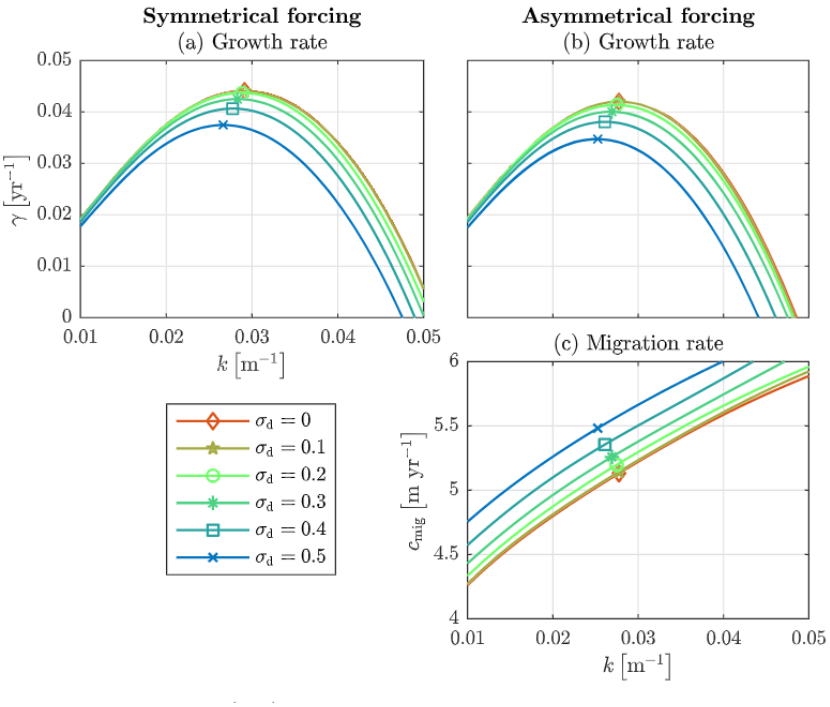

Figure 4.10: Growth and migration rate as seen in (Damveld et al., 2020) for a varying sediment diameter standard deviation

Gerwen et al. (2018) whose results are shown in Figure 4.11. The inclusion of suspended sediment clearly affected the equilibrium wave height for a case with and without residual current.
In Figure 4.12 the development of the sand wave height, for a wave length of 400 m, over the morphological time is shown. The initial growth rates of Delft3D-4 and Delft3D FM are nearly identical as was observed in the models above with shorter time-scales. The exponential growth of the sand waves for smaller wave heights, as assumed when calculating the growth rates of the sand waves, is clearly visible in the early stages of the model (up to ~130 years). Both models show a decrease in growth rate after some time. This turning point is reached at an earlier point in time in the Delft3D FM model leading to a reduced wave height at the end of the simulation compared to Delft3D-4. The final growth rates are however very similar. The wave heights at the end of the simulation (after 300 years) show a difference of approximately 3 m. In both models the sand waves

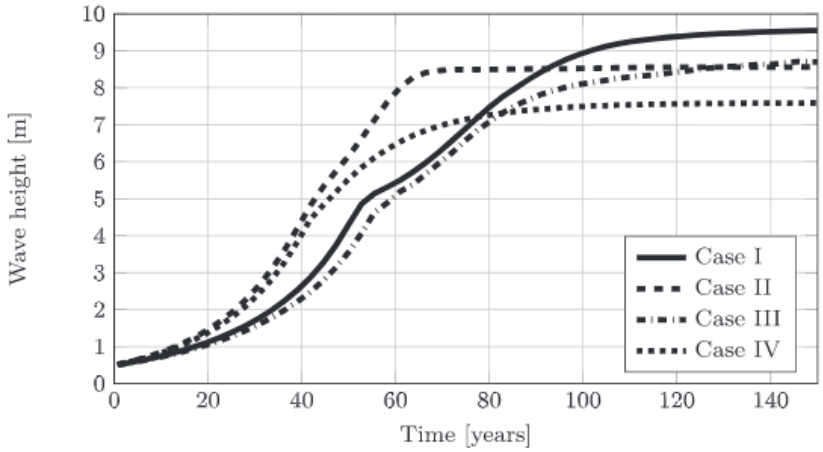

Figure 4.11: Sand wave height development towards equilibrium for symmetrical tidal conditions from Van Gerwen et al. (2018). Case I: no residual current, no suspended sediment transport, Case II: no residual current, suspended sediment included, Case III: U0 = 0.05 m/s, no suspended sediment, Case IV inclusion of 0.05 m/s residual current and suspended sediment. Sand wave lengths in the range of 204-230 m (Van Gerwen et al., 2018)

are still growing at the end of the simulation. The Delft3D-4 model shows some oscillations in wave height after around 150 years. These oscillations and the difference in wave height between the models at the end of the simulation are expected to be due to a changes in shape in the Delft3D-4 model. The 'new' trough of the sand wave, which lies closer to the crest, shows more erosion in the Delft3D-4 model relative to the Delft3D FM model. Such a small dip, as seen in the final bed level of Delft3D-4 in Figure 4.12, is not observed in real sand waves. Furthermore the sides of the final sand wave shapes coincide up to a certain point where the Delft3D-4 model has grown a kind of bump. The final sand wave shape of the Delft3D FM model is more alike the sand waves we know from nature, but since these kind of perfectly symmetrical boundary conditions do not exist in reality this comparison is debatable. The absolute difference with the results of Van Gerwen et al. (2018) is caused by a difference in sand wave length. The set-up used in this study included longer waves, which have a lower initial growth rate. The shorter wave length used by Van Gerwen et al. (2018) lies closer to the FGM as observed in Figure 4.8. This difference also resulted in a higher wave height at the transition to lower growth rates in this study, which can be explained by a smaller effect of the bed slope induced transport due to longer wave lengths.
The shape of the wave changes drastically throughout the simulation. The shape of the sand wave after 300 years of morphological change can be seen in Figure 4.12. The simulation is initiated with sinusoidal sand waves of 0.5 m in height. At the end of the simulation the lowest point of the sand wave has moved closer to the crest for both models. The crest has become slimmer in both models. Furthermore, both models showed faster growth of the crest with respect to the trough. This final shape, which is different from what is found in nature, is probably caused due to the perfect symmetry of the boundary conditions, which is unlike natural conditions.

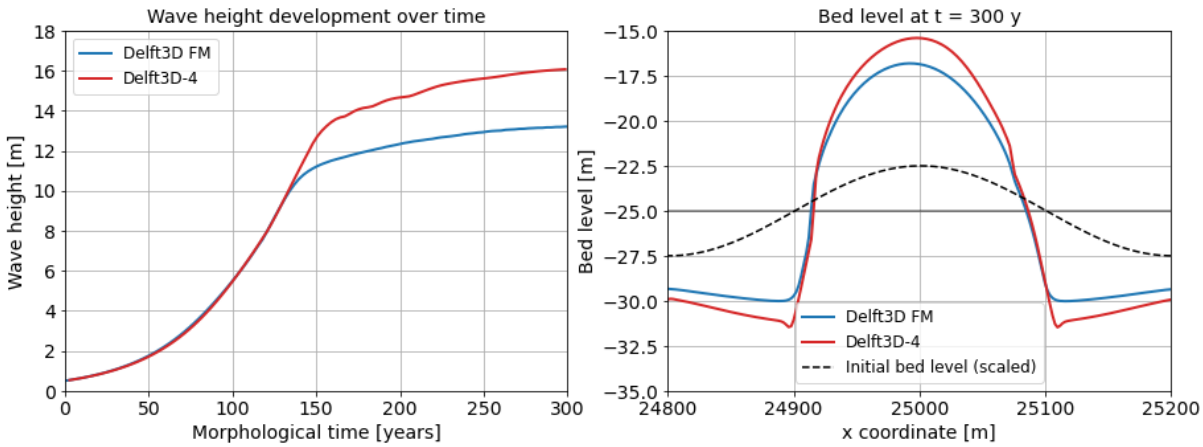

Figure 4.12: Wave height development over time (left) and final shape of the sand waves (right), Case C: symmetrical S2 forcing (L = 400 m, A_0 = 0.25 m)

4.2.4 Computation time

From the simulations above one striking difference between Delft3D-4 and Delft3D FM became apparent. The Delft3D FM model has realized vast computation time reductions relative to Delft3D-4. The computation time for the Case A model with 10 years of morphological change (7.5 days of hydrodynamics) decreased from 17.6 hours in Delft3D-4 to 8.7 hours in Delft3D FM. This reduction of over half the total time was realized while using an on average smaller time step. In the Delft3D FM model the time step is set automatically and is altered to comply with the Courant criterium for changing flow conditions. This means that at times of low flow

Table 4.2: Computation times for the 10 year morphological change model (7.5 days of hydrodynamics) for the Delft3D-4 and Delft3D FM model

Model	Time step [s]	Computation time [h]
Delft3D FM	2.1 (on average)	8.7
Delft3D-4	4.8	17.6
Delft3D-4	2	33.4

velocities the time step will be increased. The time-varying time step of the Delft3D FM model over one tidal cycle is shown in Figure 4.13. In this figure a drastic increase of the time step can be seen during slack, when the flow velocities are low. In Delft3D-4 a time step of 4.8 seconds is used (the largest value for which no Courant warnings were observed in the diagnostics file), while the average time step in the Delft3D FM model was approximately 2.1 seconds. After consultation with the software team developing Delft3D FM, the reason for these computation time reductions was identified as increased code efficiency. The computation times for Delft3D-4 with different values for the time step relative to Delft3D FM are shown in Table 4.2.

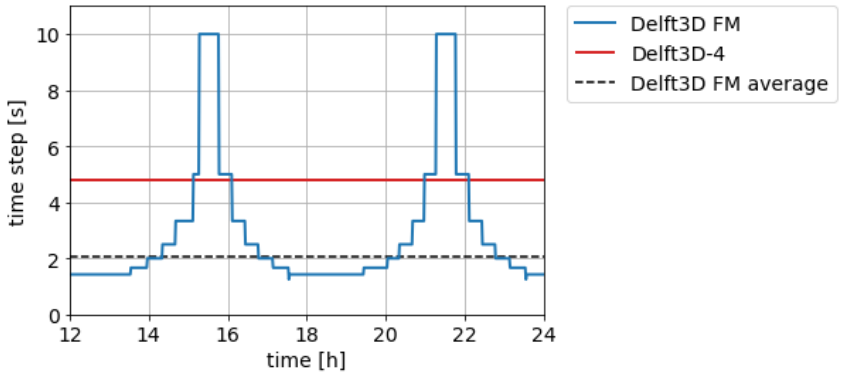

Figure 4.13: Time step size of Delft3D FM and Delft3D-4 over one tidal cycle, Case A model

Chapter recap and conclusions

In this chapter the results in terms of hydrodynamics, sediment transport and morphology of the Delft3D-4 and Delft3D FM models are compared. For this study a simplified model with sinusoidal sand waves, flat underlying bed, simple tidal forcing and a single grain size is used. In both models the vertical tide-averaged flow circulation cells which lead to sand wave growth are observed and are almost identical in shape and amplitude. For a sand wave length of 400 m the tide-averaged sediment transport and subsequent bed level changes are nearly identical between the models.

The growth rates found in both models are indistinguishable for sand wave lengths larger than 300 m. For shorter wave lengths the Delft3D-4 model shows smaller growth rates. These inequalities can be explained by the implementation of the bed slope induced transport, which differs between the models. Therefore, the bed slope parameter could easily be used to tune the Delft3D FM results to match Delft3D-4. The migration rates are much alike and show the same relations with both sand wave length and strength of the residual current in Delft3D-4 and Delft3D FM. When the sand waves are simulated towards an equilibrium wave height the initial sand wave growth (up to 130 years) is nearly identical for both models. At the end of the simulation period there is an absolute difference in sand wave height. This might be caused by unnatural changes in sand wave shape (taking place after 150 years), due to the artificial perfectly symmetrical boundary conditions. At the end of the simulation the sand waves are still growing in both models (although with a much smaller pace of up to 0.5 cm/year), which could be the result of the exclusion of suspended sediment transport.

During this comparison study a major advantage of Delft3D FM is observed: vast computation time reductions. While using a significantly smaller average time step a computation time reduction of over 50% is realized in Delft3D FM relative to Delft3D-4. These computational gains are caused by increased code efficiency in Delft3D FM.

Due to the extensive similarities in the results of both models the confidence in the Delft3D FM model for the simulation of sand waves has increased. Especially in the hydrodynamics, which are the driving forces behind sand wave growth and migration, the models are in good agreement. Furthermore, the migration rate, which is the largest source of uncertainty in bed level predictions, is comparable in both models for all tested cases. Given the good agreement between the models, we only focus on Delft3D FM in the remainder of this study.

5 | 2DV case study with Delft3D FM

For the development of offshore structures, long-term morphological predictions are required. In the previous chapter it is shown that Delft3D FM is able to simulate the growth and migration of sand waves and that the hydrodynamic and morphological results are similar to those of Delft3D-4. In this chapter the Delft3D FM model is used to predict sand wave dynamics in a real-life case study. These results will give a first indication of the suitability of Delft3D FM for these kind of predictions. First the location and set-up of the model are discussed. Since this set-up is similar to the that of the model used in the previous chapter only the differences are explained. Subsequently the results of the model and sensitivity analysis are shown.

5.1 Hollandse Kust (Zuid) Wind Farm

The case study is carried out in the Hollandse Kust (Zuid) Wind Farm (HKZWF) area (see Figure 5.1). A small section in the North of the wind farm area has been part of a previous wind farm project and is already in use. In the remainder of the area the construction will start this year (2021). As part of the early stages of offshore wind farm development extensive bathymetry measurements have been carried out at this site in 2016. These measurements, together with earlier measurements by the Dutch Navy, have been used in a morphological study of the area focused on the suitability for an offshore wind farm carried out by Deltares (Deltares, 2016a).

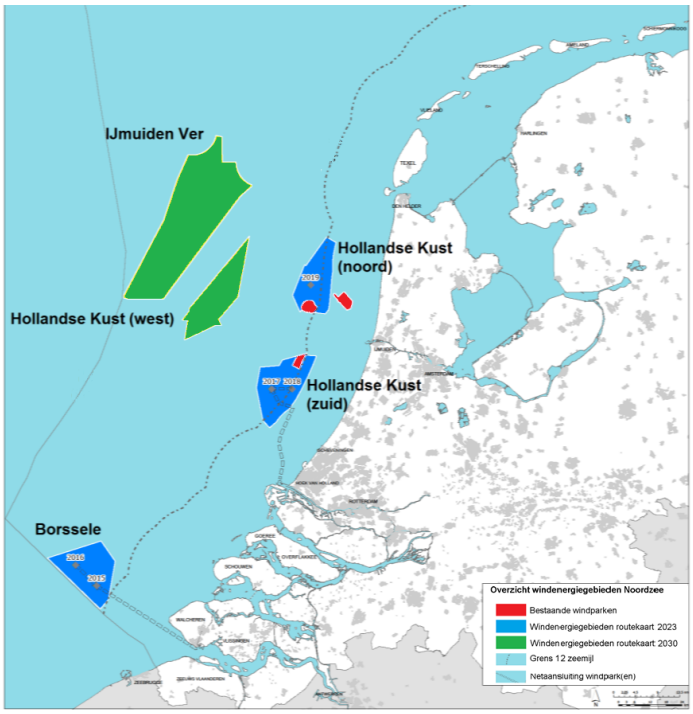

Figure 5.1: Planned and existing Dutch wind farms (Rijksoverheid, 2018)

The availability of data is in general similar for all planned wind farms and the HKZWF location is chosen for this case study because of it's relatively uniform geophysical conditions as is apparent from the regularity of the sand waves. The area is fully covered with sand waves. From data analysis it is clear that the sand waves show only minor changes in dimensions over the years. Most sand waves are thus near their equilibrium wave height. Furthermore, the sand wave characteristics (height, length, migration direction and speed) are fairly regular over the area, indicating fairly constant hydrodynamic conditions. This is preferred, since sudden changes in hydrodynamics could make 2DV simulations troublesome. In addition, the area is preferred because little human interference has taken place over the last years. Only in the far North of the area have dredging activities taken place recently, but since the sand waves are moving towards this direction, this is not expected to influence the sand wave dynamics significantly. The sand wave bathymetry extracted from the 2016 measurements is shown in Figure 5.2. More information about the (morpho- and hydrodynamics at the) Hollandse Kust Zuid Wind farm location can be found in (Deltares, 2016a).

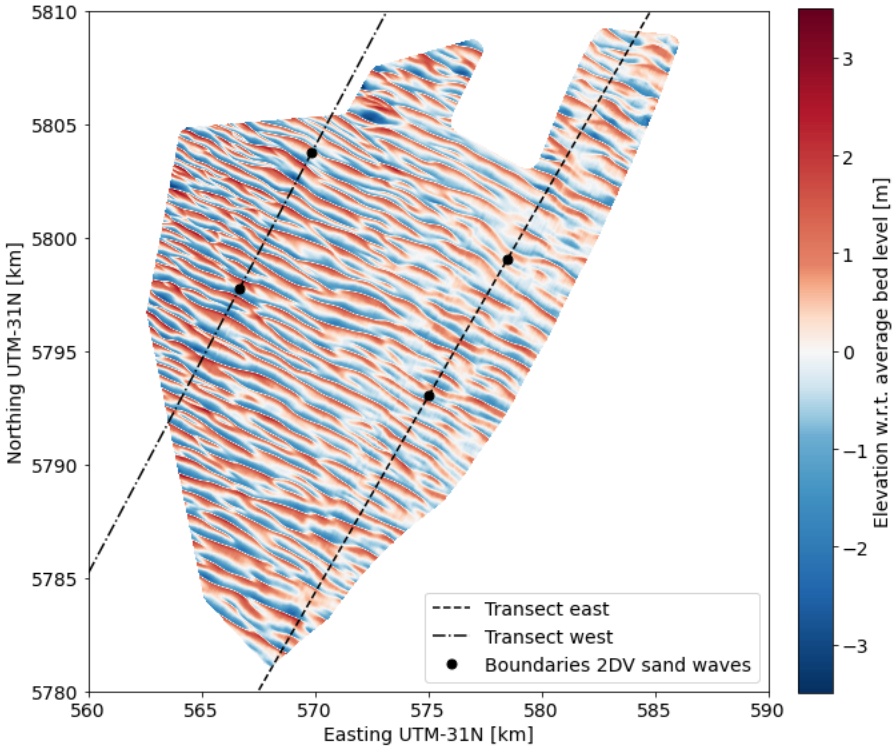

Figure 5.2: Bed level of sand wave bathymetry (w.r.t. large-scale bathymetry) extracted from the 2016 measurement survey and transects of the 'East' and 'West' 2DV models

5.2 Model set-up

Most model settings are kept the same as in the previous modelling study for the Delft3D-4 and Delft3D FM comparison. The major differences are that measured sand wave bathymetries are used for the bed level of the models and the boundary conditions are prescribed to match local conditions. In this way a hindcast model is created, which is used to simulate the hydro- and morphodynamics between two subsequent bathymetry measurements in the area.
Two transect are drawn in Figure 5.2, along which models are set up, referred to as the East and West transect. The directions of the transects are chosen such that they are approximately aligned with the migration direction of the local sand waves. The sand waves are assumed to migrate in the direction perpendicular to it's steepest slope. This migration direction was extracted by (Deltares, 2016a). The migration direction over the HKZWF area is on average 28 °N. The direction is approximately normally distributed and has a standard deviation of around 4.5 °. The migration direction is slightly more towards the East in the area closer to shore (the East). With this in mind the directions of the transects were chosen as follows: Eastern transect 30 °N and Western transect 28 °N.

5.2.1 Grid

The grid used in this model is very similar to the grid in the previous modeling study. The model area is 46800 m long. In the middle of the domain sand waves are present over an area of 6800 m, with a buffer of 20 km of flat bed on both sides. The length of the sand wave area is chosen such that the sand wave bathymetry has a zero-crossing (sand wave bathymetry = large-scale bathymetry) at the edges of the sand wave domain. As in the previous model the cells sizes increase from the sand wave domain towards the boundaries. The minimum and maximum cell size are 2 m and 1000 m respectively. The vertical grid consists of 60 sigma layers with decreasing size towards the bed. This same vertical grid was used in the previous model study and the horizontal grid sizes change in a similar manner over the area as shown in Figure 4.1.

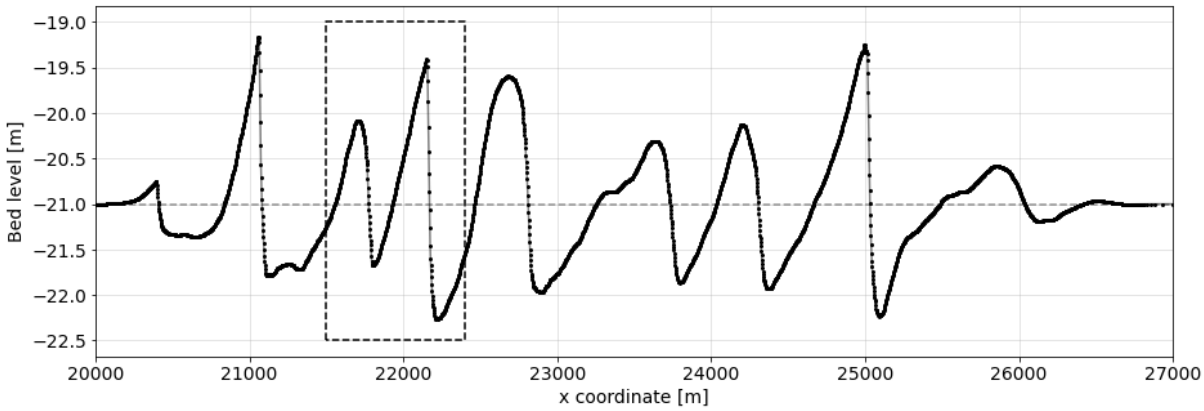

Figure 5.3: Initial bed level of sand wave domain of Eastern transect, box indicates location of Figure 5.4 and sensitivity analysis plots in Section 5.3.3

5.2.2 Bed level

For the bed level of the model a compound 2010 multi beam bathymetry dataset is used. The measurement data is first seperated into a static and a mobile bathymetry. Subsequently the mobile part is split into a sand wave and a megaripple bathymetry. Information about the dataset and the filtering process can be found in (Deltares, 2016a). From the filtered sand wave bathymetry the bed level of the sand wave area of the domain is constructed, which is superimposed on an approximation of the overall average bed level determined from the large-scale (static) bathymetry of the 2016 measurements. The sand wave bathymetry is interpolated along both transects. Since disturbances are observed in the interpolated bathymetry a filter is used to smoothen the bed level. These disturbances are expected to be present due to both measuring inaccuracies and the incomplete filtering of megaripples. The effects of filtering and the initial disturbances can be found in Appendix B. The interpolated sand wave bathymetry is dampened along the edges of the sand wave domain. Over a distance of 1.5 km the sand wave height builds up towards the measured bathymetry. The sand wave bathymetry as used in the model of the Eastern transect is shown in Figure 5.3. Outside of the sand wave area a flat bed is imposed at 21 m depth. The sand waves in the east transect are of varying shape. Some have a saw tooth shape, with a very steep slope in the direction of migration. Other sand waves are less asymmetric and have a more rounded crest. At the western transect most sand waves have a highly asymmetric shape.

5.2.3 Boundary conditions

The lateral boundaries of the 2DV model are closed. The boundary conditions at both open boundaries (South and North) are extracted from the large scale Dutch Continental Shelf Model (DCSM). In this model the tidal propagation is modelled in 2DH for the North Sea and the surrounding area. From the model output tidal water levels and velocities are extracted at the locations of the boundaries of the transect models, where the cell size of the DCSM model is 0.5 NM (0.9 km). More information about the DCSM model can be found in Zijl et al. (2018).
The DCSM model is run for a period of 1 year starting at the end of 2012. From the simulated flow velocities and water levels at the boundaries of the transect models both time series and harmonic conditions are constructed. The flow velocities parallel to the transects are used and perpendicular flow velocities are filtered out. The models are forced with one flow velocity and one Riemann water level boundary. The flow velocity at the boundary is scaled to compensate for differences in water depth, due to differences in model bathymetry between the DCSM and the 2DV model, such that the discharge is preserved. The tidal constituents used in the model are chosen to be M2, S2 and M4. The M2 and S2 constituents account for the largest tidal amplitude both in terms of water level difference and flow velocity. The M4 tide is included since this tidal constituent is known to cause migration when combined with the M2 tide. Additionally a year averaged residual current is retrieved from the DCSM model. Several combinations of these tidal constituents are applied at the boundaries to study their effects. These combinations are shown in Table 5.2. The magnitude of the tidal constituents at the boundaries of the Eastern model are shown in Table 5.1. From these harmonics the water level and flow velocity can be constructed as shown in equation 5.1. For the final case a time series boundary condition of the full tidal signal is used. This time series is constructed from the first month of the DCSM model run after spin-up. This time

series represents the flow conditions at a specific moment in the tidal cycle, which are amplified through the use of a morphological scale factor. It might therefore not fully represent the average conditions over the 6 years between the measurements, due to slow tidal variations.

Table 5.1: Forcing of the East transect Delft3D FM model at the far North and South boundary

Boundary	Variable	Constituent	Period (T) [min]	Amplitude (A)	Phase (ϕ) [deg]
South	Parallel velocity	M2	745	0.723 m/s	111
		S2	720	0.193 m/s	128
		M4	372.5	0.053 m/s	148
		U0	-	0.005 m/s	-
North	Water level	M2	745	0.573 m	138
		S2	720	0.148 m	174
		M4	372.5	0.198 m	205

Table 5.2: Cases used in 2DV case study analysis

Case	Tidal forcing	Residual current
I	M2	no
II	M2, S2	no
III	M2, S2, M4	no
IV	M2, S2, M4	yes
V	Full tidal signal	-

$$H(t) = A0 + \sum_{i=1}^{k} A_i cos(\frac{2\pi}{T_i}t - \phi_i) \quad \text{and} \quad u(t) = B0 + \sum_{i=1}^{k} B_i cos(\frac{2\pi}{T_i}t - \phi_i) \tag{5.1}$$

5.2.4 Other parameters

In the 2DV model the morphological changes are simulated for a period of 6 years, which is approximately the time between the latest bathymetry surveys in the area: 2010 and 2016. The hydrodynamics are simulated for 31 days, including one tidal cycle (~12 hours) spin-up. This simulation period covers two full spring-neap tidal cycles. Using a morphological scale factor of 72, the morphological change in the simulation represents approximately 6 years. To study the local hydrodynamics a separate model excluding morphological change is used. Other parameters in the model are kept the same as in the original model used for the comparison with Delft3D-4. These are a Chezy roughness of 75 $m^{1/2}s^{-1}$, a bed slope parameter α_{bs} of 3 and a sediment size of 350 μm. This sediment size is a reasonable estimate for the local sediment size as observed in measurement surveys (Deltares, 2016a).

5.3 Results

Since both the East and West transect model showed similar behaviour, the results in this chapter are limited to the East transect and the results of the West transect can be found in Appendix C.

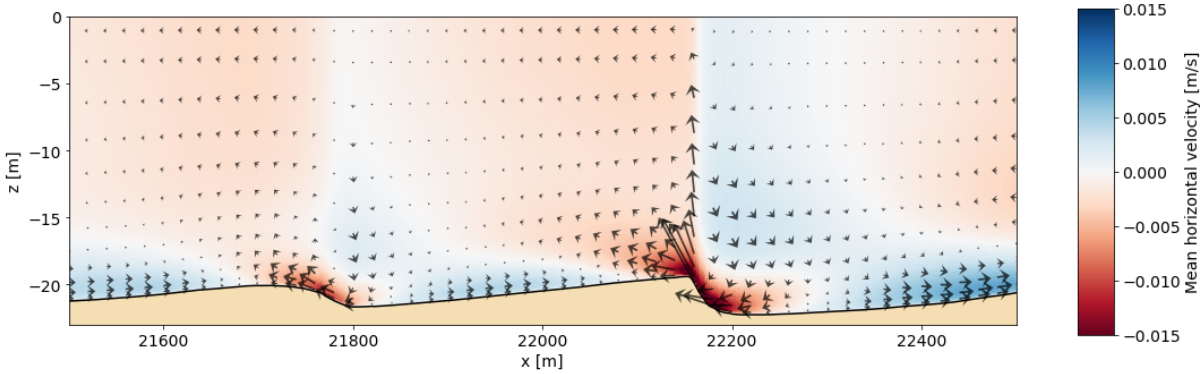

(a) Case I: M2 forcing

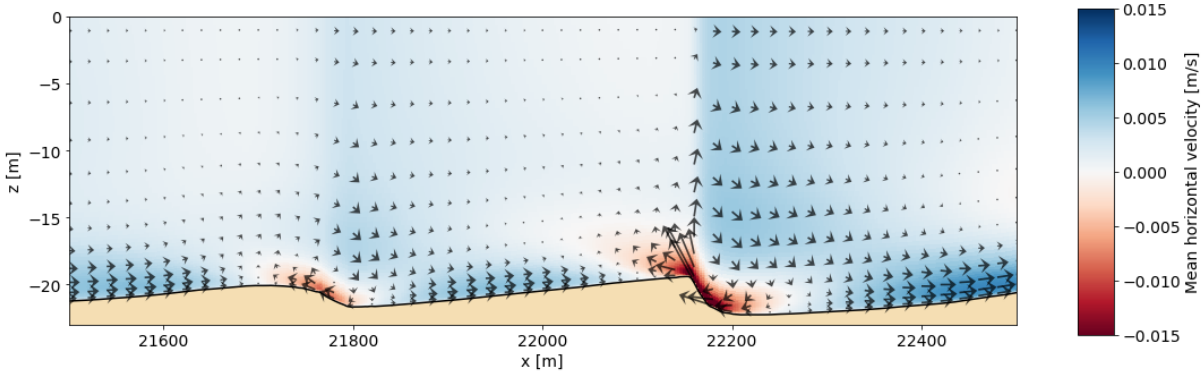

(b) Case II: M2, S2 forcing

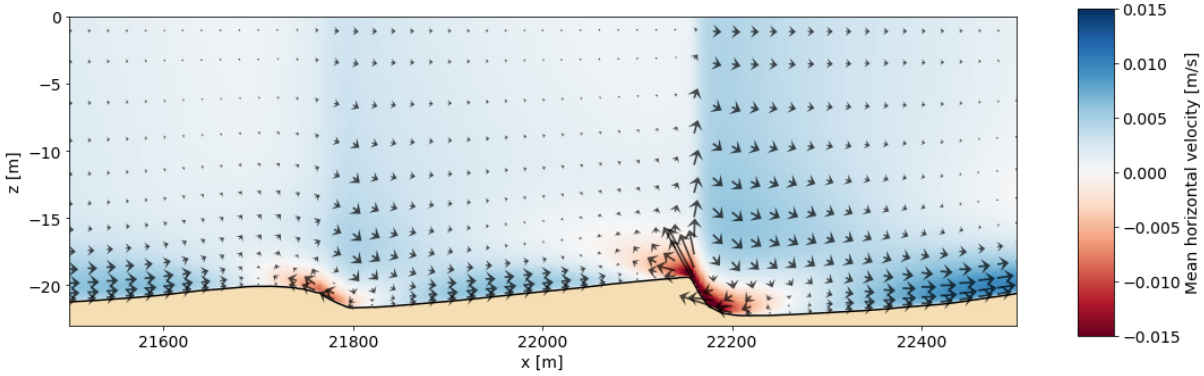

(c) Case III: M2, S2, M4 forcing

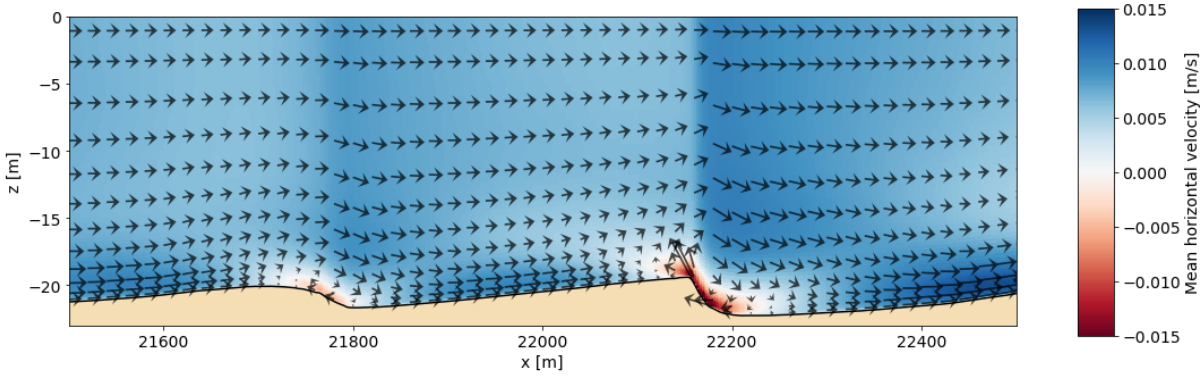

(d) Case IV: M2, S2, M4, U0 forcing

Figure 5.4: Mean velocity at location shown in Figure 5.3. Colors indicate mean horizontal velocity, arrows combine direction and magnitude of the mean horizontal and (scaled) vertical velocity

5.3.1 Hydrodynamics

The hydrodynamic results for the different cases are extracted from a model without morphological change, which is run for 29.5 days (two neap-spring tidal cycles). A comparison between the instantaneous flow velocities found within these models and the flow velocities from the original DCSM model including a wider range of tidal constituents is shown in Appendix E.1. In Figure 5.4 the mean velocities over the model duration for boundary condition with increasing accuracy are shown. The first simulation is forced with a symmetrical M2 tide. The results of this model are shown in Figure 5.4a. Even though the bathymetry is not as regular and symmetric as in the simplified model of Chapter 4, the flow circulation cells are clearly visible. Above the crest of the sand wave a transition from positive to negative mean horizontal flow velocity is present. At this point the vertical velocities are upwards directed and at the location of the trough the flow is directed towards the bed. Due to the tidal water level variations, the mean flow velocities do not cancel over the vertical. Most mean flow velocities are in the order of mm/s alike those found in the Delft3D-4 comparison. Close to the steep side of the sand wave the mean velocity however increases significantly due to the sudden changes in the bathymetry. When the S2 tide is added, leading to a spring neap tidal cycle, the mean velocities show more asymmetry as can be seen in Figure 5.4b. Above the crest there still is a transition in mean horizontal flow magnitude, but locations with a on average negative horizontal flow velocity are in this case mostly found near the bed. The addition of the M4 tidal constituent to this neap-spring cycle does not significantly influence the mean velocities (see Figure 5.4c). An addition of a residual current of 5 mm/s does however have a significant influence on this mean flow field. Figure 5.4d shows that due to this small residual current (only one tenth of the residual current used for the simulations in Chapter 4) the average flow velocities have more than doubled in large areas. This was of course to be expected taking into account the magnitude of the flow velocities in cases without residual flow, which was in most cases only a few mm/s. The negative average flow velocities are pushed back closer to the steep slope in migration direction, but this flow circulation is still present in this case. Furthermore a transition in magnitude of the horizontal flow is observed above the crest of the sand wave. The magnitude of the vertical flow and changes in horizontal flow velocity are clearly dependent on the steepness of the sand wave. Hydrodynamic results for the remainder of the domain can be found in Appendix C.1.

5.3.2 Morphology

Using a morphological scale factor the morphological change over a period of 6 years, which is approximately the time between the two subsequent measurement surveys, is simulated. The resulting bed level for the Case IV model for part of the East transect (as indicated in Figure 5.3) is shown in Figure 5.5. In the Delft3D FM model significantly more morphological change has taken place than between measurements. For both the rounder sand wave (left) and the more asymmetric sand wave (right) the slope in migration direction (to the right) has become slightly less steep in the Delft3D FM simulation, while the opposing slope has become steeper. This change in steepness is not observed in the measurement data. At some locations in the measured bathymetry the steep slope of the sand wave has even become steeper in the period between the measurements. During the simulation the sand wave has grown significantly in height. This growth is caused by both an increase in crest height and a lowering of the trough level. From the measurements only very limited change in sand wave height is observed. For the steeper sand waves in the area (around x = 22100 and x = 25000 in Figure 5.3) more artificial growth was observed form the model results than for the other, more gently sloped, sand waves. Furthermore, the steeper sand waves showed a

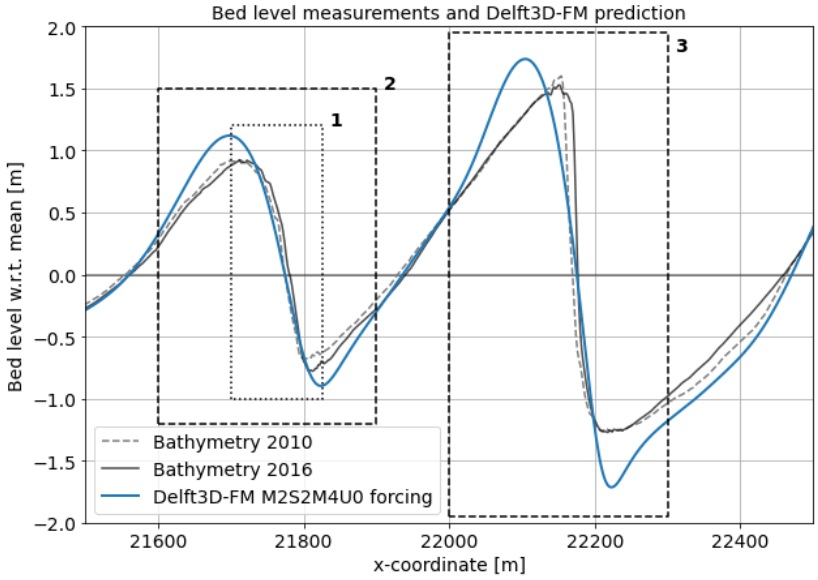

Figure 5.5: Measured levels and computed bed for Case IV after 6 years. Boxes indicate locations of: 1) Figure 5.7, 2 and 3) Figure 5.8

larger reduction in slope steepness. Taking this into account the bed level change predictions from the model are more accurate for the more gently shaped sand waves.
From the simulated bed levels it is observed that the bed level changes at the beginning of the simulation period are relatively large. This can be seen in Figure 5.6 where the bed levels and changes in bed level after 0.5 and 6 years are shown for Case IV. In the first half year, which is 1/12 of the total simulation period, nearly all change in steepness of the slope towards migration direction takes place. In the sedimentation and erosion patterns this change in slope is represented by erosion of the crest and sedimentation of the trough. In the subsequent modelling period the sand wave grows, but only very little change in steepness of this slope is observed in the model, causing the crest and through to move further apart. This initial quick bed level change may indicate a mismatch between the environmental conditions and the morphology in the Delft3D FM model. Another possible cause is an increased influence of bed slope transport relative to reality. In the remainder of the simulation period the sand waves are growing in height. An obvious cause for this growth could be the exclusion of suspended sediment transport although other possible suspects, such as the exclusion of free surface waves and the simplification of a non-graded sediment should not be ignored. This distinct difference between the earlier phases of the model and the rest of the simulation was found in all model cases.

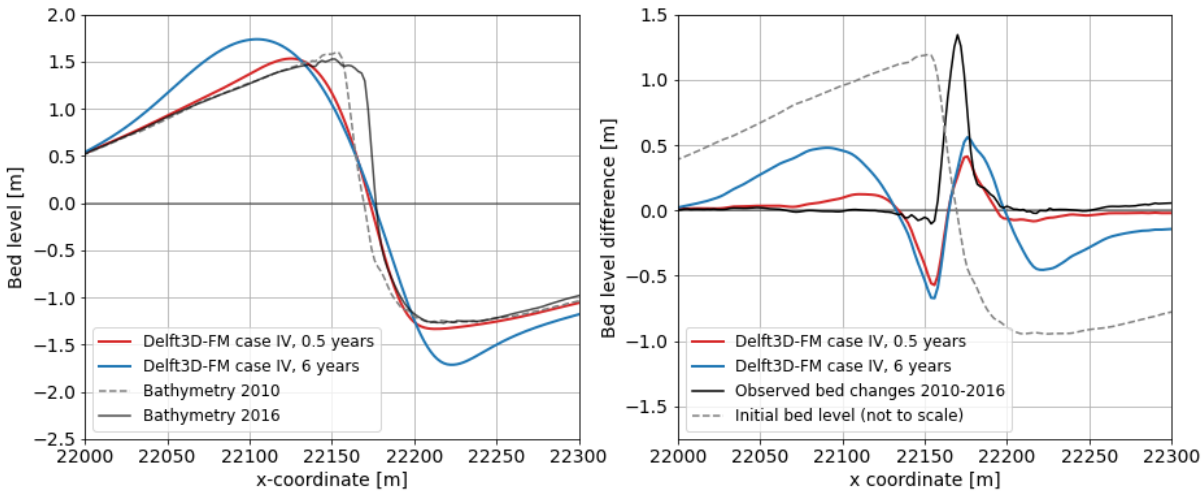

Figure 5.6: Measured and computed bed level (left) and changes in bed level (right) for the Case IV model after 0.5 and 6 years. For location see Figure 5.5, location 3

In Figure 5.7 the bed level after 6 years of morphological change for a more gentle sand waves (location 1 as indicated in Figure 5.5) is shown for different boundary conditions. The results for the other sand waves in the model can be found in Appendix C.2. For all boundary condition combination the steepest slope of the sand wave has gotten less steep during the simulation. Furthermore the wave height increased through both heightening of the crest and lowering of the trough. The increase in wave height in the model is observed for all boundary condition combinations. The symmetrical M2 case (Case I) shows the biggest overall increase in wave height. In simplified model studies the same relation was found where non-migrating waves have larger growth rates and equilibrium wave heights. When the S2 tide is added the wave becomes less steep, but no migration is taking place even though on average positive velocities were found (see Figure 5.4b). The subsequent addition of M4 showed little influence on the mean velocity field, but significantly influences the sand wave migration. The M4 tide causes a migration of the zero-crossing point of 5-10 m for all sand waves along the East transect with respect to the M2-S2 model. Since the sand waves are migrating only slowly, this makes a big difference and in most cases better resembles the migration rate from measurements. The residual current, which had the largest influence on the mean velocity field, further increases the migration rate. This difference in migration is however smaller than what is observed for the addition of the M4 tide. When instead of harmonic boundary conditions time series of flow velocities and water levels from the DCSM model are applied at the boundary, a slightly larger migration rate is found than for the other cases. The Case IV model, with the most complete harmonic boundary conditions best resembles the results of the time series. In Figure 5.8 the erosion and sedimentation patterns from Delft3D FM and measurements are shown for the sand waves included in Figure 5.5. In these patterns the change in slope is represented by an erosion of the top of the sand wave and sedimentation near the trough. In this way the crest moves in the direction opposite to migration and vice versa for the trough. The difference in migration rate between the various boundary conditions can also be observed in these patterns.

The more the sand waves in the model migrate the smaller the erosion of the crest is. Furthermore, in cases of larger migration more sand is deposited next to the crest in migration direction and this sedimentation area is wider. Overall the erosion and sedimentation patterns of the migrating waves are more similar to what is found in reality. In these patterns however still a large difference is found with reality and the bed level changes from the model are mostly too large. The results of the full domain are shown in Appendix C.2.

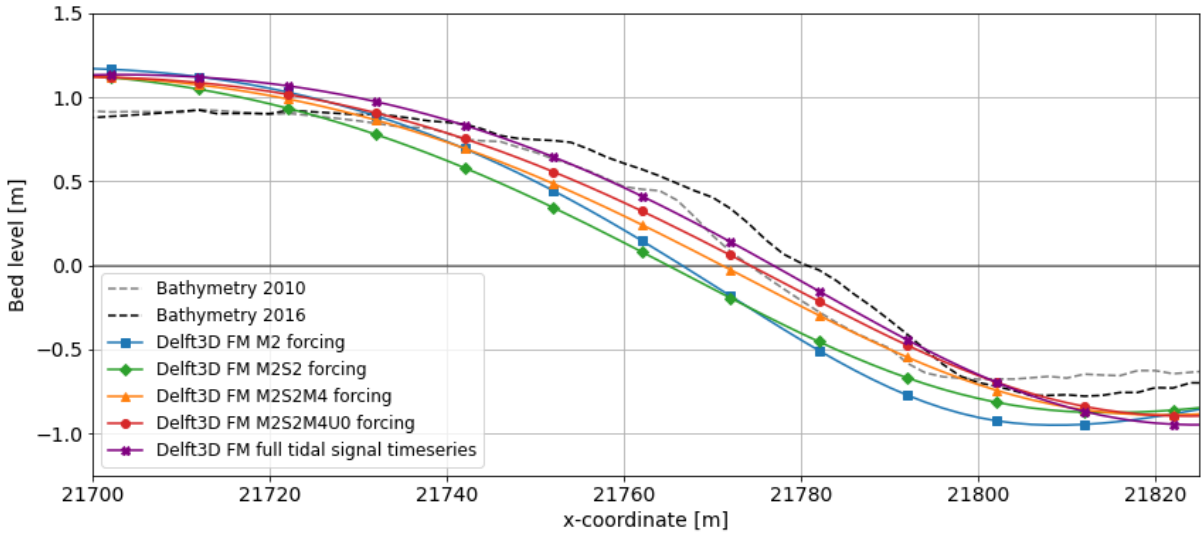

Figure 5.7: Measured and computed bed levels for all cases, for location see Figure 5.5, location 1

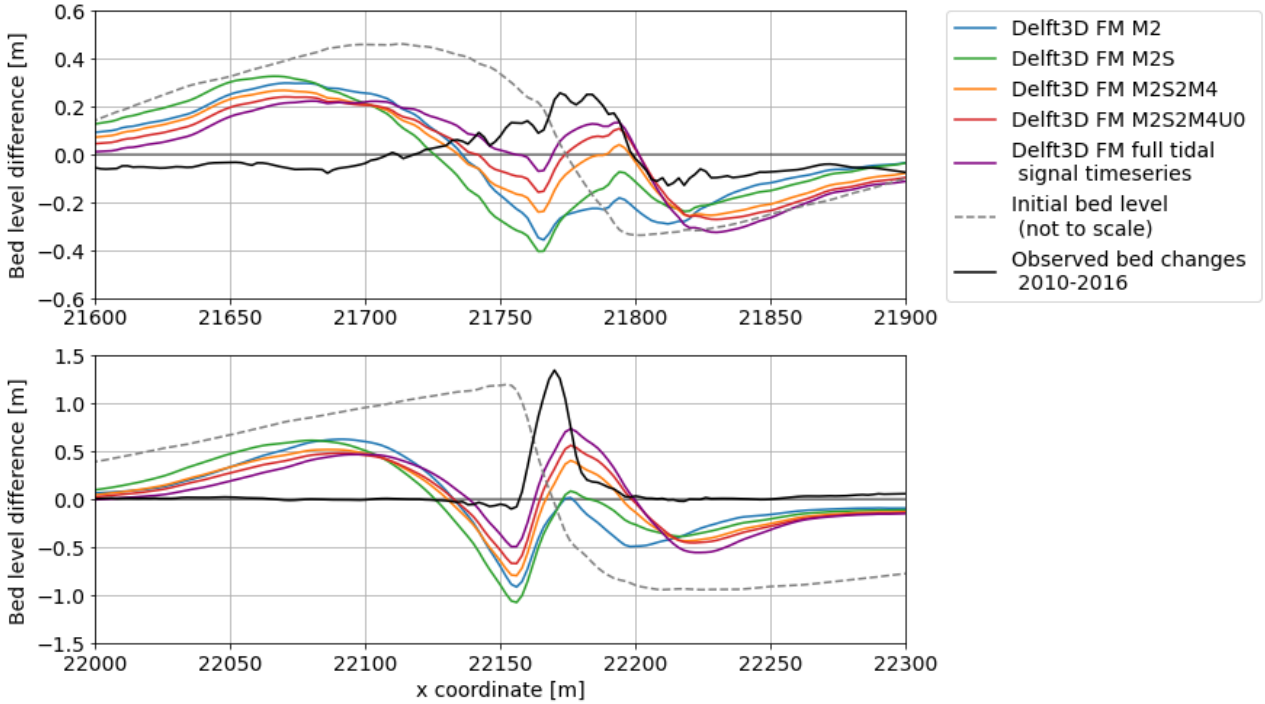

Figure 5.8: Erosion and sedimentation over 6 years from measurements and Delft3D FM for all cases, shown at location 2 (upper) and location 3 (lower) from Figure 5.5

5.3.3 Sensitivity analysis

To explore the sensitivity of the model, some input parameters are changed. For this sensitivity analysis the Case IV model (with the M2, S2, M4 and U0 boundary conditions) is used. Only one parameter is changed at

a time while the rest of the model is kept the same. The implementation of these parameters in the model can be found in Chapter 3.
First the bed slope parameter α_{bs} is varied. This parameter influences the importance of the bed slope on bed load transport. A higher bed slope parameter will increase downslope sediment transport and decrease uphill transport. In the base model a value of 3 is used for this parameter. In Figure 5.9 the effects of a varied bed slope parameter are shown. When the bed slope parameter is decreased less sediment is transported downslope. This leads to an increased steepness of the slope at the end of the simulation. In this simulation less bed level change in the first half year is observed, although some changes in slope are still present. Due to the decreased downslope transport and increased upslope transport (which has become easier) for a reduced α_{bs} the sand wave grows faster and the height of the sand wave at the end of the simulation period increases. In the resulting bathymetry the slope of the sand wave in the direction of migration retains more of it's steepness than in the base case (Case IV), which is more similar to what is observed from the measurements. With a decreased bed slope transport the sand wave is however growing significantly, which is not observed in the measurements. For an increase in bed slope parameter opposite results are found, leading to the sensitivity band shown in Figure 5.9. Through variation of this parameter either the growth of the sand wave or the steepness of the slope in migration direction is well represented, but it shows no option for improving both.
When the Chezy roughness is varied a sensitivity band as shown in Figure 5.10 is found. In this case the hydrodynamics of the model are directly affected by the change in model parameters. A higher value for the Chezy roughness indicates a smoother (less rough) bed. This means that the flow will 'feel' the bottom less and flow over it more easily. The bed boundary layer is smaller due to this reduced roughness and flow velocities close to the bed are higher. The bed shear stress is lower, despite the higher flow velocities near the bed, due to the lowered roughness. This causes less sediment to be transported and thus affects the morphology. In case of a lower roughness (higher chezy value) the flow will not be as much affected by the sand waves. This leads to less defined circulation cells in the mean flow field. In this way the growth rate of the sand wave is also affected by the roughness. From Figure 5.10 it is clear that an increase of the Chezy roughness from 75 to 85 has only a limited impact on morphology. In that case the growth of the sand wave is reduced, as is the steepness of the slope in migration direction. When the Chezy roughness is decreased form 75 to 65 a significant impact on the resulting bed level is found. In that case more sediment is transported and larger bed level changes are observed. The 'digging in' of the trough and heightening of the crest of the sand wave are amplified. Additionally more steepness of the slope in migration direction is retained. In this way the results do not improve for either option.
Finally the sediment size in the model is varied. The impact of varying this parameter is a bit more complex since it has both a dampening and an amplifying effect on the bed load transport. There is no suspended sediment included in the model and the bed load transport is modelled using the Van Rijn formula shown below.

$$|S_b| = 0.006\alpha_s\rho_s w_s D_{50} M^{0.5} M_e^{0.7} \tag{5.2}$$

The sediment size (D_{50}) itself and the settling velocity w_s in the equation cause an increase of the bed load sediment transport volume in case of increased sediment size. Both mobility parameters: M and M_e have the opposite effect. These parameters decrease for an increasing sediment size. This contradiction causes the effects of a varying sediment size to be small, as can be seen in Figure 5.11. When looking at the momentary sediment transport rates the rate increases for increasing sediment size. This is caused by the exclusion of suspended sediment transport which would cause increasing transport rates for decreasing sediment sizes.

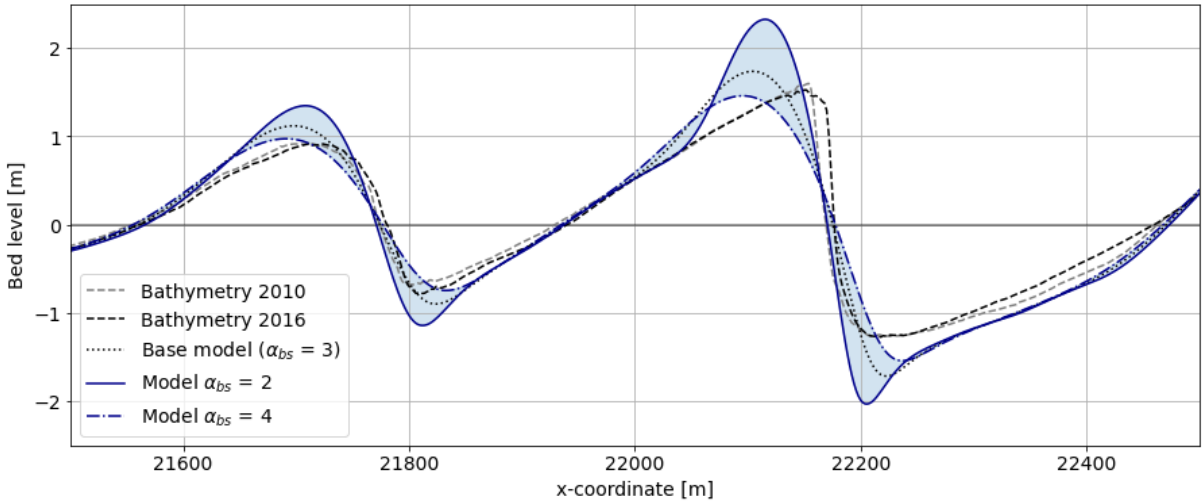

Figure 5.9: Sensitivity of Case IV model results to a variation of the bed slope parameter (α_{bs})

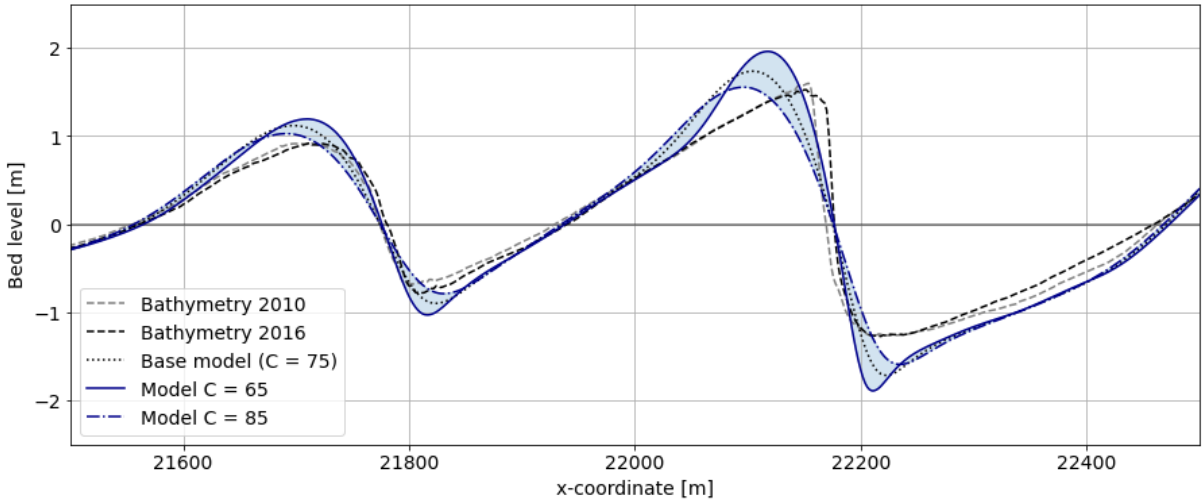

Figure 5.10: Sensitivity of Case IV model results to a variation of the Chezy roughness (C)

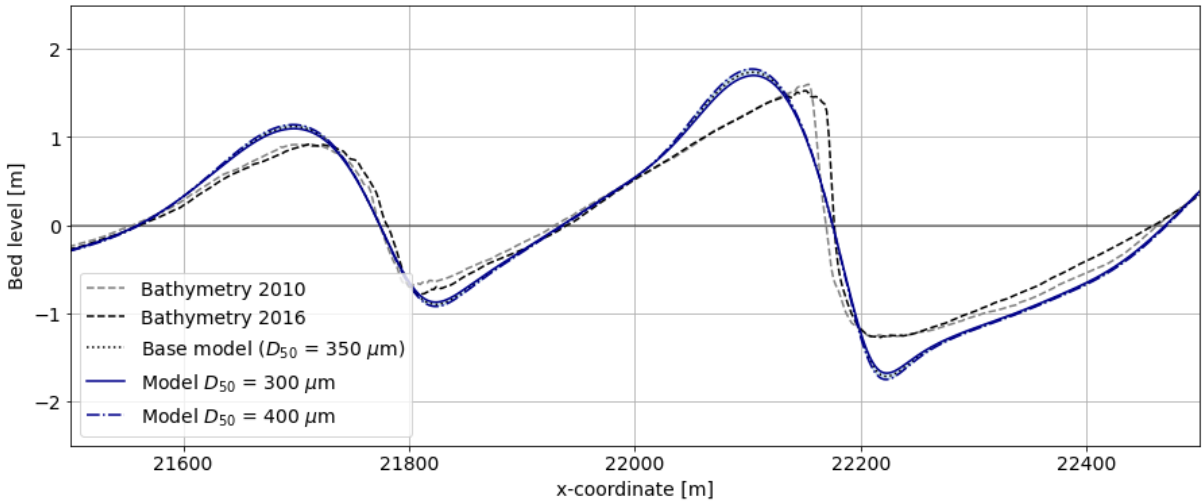

Figure 5.11: Sensitivity of Case IV model results to a variation of the sediment diameter (D_{50})

Chapter recap and conclusions

In this chapter the results of the 2DV case study are presented. The model is located at the HKZWF, which is chosen for its relatively uniform geophysical conditions, little human interference, extensive availability of data and uniform sand wave migration direction. A hindcast is performed between 2010 and 2016, the period between two subsequent surveys. The model bed level is extracted from the 2010 measurements and boundary conditions are based on the large scale DCSM model. Multiple combinations of tidal constituents are assessed as boundary conditions. These different tidal constituents significantly affect the vertical tide-averaged flow circulation cells. Especially the addition of a (weak) residual current considerably disturbs this circulation pattern. The addition of the M4 tidal constituent does not have a significant impact on the mean velocity profile although it does cause significant migration of the sand waves. The residual current causes a further increase of the migration rate.

From the morphological results it is clear that the Delft3D FM model overestimates the extend of the bed level changes. The steep slope of the sand wave in migration direction becomes more gentle during the simulation and the sand waves show a significant increase in height. Both of these phenomena are not observed in the bathymetry measurements. The change in steepness of the sand waves mostly takes place at the very beginning (first 6 months) of the simulation. This initial quick bed level change may indicate a mismatch between the environmental conditions and the morphology in the model. Another possible cause is an increased influence of bed slope transport relative to reality. In the remainder of the simulation period the sand waves are growing in height. An obvious cause for this growth could be the exclusion of suspended sediment transport although other possible suspects, such as the exclusion of free surface waves and the simplification of a non-graded sediment should not be ignored.

The sensitivity analysis shows a large dependency of the morphological results on both the bed slope parameter and the Chezy roughness. An increase of the Chezy roughness (indicating a less rough bed) or an increase of the bed slope parameter lead to a reduced growth rate, but increased slope flattening. The opposite happens for a decrease of either parameter. In this way changing these parameters separately would improve either the growth rate or the steepness of the slope in migration direction in the model results, relative to the measurements.

6 | 3D case study with Delft3D FM

Sand wave fields have a profoundly 3D character. Along sand wave crests changes in direction as well as bifurcations are observed. Underlying bed forms add to this variation in two directions. Furthermore, the tidal motion has an elliptical character and can thus not fully be prescribed in a 2DV setting. To study the importance of 3D effects for the modelling of sand waves a 3D model is set up around the East transect. This model study will give insight into the viability of 2DV models for sand wave predictions. Furthermore a first exploration is done into the possibilities of Delft3D FM for these kind of models, such as running in parallel.

6.1 Model set-up

The 3D model is set-up around the location of the Eastern transect 2DV model. The grid lines are aligned with the approximate sand wave migration direction, alike in the 2DV model. In the center of the model area sand waves are present over an area of 7 by 2 km. This sand wave domain is enclosed by an area without sand waves leading to a full model domain of 47 by 12 km. The location of the model area and sand wave domain are shown in Figure 6.1

6.1.1 Grid

Similar to previous models the grid sizes decrease from the boundaries towards the sand wave domain. The grid cells at the boundary are approximately 1 by 1 km. At the location of the sand waves the grid cells have a size of 2 m in the direction perpendicular to the sand wave crest (which is approximately the direction of migration). This grid length and resolution are identical to that used in the 2DV modelling studies. In the direction along the crest the grid size is 10 m in the sand wave domain. Since the grid is aligned with the sand waves the slopes in this direction are much gentler allowing for bigger grid sizes. Mostly rectangular cells are used with some triangular cells at transitions (see Figures in Appendix F). The orthogonality and smoothness of the grid were kept in mind while constructing the grid. The vertical grid is equal to the previous models with 60 sigma layers.

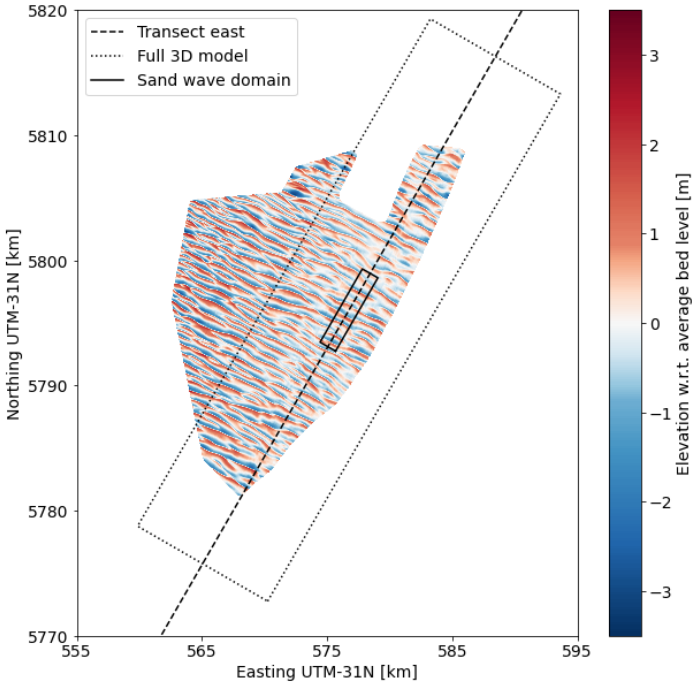

Figure 6.1: 3D model domains and HKZWF sand wave bathymetry filtered from 2016 measurement survey

6.1.2 Bed level

The full model area partly exceeds the 2016 survey area. For the sand wave bathymetry in the center of the model the 2010 compound survey data is used, from which large-scale bathymetry as well as smaller bed forms are filtered (see Section 5.2). The measurement data is interpolated to the grid and the same smoothing filter

is used to remove disturbances as in the previous case study. The filter is used in two directions and especially in the along crest direction signs of measurement errors, most probably due to vertical referencing issues, were found (see Appendix B). The sand waves are dampened towards the edges of the sand wave domain over an area of 1.5 and 0.3 km in cross- and along-crest direction, respectively. This sand wave bathymetry is superimposed on to the bed level from the DCSM model, which is interpolated to the grid. The final bed level is shown in Figure 6.2

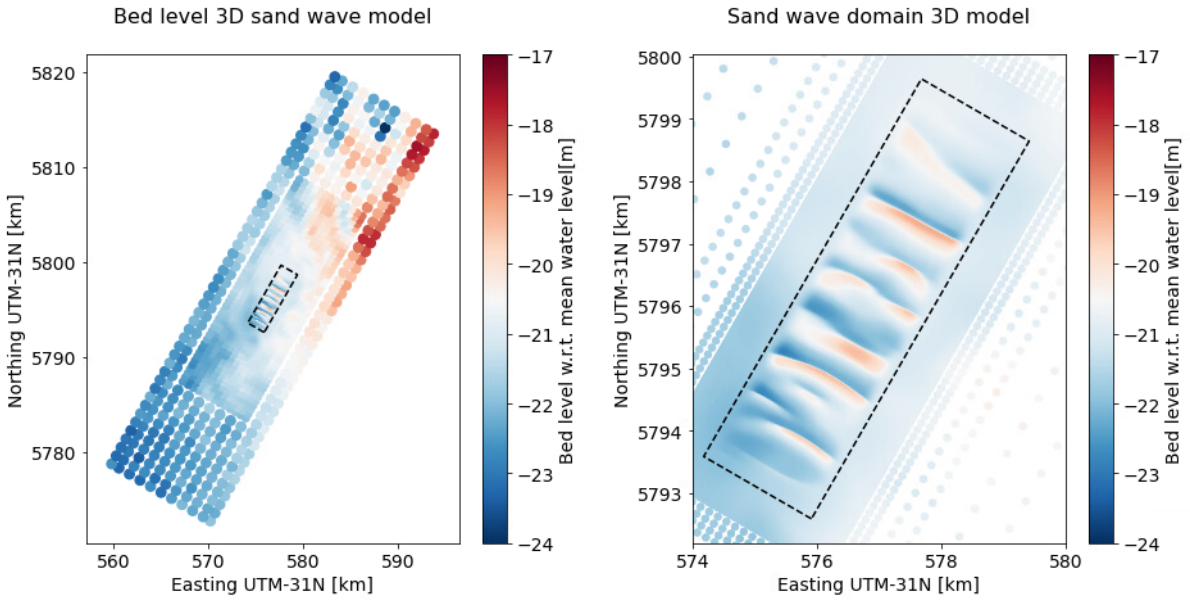

Figure 6.2: Bed level of the 3D model, plotted at grid points for the full domain (left) and an enlargement of the sand wave domain in the center (right)

6.1.3 Boundary conditions

For this 3D model a new type of boundary condition available in Delft3D FM is used: the advection velocity boundary condition (Dobrochinski, 2021). This boundary condition imposes a water level combined with a flow velocity profile over the depth in both horizontal directions at all boundary points with incoming flow velocities. A schematic overview of the imposed conditions at inflow boundaries is shown in Figure 6.3. At outflow boundaries the boundary condition has a Neumann like behaviour where cell centre velocity is copied to the virtual cell lying outside the model domain. In this way a good match for both water levels and flow velocities is reached. This match between the flow velocities and water levels is shown in Appendix E.2. Through the use of this boundary condition no compromises between a good representation of water levels or good representation of flow velocities are necessary when dealing with small model areas. Furthermore, the effects of features, such as gullies or banks, outside the model domain can easily and accurately be included in a smaller model. The advection velocity boundary is used for all 4 boundaries of the model domain. The water levels and flow velocities are extracted as time series from the DCSM model starting from the end of 2012 (see Zijl et al. (2018)).

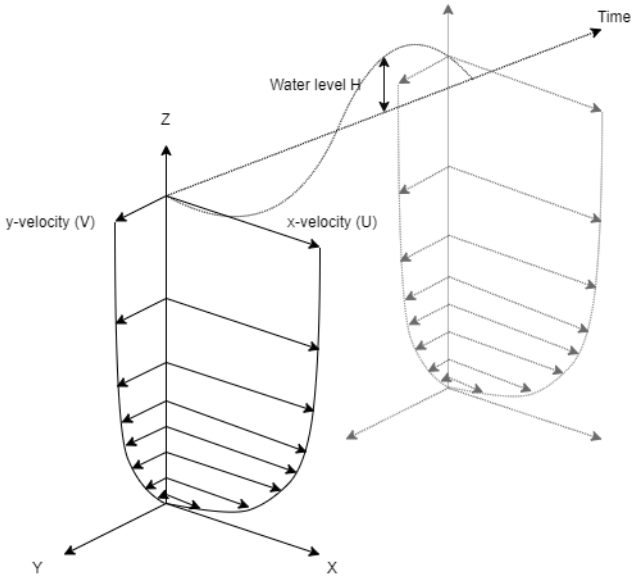

Figure 6.3: Schematic overview of the advection velocity boundary condition for inflow boundaries

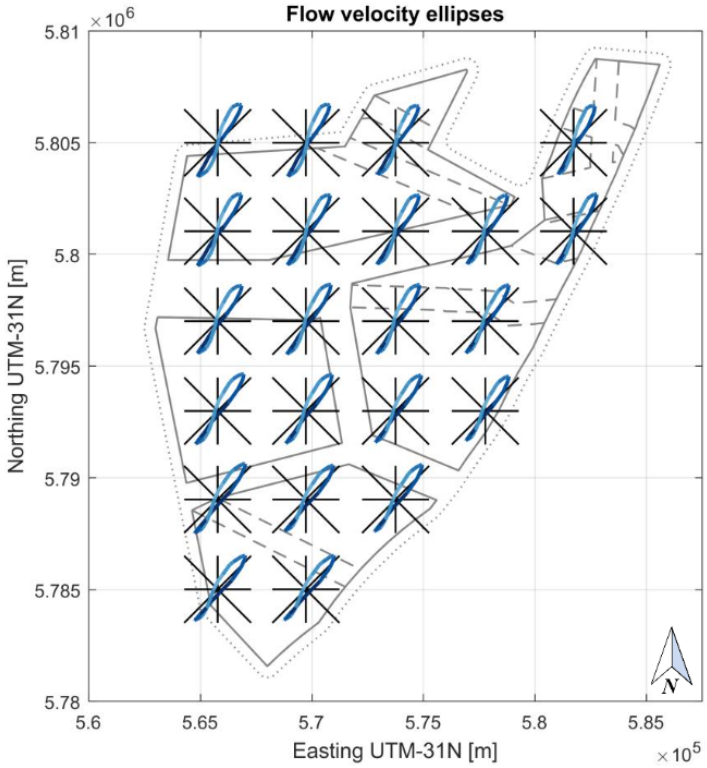

Figure 6.4: Tidal ellipse representing flow velocity magnitude and direction for one tidal cycle over the HKZWF area (Deltares, 2016a)

6.2 Results

In this section the results of the 3D case study model are shown. First the hydrodynamics over the full sand wave domain are presented. Subsequently a more in-depth analysis of the bed load transport and morphology in the 3D model is carried out. For this analysis, the focus is put on the East transect location used in the previous chapter, which runs through the middle of the sand wave domain in the 3D model (see Figure 6.1).

6.2.1 Hydrodynamics

From a simulation without morphological change the flow velocities and directions are extracted. For approximately maximum flood flow these variables are shown in Figure 6.5. Especially the flow velocity magnitude shows a significant influence of the three dimensional bed profile. The depth averaged flow velocities are amplified above sand wave crests due to a reduced water depth. The opposite happens at the location of the troughs. The depth averaged velocity directions are more homogeneous. Some influences of the individual sand waves on flow direction are found, but mostly a gradual change in flow direction over the area is observed. The flood flow direction over the area is on average not aligned with the 2DV transect direction based on the steepest slope, which is 30 °N. A similar deficit between the transect direction and the ebb flow direction is observed although the flow direction is in that case more consistent over the area. The gradual change of flood flow direction over the area was also found in the morphological study performed by Deltares (2016a). In Figure 6.4 the tidal ellipses over the HKZWF area from this study are shown. This pattern of flow directions is thus not influenced significantly by the presence of sand waves. Since the area is flood dominant and the sand waves are migrating in that direction this change in average flood flow direction over the area could be quite important for the morphology.

6.2.2 Sediment transport

The bed load transport and morphology are studied along a few transects drawn across the area. The middle transect is equal to the East transect used in the 2DV study (see Figure 6.1) and results for this transect are shown. The results at the locations of the other transect, which have the same direction, but located at 250 and

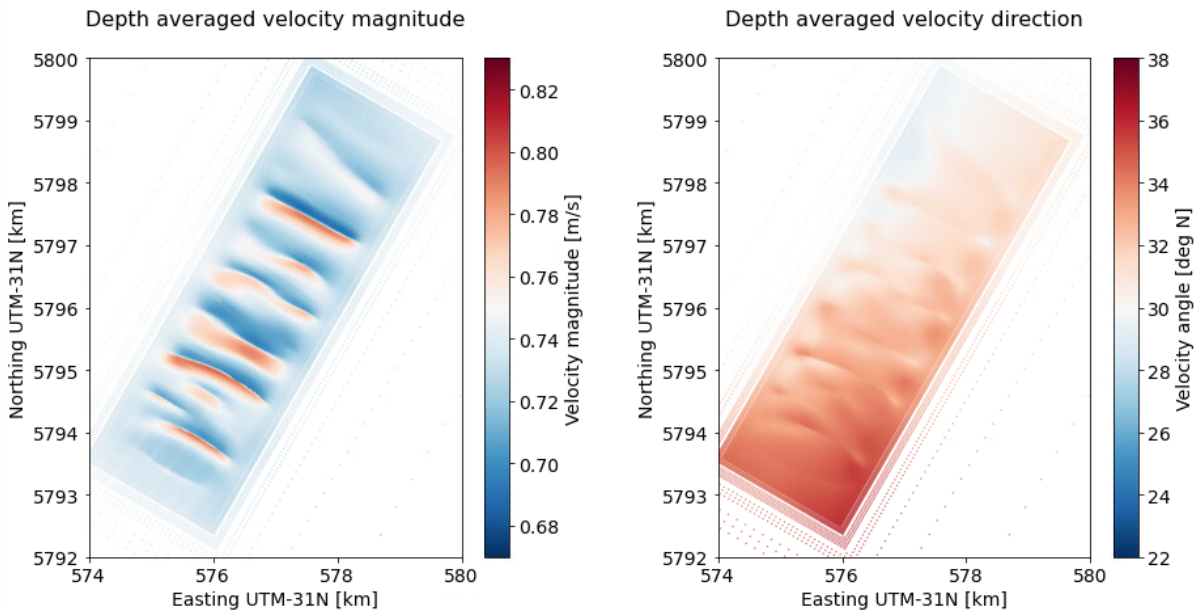

Figure 6.5: Depth averaged velocity magnitude (left) and depth averaged velocity direction (right) during peak flood flow

500 m towards the North-West and South-East of the middle transect, showed similar relations. In Figure 6.6 the direction of the net sediment transport over the East transect is shown. A similar gradual change in direction is found as is present in the flow directions. At the locations of steep slopes in the sand wave bathymetry some influence of the sand waves on the net sediment transport direction can be seen. The direction of the transect used in the 2DV study, which is 30°N, is similar to the mean transport direction over the transect, but at the edges of the domain a significant deviation from this transect direction is found. For the locations indicated in Figure 6.6 the direction of sediment transport, velocity at the bed and depth averaged velocity over time are shown in Figure 6.7. The shaded color indicates the instantaneous sediment transport at that location. During flood flow, which accounts for the most sediment transport (the darkest band in the figure), the direction of the current and sediment transport is changing significantly over time. This behaviour, with a quite unidirectional ebb flow and a more elliptical flood flow was also found in a 2DH modelling study by Deltares (2016a), of which the tidal ellipses are shown in Figure 6.4. However, from Figure 6.7 it is clear that the velocity near the bed, which shows the most similarity with the sediment transport direction, deviates from the depth averaged

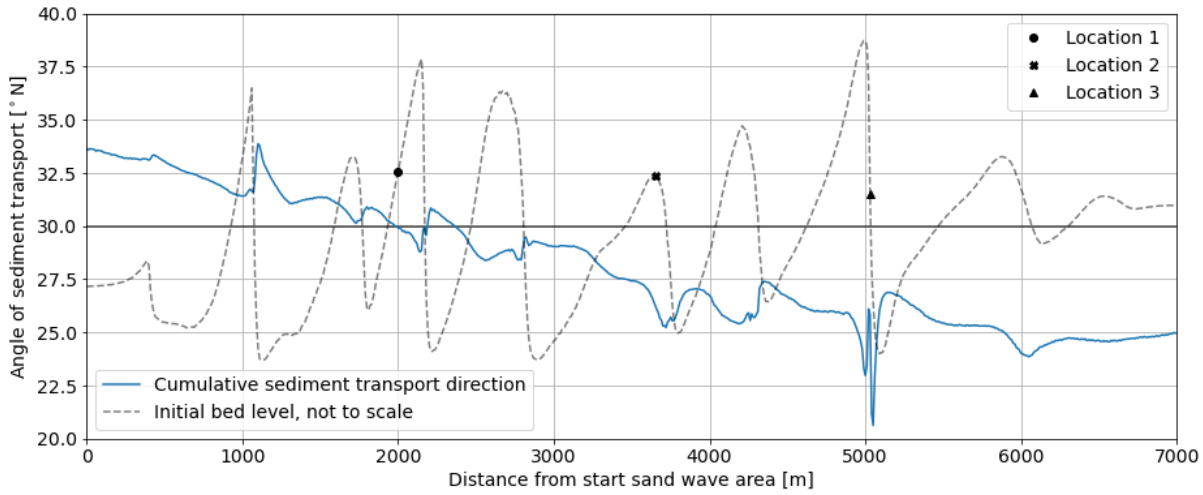

Figure 6.6: Net sediment transport direction along the East transect (see Figure 6.1 for location) over 4 tidal cycles (2 days), transect direction is 30°N, markers indicate locations used in Figure 6.7

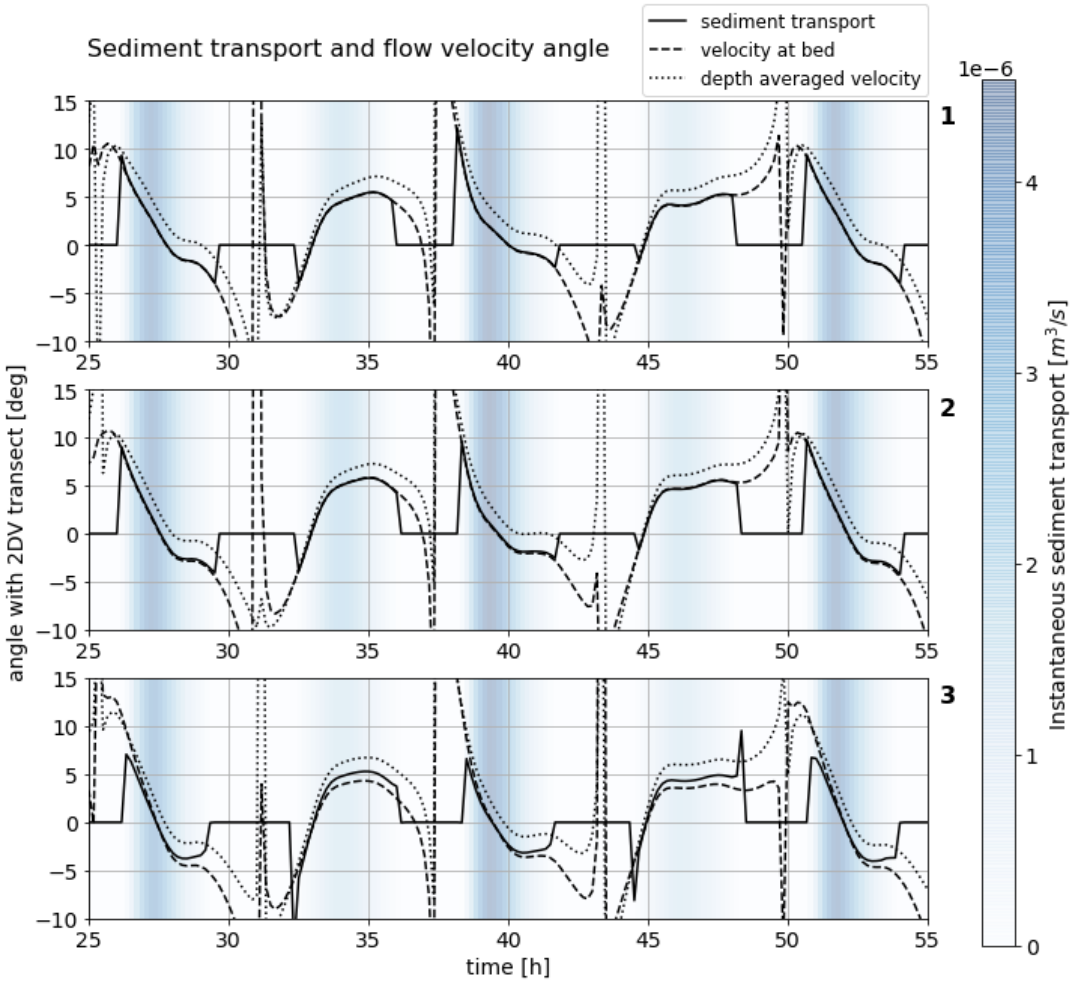

Figure 6.7: Sediment transport direction over time at 3 locations along the East transect (see Figure 6.6), including flow direction at the bed and depth averaged flow velocity direction

velocity direction by a few degrees. In the third plot of Figure 6.7 a location at the steep slope of a sand wave is shown. At that location the sediment transport direction deviates more from the direction of the flow at the bed. This is caused by the increased influence of bed slope transport. During flood flow, which is directed down-slope, the direction of sediment transport is closer to the transect orientation, which was chosen based on the steepest slope. During ebb flow the effect is larger and the sediment transport direction deviates further from the steepest slope direction than the flow. These steep slopes of the sand waves thus do steer the sediment transport in a certain direction.

6.2.3 Morphology

Due to the size of the model (approximately 700 000 cells with 60 sigma layers), simulating for 6 years until the next measurement (as was done in the 2DV case study) was not possible in terms of computation time. The model is run for 4 tidal cycles (excluding 1.5 tidal cycles spin-up). With a morphological scale factor of 72 the morphological duration of the simulation is approximately 150 days. The sedimentation and erosion patterns from measurements and those from the Delft3D FM model are shown in Figure 6.8. Since the sand waves in the model are dampened close to the edges of the sand wave domain the bed level changes caused by the sand waves do not extend to these edges. The most active locations in terms of bed level change do coincide between the Delft3D FM model and the measurements. These active locations are mostly found on the steep slope of the sand waves in migration direction. Indications of similar behaviour as the 2DV models can be seen in the form of erosion at the location of the sand wave crests. In the measurements especially sedimentation is present on lee side of the sand waves. The model results show both significant sedimentation on the lee slope and some erosion at the top of the sand wave. This pattern, which indicates a decrease in slope steepness, is

clearly visible when comparing the results along the East transect, which is done in Figure 6.9. In this Figure the results of both the 2DV and 3D model after 150 days of morphological change (approximately 2 days of hydrodynamics) are shown. For this purpose the 2DV model was run again with the smoothened bathymetry along the transect of the 3D model. Since errors in the lateral direction were filtered out, this bathymetry was slightly different from the original 2DV bathymetry.

The location of sedimentation on the lee side of the sand waves from the 3D model is similar to what is found in the measurements. Compared to the 2DV model, the 3D model shows lowered erosion of the top of the sand wave and increased sedimentation on the lee slope. This pattern better matches the bed level changes from measurements. The initial bed level change in the 3D model is however still disproportionally large compared to the duration between the measurements. Since the three dimensional tidal flows and tidal asymmetry from the DCSM model are better represented in the 3D model (compared to the 2DV model) this could cause the difference in model results. Sand wave growth, as was observed in the 2DV model, is not yet distinguishable in the results of the 3D model. However, since the model is only run for a short period this might still happen on the longer time scales.

The morphological results of the 3D case study model still show room for improvement. The initial bed level changes in the model are large relative to the bed level changes over 6 years from measurements. These initial quick bed level changes might indicate that the model is forced towards a different equilibrium sand wave shape. Some differences in hydrodynamics with reality might thus still be present. Since 3D tidal flows from the DCSM model are well represented in the 3D case study model (see Appendix E.2), differences with reality should be found elsewhere. Further improvements of the model towards more realistic hydrodynamics are discussed in Chapter 7. These model alterations include more realistic peak flow velocities and inclusion of wind-driven currents. These changes might decrease or eliminate the artificial slope reduction. Furthermore, optimization of the 3D model will decrease the computation times such that long term morphological 3D simulations could be carried out. These long term results will show the predictive capacities of such models.

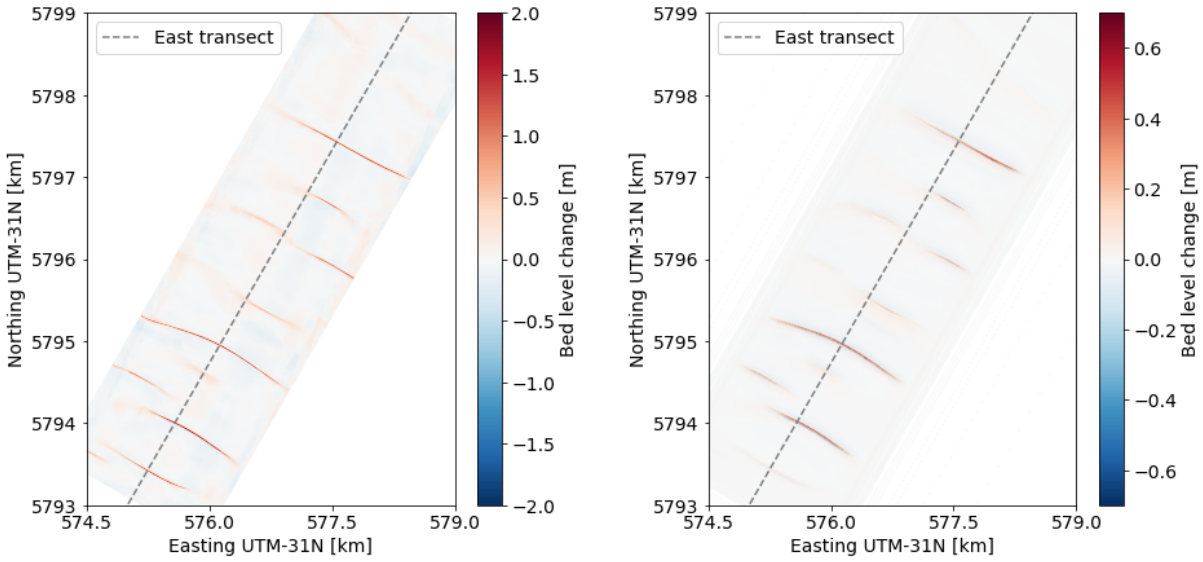

Figure 6.8: Observed bed level changes after 6 years (left) and computed bed level changes after 150 days (right). Dashed line indicates the location of the East transect used in Figure 6.9 Please note the difference in color scales

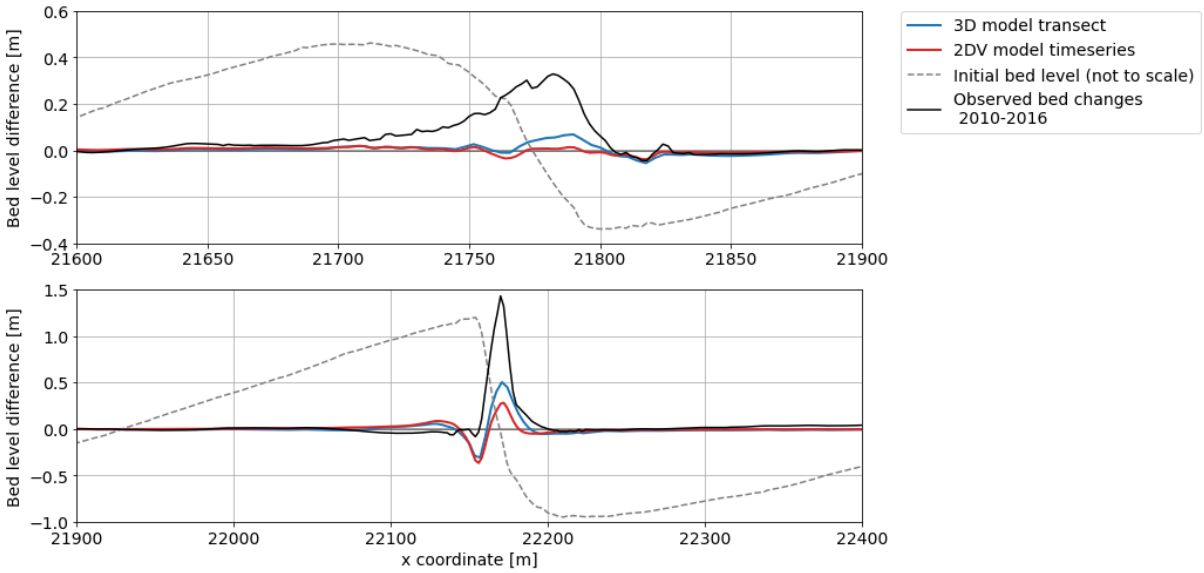

Figure 6.9: Sedimentation and erosion along transect East from the Delft3D FM simulation after 150 days for 3D and 2DV settings, compared to differences between measurements. Please note duration between measurements was 6 years

Chapter recap and conclusions

In this chapter a 3D case study is set up. The center of the 3D model domain coincides with the location of the transect used in the previous chapter. The bed level consists of the large-scale bathymetry from the DCSM model, with an area of superimposed sand waves in the middle of the model domain. A new type of boundary condition: the advection velocity boundary is used in the 3D model. This boundary condition imposes both a water level and a flow velocity profile over depth in both directions. In this way a good match for both water levels and flow velocity magnitude and direction is reached in the model. Moreover, the 3D model has an unstructured grid and is run in parallel.

As was apparent from the tidal ellipses found by Deltares (2016a), the flood flow direction changes significantly over time and space. This leads to a mismatch of the flow direction, and thus sediment transport, with the transect direction used in the 2DV case study. Furthermore, at the locations of a steep sand wave slopes, influences of bed slope related transport on the local sediment transport direction are found. The variability of flow velocity and sediment transport directions over space and time show the influence of the addition of a third dimension.

The 3D sedimentation and erosion pattern matches the measurements in terms of active zones. At the crest of especially steep sand waves some erosion is present in the model results. The location of the sedimentation on the lee side of the sand waves is similar to what is found from measurements. Due to the size of the model it was not possible to run the simulation for the 6 years between the subsequent measurements. A quantitative comparison is thus troublesome. However, indications of similar behaviour as found in the previous Delft3D FM models are present. The reduction of slope steepness in the model might be caused by a mismatch of the boundary conditions and the bathymetry in the Delft3D FM model. Since 3D tidal flows from the DCSM model are well represented in the 3D case study model the focus for improvement of morphological results should lay elsewhere. Identified possible causes are differences between the DCSM model hydrodynamics and reality and the exclusion of wind-driven currents. These differences are discussed in more detail in Chapter 7.

7 | Discussion

In this chapter the limitations of the applicability of the results shown in this thesis are discussed. When applying the results to practice it is important to keep these limitations in mind as they may result in uncertainties.

Differences between Delft3D-4 and Delft3D FM results

The hydrodynamic results of Delft3D-4 and Delft3D FM show great similarity, as can be seen in Table 7.1 where some results from the base case used in Chapter 4 are shown. Small differences in the velocity profile over the depth are apparent from these figures, which could be caused by the difference in boundary condition type or computational differences. The relations between flow velocity near the bed, bed shear stress and bed load transport in Delft3D FM are in line with those found in Delft3D-4. The local tide-averaged bed load transport is slightly larger in Delft3D FM indicating an increased inequality between ebb and flood transport. The growth rate curves show slight differences between the models as is apparent from the wave length of the FGM which is slightly smaller in Delft3D FM compared to Delft3D-4. This inequality is caused by differences in the implementation of the bed slope related transport. Through extensive research the Delft3D-4 model parameters have been tuned to fit sand wave observations in the North Sea. These tuned parameters have been copied to Delft3D FM in this model study. These input parameters, such as the bed slope parameter (α_{bs}) do however have a considerable impact on the growth rate curve. When the bed slope parameter is increased slightly in the Delft3D FM model, the growth rate curve changes as is shown in Figure 7.1. From this figure

Table 7.1: Comparison of results between Delft3D-4 and Delft3D FM for hydrodynamics (top) morphology (middle) and computational performance for single core (bottom). Hydrodynamic and sediment transport at flank location facing flood current, L = 400 m

Description	Delft3D-4	Delft3D FM	Dimension
Depth averaged flood velocity	0.608	0.606	ms^{-1}
Maximum eddy viscosity	0.058	0.053	m^2s^{-1}
Peak tide-averaged velocity	1.677	1.671	mms^{-1}
Height point of flow reversal (σ_r)	-0.855	-0.870	-
Peak flow velocity at bed	0.170	0.157	ms^{-1}
Peak bed shear stress	0.713	0.651	Nm^{-2}
Peak bed load transport	$1.31*10^{-6}$	$1.16*10^{-6}$	m^2s^{-1}
Tide-averaged bed load transport	$7.26*10^{-9}$	$7.36*10^{-9}$	m^2s^{-1}
FGM wave length	231	193	m
Growth rate FGM	0.033	0.039	$year^{-1}$
Migration rate FGM (U0 = 0.05)	3.27	3.29	$myear^{-1}$
Average timestep	4.8	2.1	s
Computation time (7.5 days)	17.6	8.7	h

it is clear that the growth rate curve from the Delft3D FM model could be identical to the original one from Delft3D-4, for certain parameter settings which lie within acceptable ranges.
When comparing the computational performance of the models it can be seen that the computation time of the Delft3D FM model is significantly reduced with respect to Delft3D-4. The computational gains for a single core simulation using a regular grid can be attributed to improved efficiency of the code. When using multiple cores the computational gain of Delft3D FM will increase further.

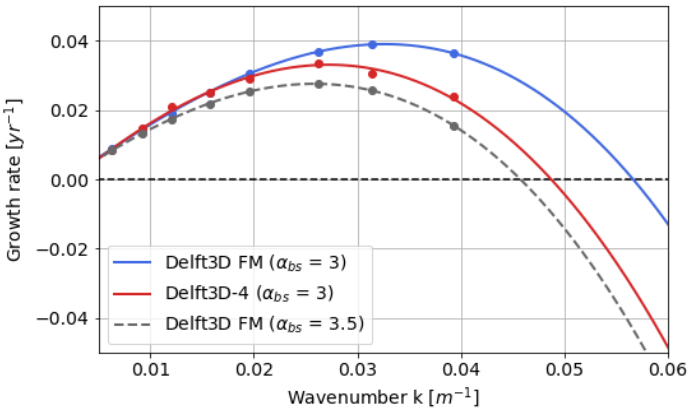

Figure 7.1: Growth rate for Delft3D-4 and Delft3D FM with different values of the bed slope parameter for varying sand wave length.

Delft3D FM, a work in progress

While running simulations significant differences between the results of different versions of Delft3D FM were observed. These distinctions were found in the sediment transport module, which is still in development. In the this study one of the latest versions of Delft3D FM (version 2.16.03.70963) is used. This version shows very similar relations between flow and sediment transport compared to Delft3D-4. The development of the Delft3D FM model is being carried out in collaboration with users, which ensures quick feedback for different model cases and thus stimulates improvement of the results between versions. These differences however need to be kept in mind when applying Delft3D FM to sand wave cases and could, for instance, impact the calibration of the model.

Simplifications of the residual current

The boundary conditions for the case study models were extracted from the DCSM model. This large scale model simulates tidal propagation in 2DH. For this model study the atmospheric pressures, which induce wind-driven currents, were excluded due to the focus on the influence of tidal constituents. These currents are however significant and often have an asymmetrical character. To give an indication of the strength of these currents, the DCSM simulation is repeated including atmospheric pressures. The strength of the wind-driven currents from this run, at one of the boundaries of the 2DV model, is shown in Figure 7.2. Part of the time series shown here includes stormy conditions. The wind-driven currents reach strengths of up to 0.45 m/s, which approaches the local amplitude of the M2 tide. When a year averaged residual current is extracted, the strength of the current is 0.0145 m/s (in sand wave migration direction), which is almost thrice the strength of the original current due to tidal propagation.
Velocity and water level time series from the DCSM model run including atmospheric pressures have been applied at the boundaries of the 2DV model. The resulting morphology is shown in Figure 7.3. Since rather stormy conditions are included in this time series, which are amplified through a morphological scale factor, the

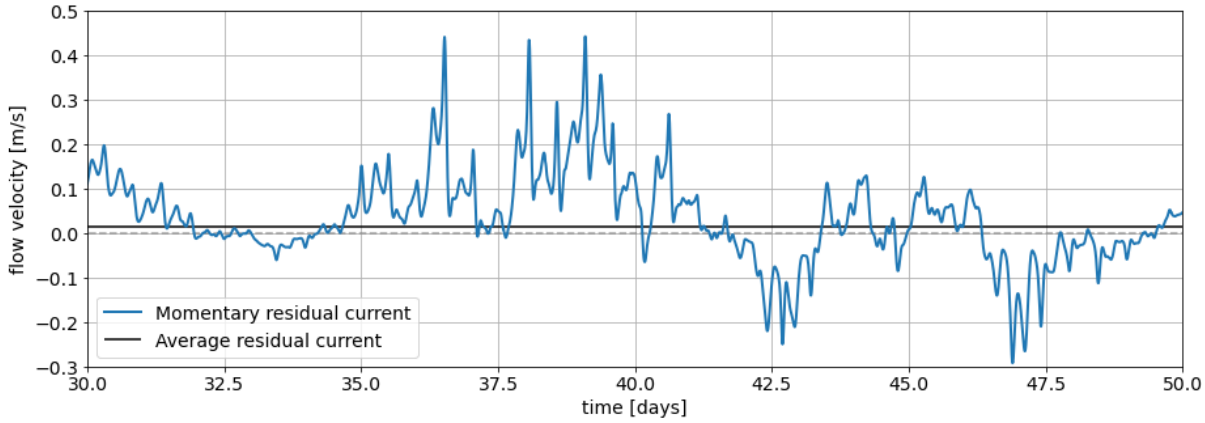

Figure 7.2: Residual current induced by atmospheric pressures from the DCSM model at South boundary East transect. Period shown: January and February 2013

resulting sand wave migration is much larger. The strength of the residual current is probably overestimated in this case. To arrive at a more realistic estimation of the bed level changes, a representative forcing data-set should be created. In Figure 7.3 the effects of two simplifications are thus shown. Firstly the exclusion of wind driven currents and secondly the change from an averaged residual current to simulating the momentary strength and direction of this current. Averaging the current, as was done in the 2DV case study, does not represent the time-varying strength of the current which, especially due to the non-linear relation between flow velocity and sediment transport, significantly influences morphology.

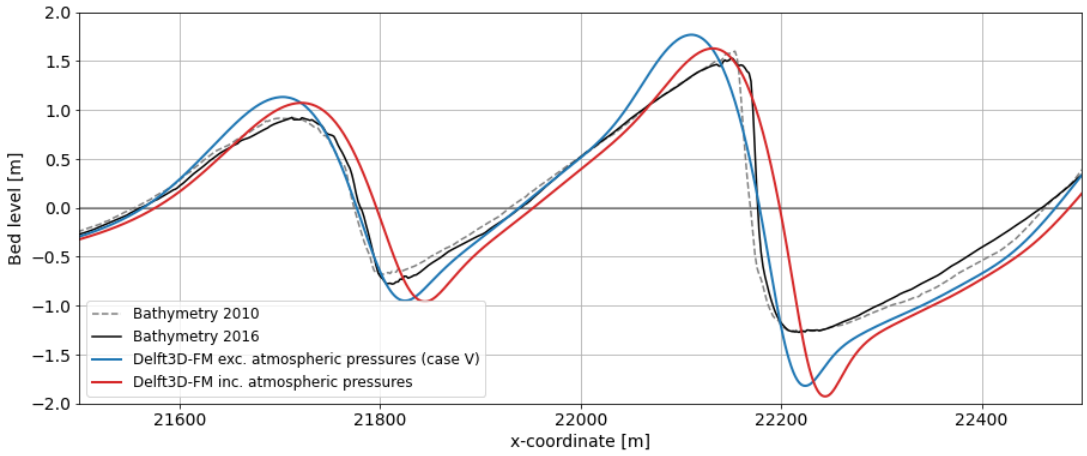

Figure 7.3: Bed level from measurements and after Delft3D FM simulation of 6 years with full tidal forcing including and excluding currents induced by atmospheric pressures, from DCSM model.

Boundary conditions from DCSM model

The DCSM model (including atmospheric pressures) has been validated with buoy measurements in (amongst others) the HKZWF area (see Deltares (2016a) and Zijl et al. (2018)). From these validations it was concluded that the water level and velocity match between the model and measurements was quite good although peak velocities are a bit off. The velocity bias of the model is 0.07 m/s for a buoy in the HKZWF area indicating an overestimation of the velocities by the model. The correlation between flow velocities in the DCSM model with measuremed flow velocities is approximately 0.95 (Zijl et al., 2018). This small difference could however have a significant impact on morphology for the time-scales considered in this study. A comparison between the measurements and the DCSM model run in 3D mode is shown in Figure 7.4. Especially for the (weaker) ebb tide the velocity magnitude is clearly overestimated by the DCSM model.

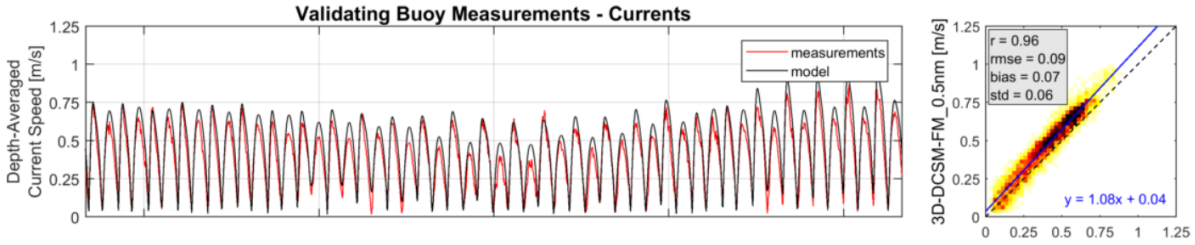

Figure 7.4: Depth averaged velocity magnitude from DCSM model and measurements at HKZB buoy for the first two weeks of December 2016 (Zijl et al., 2018)

Improving morphological results: excluded and simplified processes

The morphological results of the case studies show room for improvement and some of the excluded or simplified processes might be the key to more accurate predictions of sand wave dynamics. During the 2DV case study interesting results were found for a model set-up with two Riemann water level boundaries. This specific combination of boundary conditions was unable to properly represent the local hydrodynamic conditions. However, the morphological results were surprisingly accurate, as can be seen in Figure 7.5. The final bed level shows that the steep slope of the sand wave is maintained and only little growth has taken place during the simulation period of 6 years. The migration of the sand waves is slightly overestimated, but otherwise the morphological

results are quite good. The upper right plot in Figure 7.5 shows the flow velocity at the boundary of the sand wave domain for this model run. It is clear that especially the ebb flood velocities are vastly underestimated, even when taking into account the differences between the DCSM model and measurements mentioned in Section 7. Even though the hydrodynamics of the model are inaccurate, these results might indicate where the the differences in morphology between the model results and measurements originate. The model with two Riemann boundaries deviated in terms of sediment transport rates from the other simulations in two ways: the sediment transport rates are reduced and sediment transport in ebb direction is negligible.
The results of this simulation might be another indication of a mismatch between the boundary conditions and reality. The first indication of this deviation was found in the quick decrease of slope steepness in the 2DV case study models. The bed level changes during the first half year of the simulations were of the same order as the changes during the remaining 5.5 years, as is seen in Figure 5.6. This might show that after this initial period an equilibrium between the morphology and the boundary conditions is reached, which is different from what is observed in reality. As stated in the previous sections, the boundary conditions show some deviation from measurements and are incomplete. In case of more accurate boundary conditions, the peak velocities would be somewhat reduced and the asymmetry between ebb and flood velocity would increase. This is caused both by the overestimation of peak velocities (especially ebb) in the DCSM model and addition of wind-driven currents, which are often aligned with the flood direction. More accurate boundary conditions would in that way create a situation more like what is seen in the model with two Riemann water level boundaries.
Another possible cause for the differences in morphological results and the quick slope decrease could be found in the relations between hydrodynamics and morphology. It could be that the model is overestimating the amount of sediment transport caused by the flow over the sand waves. In reality the threshold for sediment transport could be higher. This might be resolved through the use of a different sediment transport formula or the inclusion of multiple sediment fractions allowing for armoring of the bed.
After the initial stages of the simulations, growth of the sand waves was observed. In the bed level measurements only minor changes in sand wave height are observed. This sand wave growth might be caused by the exclusion of suspended sediment transport. Van Gerwen et al. (2018) found that when excluding suspended sediment transport, sand waves would still be growing at the end of long term simulations, when simulations including suspended sediment transport already reached an equilibrium wave height. During the sensitivity analysis in Chapter 5 other possible (partial) causes were found. The bottom roughness and bed slope parameter have a significant influence on the growth rate of the sand waves in the model. Additionally the simplification of the sediment used in the model could be a cause for this artificial growth. When instead of a uniform sediment multiple sediment fractions would be included this would have a dampening effect on sand wave growth. This effect was observed in a study by Damveld et al. (2020), of which some results are shown in Figure 4.10. This

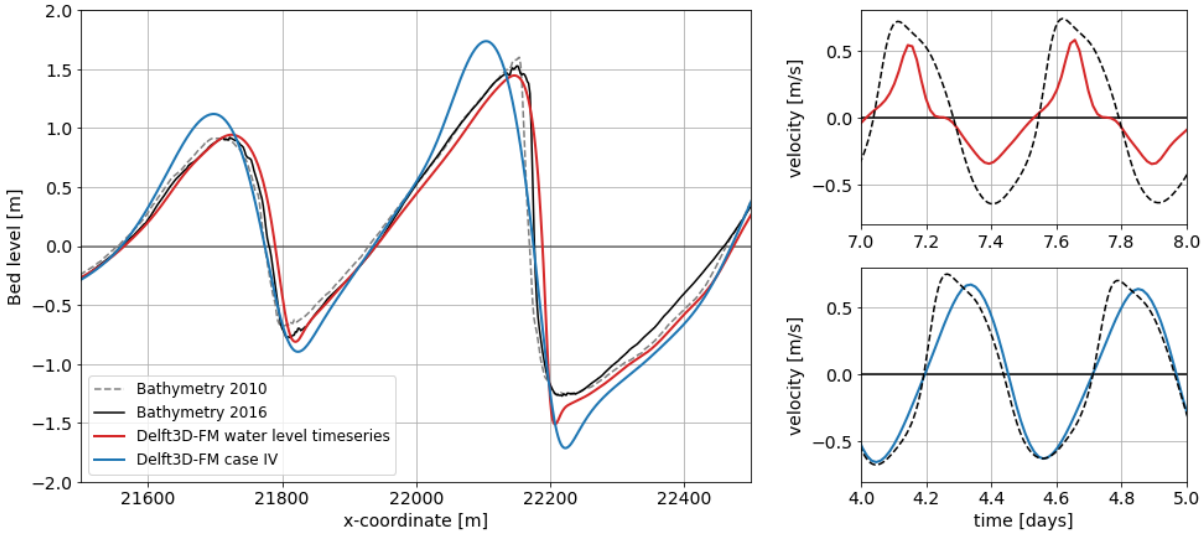

Figure 7.5: Left: bed level from measurements and after Delft3D FM simulation of 6 years with Case IV forcing used in 2DV case study (combination of M2, S2, M4 and U0) and two timeseries Riemann water level boundaries from DCSM model. Right: Tidal velocity signal at south boundary of the sand wave domain for simulation with two waterlevel boundaries (up) and Case IV model (down) compared to tidal signal from DCSM model (dashed line)

reduced growth rate is a result of armoring of the bed. Additionally, free surface waves were excluded in the modelling study. Free surface waves are known to have a dampening effect on sand wave heights (Campmans, 2018). Further study into the influences of these effect on the morphology at the location considered could help improve the predictive capacities of the model.

Chapter recap and conclusions

In this chapter some of the limitations of the research are discussed. The hydrodynamic results of a simplified sand wave case (see Chapter 4) show a good match between Delft3D-4 and Delft3D FM. In the morphological results some inequalities were found. These inequalities were attributed to differences in the implementation of bed slope related transport. In Figure 7.1 it is shown that changes in the bed slope parameter indeed could lead to a better agreement between the model results.
During this model comparison differences between the subsequent versions of Delft3D FM were observed. A recent version of Delft3D FM, used in this study, showed extensive similarities with Delft3D-4. Care should however be taken when applying a different version.
The boundary conditions of the case study models were extracted from the large-scale DCSM model. Although the main tidal flow is well represented by this model, some slight differences are present. In the DCSM model especially the peak ebb tidal flow velocity is overestimated, which could explain the reduced steepness of the sand waves in the model results. Further differences with reality are present due to the simplification of the residual current. Through the use of a morphological scale factor, the computation time is reduced significantly. Information about the momentary strength and direction of the residual current is in that case however lost. In combination with the exclusion of wind-driven currents, this leads to significant deviations from reality.
The best match between morphological simulation results and measured bed level changes was found through a model unable to properly represent the local hydrodynamics. This model might however give indications where the causes for the differences in morphological results originate. In this simulation run the sediment transport in ebb direction was negligibly small. It might be that the ebb velocities are indeed overestimated in the model, or the relation between flow velocity and sediment transport in the model differs from reality. Further causes for differences in morphological results are found amongst others in the exclusion of suspended sediment transport, free surface waves and sediment gradation.

8 | Conclusions

In this thesis the application of Delft3D FM to sand waves in the North Sea area is explored. With the knowledge gained through simulations the research questions will be answered in this chapter. First the answers to the sub questions as stated in Section 1.3 will be discussed. Subsequently these conclusions will be combined with other observations to arrive at the answer to the main research question. In that section the opportunities and challenges of Delft3D FM for modelling sand wave dynamics are discussed.

1) To what level is the Delft3D FM model capable of reproducing the key processes leading to sand wave formation in comparison with Delft3D-4?
Analysis of the hydrodynamic and morphological result of Delft3D FM shows that the model is capable of reproducing the key processes leading to sand wave growth. The tide-averaged vertical flow circulation cells which form the basis of sand wave growth are reconstructed in Delft3D FM under symmetrical tidal forcing. Moreover, these circulation cells lead to sand wave growth in the model for a certain wave length range. The dependencies of growth and migration rates on hydrodynamic forcing and sand wave length are similar between Delft3D-4 and Delft3D FM. Furthermore, the behaviour towards equilibrium is comparable for both models.

2) What tidal components should be included in the model boundary conditions to more accurately predict real-life sand wave dynamics in the North Sea?
Through a 2DV case study model the influence of various combinations of tidal forcing was analyzed for a real-life situation. Clear dependencies of sand wave growth and migration on boundary conditions were found. The M4 tidal component is identified as an important driving force for the local sand wave migration. Moreover, the addition of a residual current, although much smaller than used in most idealized studies, caused further migration of the sand waves. The differences in morphological results with the simulation including the full tidal signal indicate that other tidal components might also be of importance. The dependencies found were similar to those from studies using simplified models. Since the majority of previous research is carried out on these simplified sinusoidal sand waves, this could pave the way for real life application of process based models.

3) What is the sensitivity of the model to changes in input values?
A sensitivity analysis is carried out using the 2DV case study model. The bed slope parameter is found to have a significant influence on both the wave height and the maximum slope steepness of the sand waves at the end of the simulation. For a higher value of the bed slope parameter, which lead to stable sand wave heights, the slope steepness would reduce significantly. On the other hand, for a decreased bed slope parameter, the steepness of the sand wave would be better maintained throughout the simulation, but sand waves showed considerable growth. The bed roughness showed a similar dependency, where a rougher bed resulted in amplified sand wave growth and steeper slopes. For a more smooth bed, the sand wave growth was reduced and the steep slopes became more gentle during the simulation. The influence of the sediment diameter on the morphological results was found to be limited, although this might be caused by the exclusion of suspended sediment transport.

4) What is the importance of 3D effects for the local sand wave dynamics?
Even in a fairly regular sand wave field, without much variation in sand wave migration direction, 3D effects in hydrodynamics can be of importance to morphology. In a 3D flow field the variations in flow velocity and direction over a sand wave field are better represented. Furthermore, the ellipsoidal character of the tide leads to 2D pattern of bed load transport directions. At the location of steep sand waves slopes the direction of sediment transport is significantly influenced by bed slope transport. This might cause deviations between the sediment transport direction and the flow direction at the bed. These factors make the inclusion of a third dimension in sand wave modelling essential for a good representation of hydrodynamics and sediment transport. In areas where tidal sand banks are present, these 3D effects are expected to be even larger (Leenders, 2018).

Opportunities and challenges of Delft3D FM for prediction of sand wave field dynamics

The goal of this research is to explore the opportunities and challenges of Delft3D FM for quantitative modelling of sand wave dynamics in the North Sea. These opportunities and challenges are found in various domains and are summarised below.

Opportunities

1. **Reduction of computation times**
    - **Increased code efficiency**
      In Chapter 4 it is shown that even for a smaller average time step a computation time reduction of over 50% is realized in Delft3D FM relative to Delft3D-4.
    - **Running in parallel**
      The Delft3D FM model has the unique ability to split the model domain into partitions which can be run in parallel. The results of a 2DV sand wave model simulated as a whole are identical to those generated when a model is run in parallel, see Appendix D. In 2DV set-up a model with 8 partitions showed an approximately linear increase in computational speed compared to a model run on a single core.
    - **Unstructured grids**
      Another important improvement which is implemented in Delft3D FM is the use of unstructured grids. Such a grid was used in the 3D modelling study in Chapter 6. While orthogonality and smoothness of the grid were kept in mind, no significant impacts of the coupling of grid cells of different shapes and sizes were found. Through the use of these kind of grids local refinements can be made inside the model domain. The fine grids needed in the sand wave area in that case do not have to be extended throughout the whole modelling domain. These refinements can also be used to increase accuracy around structures such as monopiles without the need for domain decomposition.
    - **Morphological scale factor**
      In this study a morphological scale factor (MF) was used to obtain the presented results. This method to accelerate morphological changes is also present in other numerical models like Delft3D-4. Because of the repetitiveness of the hydrodynamic forcing, sand wave growth and migration represents a suitable case for the use of a MF. The results for different values of this factor are practically identical at least up to an acceleration of 2000 times, see Appendix A.2.
    - **Optimized time-step management**
      In contrast to Delft3D-4 the Delft3D FM model uses a time-varying, model defined time step. This time step can thus be adjusted during the simulation to match changes in flow velocity (see Figure 4.13). Especially at times with low flow velocities (e.g. during slack) this increases the time-step significantly, leading to shorter computation times for Courant limited computations.
    - **Accurate boundary conditions**
      Increased accuracy of boundary conditions could potentially reduce the needed buffer zone (see 3).
2. **Embedding in existing models**
   Through the use of unstructured grids, existing Delft3D FM models can be adjusted to include sand wave areas with local fine grids. This significantly reduces the set-up time for the model as the boundary conditions, calibration and validation of the overarching model has already been carried out. Furthermore this introduces the possibility of including multiple areas of interest in one model (with local grid refinements) and carrying out calculations for both areas at once.
3. **Good representation of velocity and water level**
   Using the new advection velocity boundary type a good match of water levels and velocities can be accomplished. More information than usual has to be prescribed, but when this data is available (which is the case for nesting in regional models) the water level and velocity match is improved significantly. This shows opportunities for decreasing the buffer area between the area of interest and the model boundaries, or even removing this area all together. Without a buffer area the computation time will be reduced and if the match of the boundaries is good enough the accuracy of hydrodynamics could be improved. Moreover, non-tidal currents (e.g. surge currents and currents due to tidal sand banks) can be incorporated more easily using this boundary condition.

Challenges

1. **Accuracy limited by available data**
   One of the limiting factors for the accuracy of simulations is the availability of in-situ data. The results of the model are only as good as its input. In the HKZWF case an extensive amount of data on local hydrodynamics and morphology is available. When less data is available the accurate representation of local processes driving sand wave dynamics becomes more difficult. This in turn results in increased uncertainties in sand wave predictions.

2. **Inclusion of small scale processes**
   Some processes influencing hydrodynamics and morphology are of a smaller scale than the cell sizes used in the model. These processes could be difficult to include in the model, while in data analysis they are implicitly included. One of such processes is the growth and migration of megaripples. These megaripples influence the local hydrodynamics through the bed roughness. Furthermore, being quite dynamic, they are responsible for some transport of sediment. Roughness predictors based on ripples have been developed and should be tested for this case. Difficulties do however arrive because of the variable character of these megaripples. Damveld et al. (2018) showed significant differences between the ripples in crest and trough areas of the sand waves. Ripples are also largely affected by momentary flow conditions and could therefore vanish during storms and sometimes show seasonality. Further study into the impact of these ripples on hydro- and morphodynamics could determine their importance in predicting sand wave dynamics.

3. **Calibration effort**
   The HKZWF 2DV and 3D models were not calibrated during the study. Further study should point out whether extensive calibration is needed. Especially when calibration is needed between different sites this could be limiting for the practical use of these predictions, due to the time and data needed for calibration (and validation).

These challenges could be resolved through further research. In this way the full potential of the Delft3D FM model could be discovered and prepared for future engineering applications.

Practical applications of Delft3D FM for the predictions of sand wave dynamics are found in numerous cases. The use of Delft3D FM could lead to deeper understanding of complex sand wave systems, especially in case of influences of underlying large scale bathymetry. In addition the Delft3D FM model could assist in understanding the migration of sand waves between two bathymetry measurements by increasing the temporal resolution. In this way seasonal or event based migration of sand waves can be identified. Since the model shows the ability to predict the influence of variations in environmental condition, these applications could already be explored, although the quantative morphological results still show room for improvement. When the morphological results of the Delft3D FM model are improved, through calibration or the inclusion of additional processes, the model could provide more accurate future seabed predictions. Thereby, Delft3D FM could provide a solution for data-sparse areas where sand wave predictions based on data-analysis are troublesome. Lastly the Delft3D FM model could provide insight into the recovery of sand waves after dredging (e.g. in case of pipeline installation).

The use of Delft3D FM for morphological predictions in sand wave areas may drastically change the way sand waves are dealt with in case of offshore construction. More insight into the processes paves the way for more nature based solutions, reducing the need for dredging. In this way Delft3D FM could contribute to reducing risks, costs and environmental impact of offshore construction projects in sand wave areas.

9 | Recommendations

Further research will increase the potential of the Delft3D FM model for sand wave predictions for engineering applications. The challenges found in the use of Delft3D FM, mentioned in the previous chapter, can (partly) be overcome through such research. Moreover, extended knowledge about the processes influencing sand wave dynamics in a 3D setting, which can be gained through the use of Delft3D FM, will improve predictions of sand wave dynamics as a whole. In this chapter some recommendations are discussed for further research.

Exploring the influences of different processes in 3D setting
In previous studies the effects of different processes on sand wave dynamics have been studied extensively. However, this was mostly done in a 2DV setting. Adding a third dimension could impact the influence of variability in environmental parameters and additional processes. Especially if these processes are inherently 3D, such as the ellipticity of the tide, this could have a significant impact on morphology. Moreover, Leenders (2018) showed that underlying 3D topography influences the migration of sand waves. Through 3D modelling the interaction of various processes with underlying bed forms can be explored.

Improving morphological results through calibration and/or inclusion of more processes
The morphological results of the case studies still showed significant deviation from measurements. The deviations of the morphological results could indicate incompleteness of the model. Since various processes have not been included, these could be the key to more accurate predictions. One of such processes is suspended sediment transport. Borsje et al. (2014) showed that suspended sediment has a dampening effect on sand wave growth and since the results of the case study show artificial growth of the sand waves, this process could be a missing piece. Other factors to consider are for example the inclusion of waves and wind driven currents. Moreover, further improvement of the boundary conditions could lead to more accurate morphological results.

Application of the model under different geophysical conditions
To explore the accuracy of the model under different geophysical conditions, different locations should be included in future model studies. For the case studies a location in the North Sea was chosen and the models were set-up in a limited area of the HKZWF. This means that the geophysical conditions were fairly regular throughout the model studies in this thesis. Differently shaped and sized sand waves as well as different environmental parameters could significantly influence the accuracy of the model results. The sand waves in the HKZWF area have a relatively high asymmetry compared to other locations in the North Sea (Damen et al., 2018). Since the morphological results from Delft3D FM were more accurate for the more gently shaped sand waves, this could mean that the model is more easily applicable than would seem from this study. Furthermore, especially in sand wave areas with large underlying bed forms the expansion to a third dimension is vital. The performance of the model should therefore be tested in such an area.
When calibrating the model to more accurately predict sand wave dynamics, these factors should be taken into account. Further study at different locations will indicate whether calibration between sites would be necessary. This will impact the effort needed for model predictions and thus affect the applicability of the model in an engineering setting.

Model optimization
Due to time restrictions of this research the models used are not optimized in terms of set-up. Especially in case of the 3D model such an optimization could potentially cause large reductions of computation times. Factors to consider in such an optimization are amongst others: number (and distribution) of sigma layers, size of the buffer area, grid size in area of interest, number of cores in parallel runs and value of the morphological scale factor. Through optimization (and possibly automation) the value of these models for engineering applications will increase.

References

4COffshore . Global Offshore Map. 2021. https://www.4coffshore.com/offshorewind/.

Algemene Rekenkamer . Kosten windenergie op zee. 2018. https://www.rekenkamer.nl/publicaties/rapporten/2018/09/27/focusonderzoek-kosten-van-windparken-op-zee.

Bao J., Cai F., Shi F., Wu C., Zheng Y., Lu H., Sun L. Morphodynamic response of sand waves in the Taiwan Shoal to a passing tropical storm // Marine Geology. 8 2020. 426.

Besio G., Blondeaux P., Brocchini M., Hulscher S.J.M.H., Idier D., Knaapen M.A.F., Németh A.A., Roos P.C., Vittori G. The morphodynamics of tidal sand waves: A model overview // Coastal Engineering. 7 2008. 55, 7-8. 657–670.

Besio G., Blondeaux P., Brocchini M., Vittori G. Migrating sand waves // Ocean Dynamics. 2003. 53, 3. 232–238.

Besio G., Blondeaux P., Brocchini M., Vittori G. On the modeling of sand wave migration // Journal of Geophysical Research. 4 2004. 109, 4.

Bijvelds M.D.J.P. Numerical modelling of estuarine flow over steep topography. 2001.

Blondeaux P., Vittori G. Formation of tidal sand waves: Effects of the spring-neap cycle // Journal of Geophysical Research. 2010. 115, 10.

Bomers A., Schielen R.M.J., Hulscher S.J.M.H. The infuence of grid shape and grid size on hydraulic river modelling performance // Environmental Fluid Mechanics. 2019. 19. 1273–1294.

Borsje B.W., Kranenburg W.M., Roos P.C., Matthieu J., Hulscher S.J.M.H. The role of suspended load transport in the occurrence of tidal sand waves // Journal of Geophysical Research: Earth Surface. 2014. 119, 4. 701–716.

Borsje B.W., Roos P.C., Kranenburg W.M., Hulscher S.J.M.H. Modeling tidal sand wave formation in a numerical shallow water model: The role of turbulence formulation // Continental Shelf Research. 6 2013. 60. 17–27.

Campmans G.H.P. Modeling storm effects on sand wave dynamics (PHD thesis). 2018. 118.

Cheng C.H., Soetaert K., Borsje B.W. Sediment characteristics over asymmetrical tidal sand waves in the Dutch north sea // Journal of Marine Science and Engineering. 6 2020. 8, 6.

Choy D.Y. Numerical modelling of the growth of offshore sand waves, A Delft3D model study. 2015. http://repository.tudelft.nl/.

Damen J.M., Van Dijk T.A.G.P., Hulscher S.J.M.H. Spatially Varying Environmental Properties Controlling Observed Sand Wave Morphology // Journal of Geophysical Research. 2018. 123. 262–280.

Damveld J.H., Borsje B.W., Roos P.C., Hulscher S.J.M.H. Horizontal and vertical sediment sorting in tidal sand waves: modeling the finite-amplitude stage // Journal of geophysical research. Earth surface. 2020. 125, 10.

Damveld J.H., Reijden K.J. van der, Cheng C., Koop L., Haaksma L.R., Walsh C.A.J., Soetaert K., Borsje B.W., Govers L.L., Roos P.C., Olff H., Hulscher S.J.M.H. Video Transects Reveal That Tidal Sand Waves Affect the Spatial Distribution of Benthic Organisms and Sand Ripples // Geophysical Research Letters. 11 2018. 45, 21.

De Koning R J. Sand Wave Dynamics Bedform analysis and dredging strategy design for South Channel, Melbourne, Australia. 2017. http://repository.tudelft.nl/.

Deltares . D-Flow Flexible Mesh User Manual. 2020a. https://content.oss.deltares.nl/delft3d/manuals/D-Flow_FM_User_Manual.pdf.

Deltares . Delft3D-FLOW User Manual. 2020b. https://content.oss.deltares.nl/delft3d/manuals/Delft3D-FLOW_User_Manual.pdf.

Deltares , Hasselaar R., Raaijmakers T., Riezebos H., Van Dijk T., Borsje B., Vermaas T. Morphodynamics of Borssele Wind Farm Zone WFS-I and WFS-II-final report. 2015.

Deltares , Luijendijk A., Roetert T., Dagalaki V., Forzoni A. Morphodynamics for Hollandse Kust (west) Wind Farm Zone. 2020.

Deltares , Paulsen B.T., Roetert T., Raaijmakers T., Forzoni A., Hoekstra R., Van Steijn P. Morphodynamics of Hollandse Kust (zuid) Wind Farm Zone. 2016a.

Deltares , Raaijmakers T., Roetert T., Bruinsma N., Riezebos H.J., Van Dijk T., Forzoni A., Vergouwen S., Grasmeijer B. Morphodynamics and scour mitigation for Hollandse Kust (noord) Wind Farm Zone. 2019.

Deltares , Raaijmakers T., Roetert T., Riezebos H.J., Van Dijk T., Borsje B., Vermaas T. Morphodynamics of Borssele Wind Farm Zone WFS-III, WFS-IV and WFS-V. 2016b.

Dobrochinski J. based on personal communication with the Deltares Software department. 2021.

Hulscher S.J.M.H. Tidal-induced large-scale regular bed form patterns in a three-dimensional shallow water model // Journal of Geophysical Research. 9 1996. 110, 9. 20727–20744.

Knaapen M.A.F. Sandwave migration predictor based on shape information // Journal of Geophysical Research. 12 2005. 110, 4.

Leenders S. Numerical modelling of the migration direction of offshore sand waves using Delft3D Including underlying seabed topography. 2018.

Matthieu J., Borsje B.W., Hulscher S.J.M.H. Self-organizational properties of tidal sand wave fields modeling. 2013.

Matthieu J., Raaijmakers T. Interaction Between Offshore Pipelines and Migrating Sand Waves // Proceedings of the 31st International Conference on Ocean, Offshore and Arctic Engineering. 2012.

Morelissen R., Hulscher S.J.M.H., Knaapen M.A.F., Németh A.A., Bijker R. Mathematical modelling of sand wave migration and the interaction with pipelines // Coastal Engineering. 2003. 48, 3. 197–209.

Nemeth A.A. Modelling offshore sand waves. 2003. 141.

Nemeth A.A., Hulscher S.J.M.H., De Vriend H.J. Offshore sand wave dynamics, engineering problems and future solutions. 2003.

O'Flaherty-Sproul Mitchell. ttide_py. 2021. https://github.com/moflaher/ttide_py.

Rijksoverheid . Kabinet maakt plannen bekend voor windparken op zee 2024-2030. 2018. https://www.rijksoverheid.nl/actueel/nieuws/2018/03/27/kabinet-maakt-plannen-bekend-voor-windparken-op-zee-2024-2030.

Rijksoverheid . Windenergie op zee. 2020. https://www.rijksoverheid.nl/onderwerpen/duurzame-energie/windenergie-op-zee.

Roos P.C., Hulscher S.J.M.H. Large-scale seabed dynamics in offshore morphology: Modeling human intervention // Reviews of Geophysics. 2003. 41, 2.

Tonnon P.K., Rijn L.C. van, Walstra D.J.R. The morphodynamic modelling of tidal sand waves on the shoreface // Coastal Engineering. 4 2007. 54, 4. 279–296.

Van Gerwen W., Borsje B.W., Damveld J.H., Hulscher S.J.M.H. Modelling the effect of suspended load transport and tidal asymmetry on the equilibrium tidal sand wave height // Coastal Engineering. 6 2018. 136. 56–64.

Van Raaij Volkskrant. Fors meer windparken op zee in 2050: de EU mikt op 25 keer zoveel als nu. 2020. volkskrant.nl/nieuws-achtergrond/fors-meer-windparken-op-zee-in-2050-de-eu-mikt-op-25-keer-zoveel-als-nu~b507cf23/.

Van Rijn L.C. Principles of sediment transport in rivers, estuaries and coastal seas. 1993.

Wang Z., Liang B., Wu G., Borsje B.W. Modeling the formation and migration of sand waves: The role of tidal forcing, sediment size and bed slope effects // Continental Shelf Research. 11 2019. 190.

Zijl F., Veenstra J., Groenenboom J. The 3D Dutch Continental Shelf Model-Flexible Mesh (3D DCSM-FM) Setup and validation. 2018.

van Oyen T., Blondeaux P. Grain sorting effects on the formation of tidal sand waves // Journal of Fluid Mechanics. 2009. 629. 311–342.

A Additional results Delft3D-4 and Delft3D FM comparison

In this Appendix additional hydrodynamic and morphological results are shown for the simplified models used in Chapter 4. First the hydrodynamics over time are displayed for the 400 m wavelength model. Secondly the morphological results of the 1 year model are shown. Lastly the results for another wavelength: L = 160 m, where the difference between the models is slightly larger, are presented.

A.1 Additional hydrodynamic and morphological results

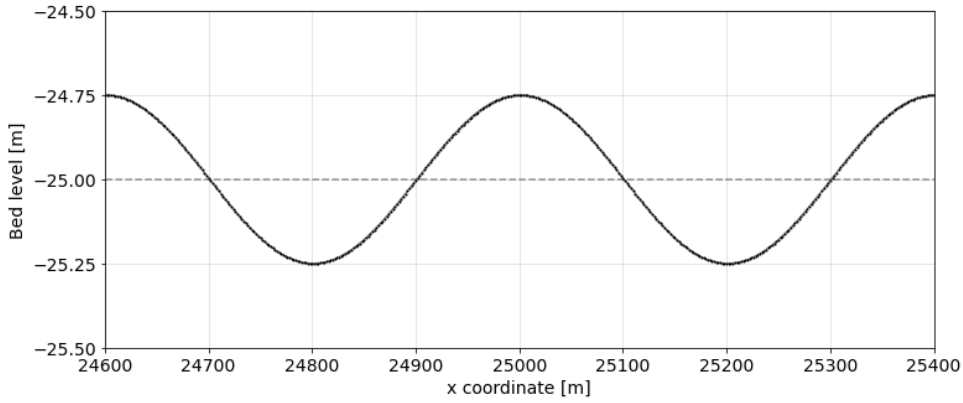

Figure A.1: Bed level at center of the domain, for L = 400 m

In Figure A.2 and Figure A.3 the variations in eddy viscosity and horizontal velocity over time for both models are shown. There is a clear difference in magnitude of the eddy viscosity between the models. The horizontal velocities are very similar between the models. In both the eddy viscosity and the horizontal velocity a small

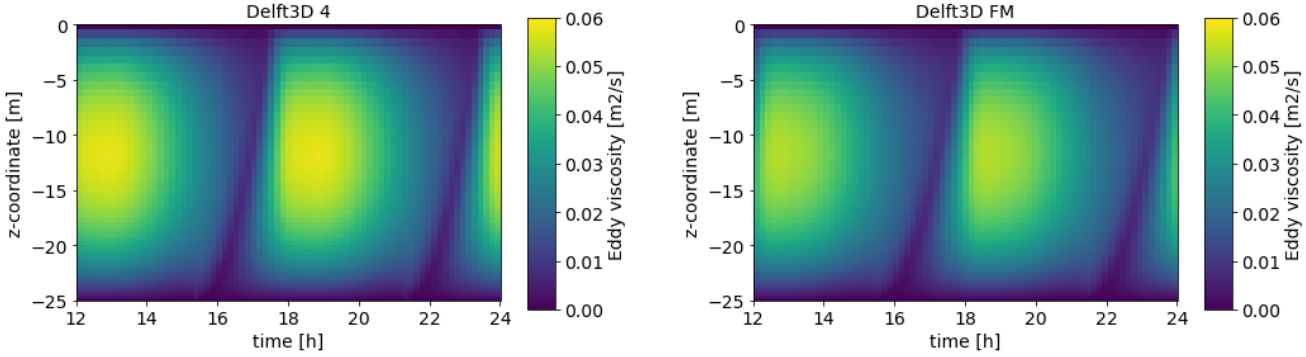

(a) Eddy viscosity over time from Delft3D-4

(b) Eddy viscosity over time from Delft3D FM

Figure A.2: Eddy viscosity over time at the middle of the sand wave domain (x = 25000 m) above the crest of the sand wave

phase lag (of around 10 minutes) is present in the Delft3D FM model compared to the Delft3D-4 model. This lag is probably caused by the difference in boundary condition definition. Where in Delft3D-4 the velocity is directly affected at the boundaries in Delft3D FM the change in water level still has to induce flow velocities.

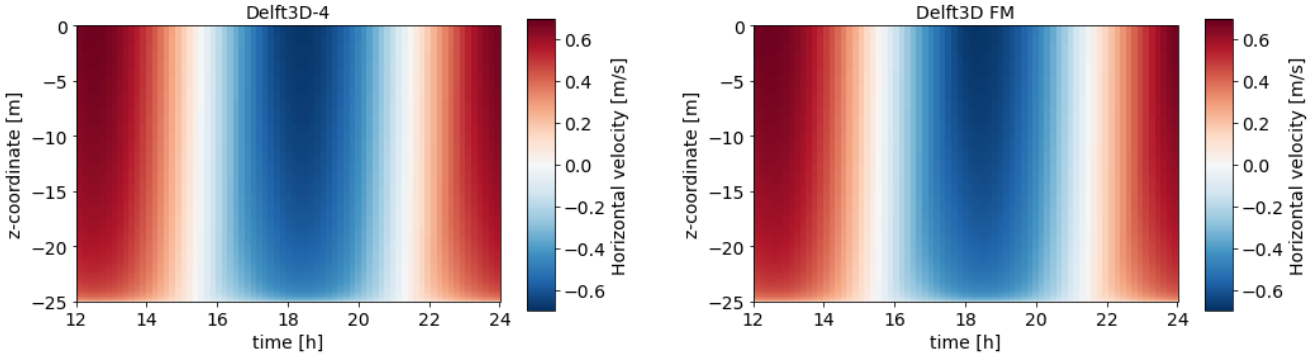

(a) Horizontal velocity over time from Delft3D-4

(b) Horizontal velocity over time from Delft3D FM

Figure A.3: Horizontal velocity at the middle of the sand wave domain (x = 25000 m) above the crest of the sand wave

In Figure A.4 the horizontal flow velocity at bed, bed shear stresses and bed load transport over time are shown. The Delft3d-4 model has a higher flow velocity in the cell closest to the bed, resulting in a higher bed shear stress and an increased bed load transport magnitude relative to Delft3D FM. The relations between these variables are observed to be similar between the models. Since these variables are extracted at the middle of the (left) flank, where the tide-averaged bed load transport is maximized, some inequalities between the flood and ebb values are seen.

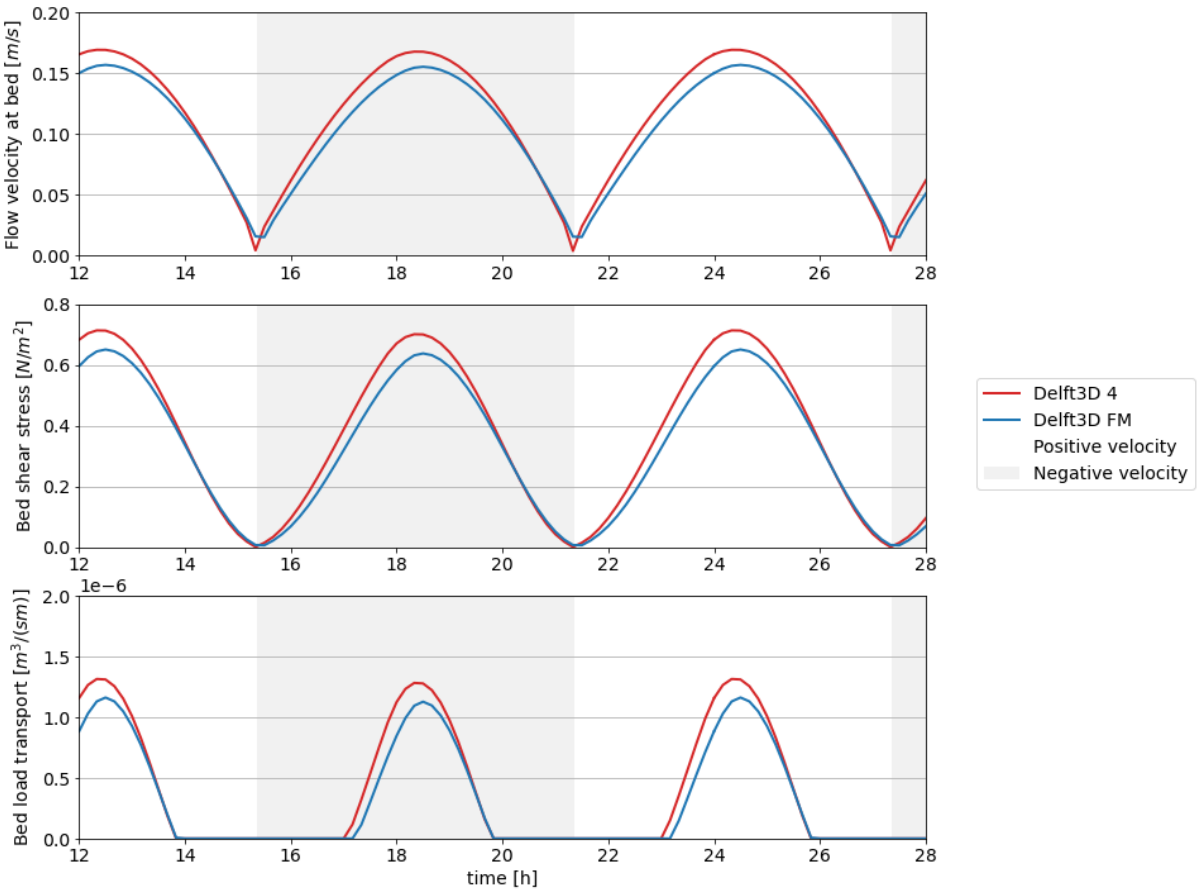

Figure A.4: Horizontal flow velocity at bed, bed shear stress and bed load transport over time at the middle of the left flank of the center sand wave (x = 24900 m)

In addition to the model with a duration of 10 years, a model was set up with 1 year of morphological change. The model has an identical set up as the the model discussed in Chapter 4, except from a lower morphological scale factor, which is in this case 52 (instead of 520). The hydrodynamics are modelled for 7 days (excluding one tidal cycle spin-up) to reach a morphological period of 1 year.
In Figure A.5 the bed level difference between the final and initial bathymetry is shown for the case with and without residual current. Again the changes in bed level are larger for the case including residual current. Both models show a small trench at the center of the domain, the initial location of the sand wave crest, in the final bathymetry of the model without residual current. This small trench has disappeared in the results after 10 years. Apart from this the shape of the bed level change curve is very similar to the results after 10 years. The magnitude of the erosion and sedimentation is less than 1/10 of the volume after 10 years, indicating non linear erosion and sedimentation.

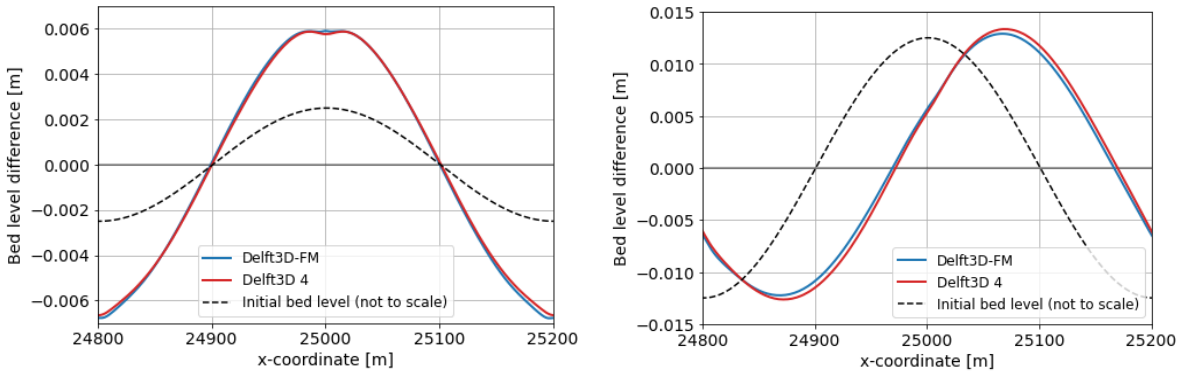

(a) Bed level change after 1 year excluding residual current

(b) Bed level change after 1 year with residual current U0 = 0.05 m/s

Figure A.5: Bed level change after a morphological period of 1 year for Case A: symmetrical (S2) and Case B: asymmetrical (S2 and U0) boundary conditions

A.2 Validation morphological scale factor

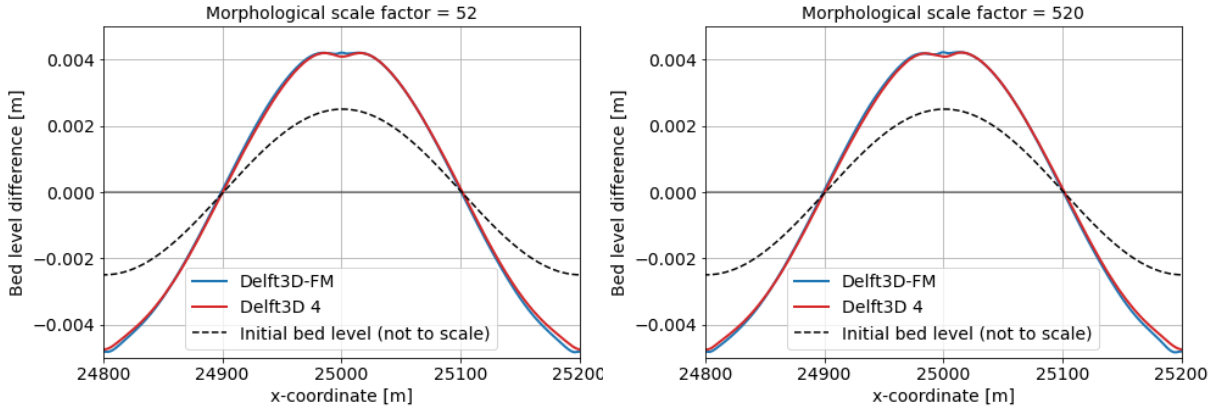

Figure A.6: Bed level change after a morphological period of 260 days for a morphological scale factor of 52 (left) and 520 (right)

With the results of the one year model the value used for the morphological scale factor can be validated. Since the only difference between the 1 year and 10 year models is the value of the morphological scale factor, the results should be identical for the same morphological time-spans. Both models have run for a whole number of tidal cycles at the moment of 260 days of morphological change. The bed level changes up to that point for both models can be seen in Figure A.6. From this Figure it is clear that a morphological scale factor as high as 520 does not significantly affect the morphological results. For the case with residual current similar results

were found.
The long-term model, run for 300 years of morphological change, uses a morphological scale factor of 2000. After one tidal cycle 1000 days of morphological change are simulated. Approximately the same time-span is used after 2 days of hydrodynamics in the 10 year model. The resulting bed level changes are shown in Figure A.7. The results are again very similar, indicating that a morphological scale factor of as high as 2000 is still acceptable in this case. The 10 year model shows slightly bigger changes in bed level, since the morphological times are not perfectly matched (the morphological time is 40 days longer in the left plot).

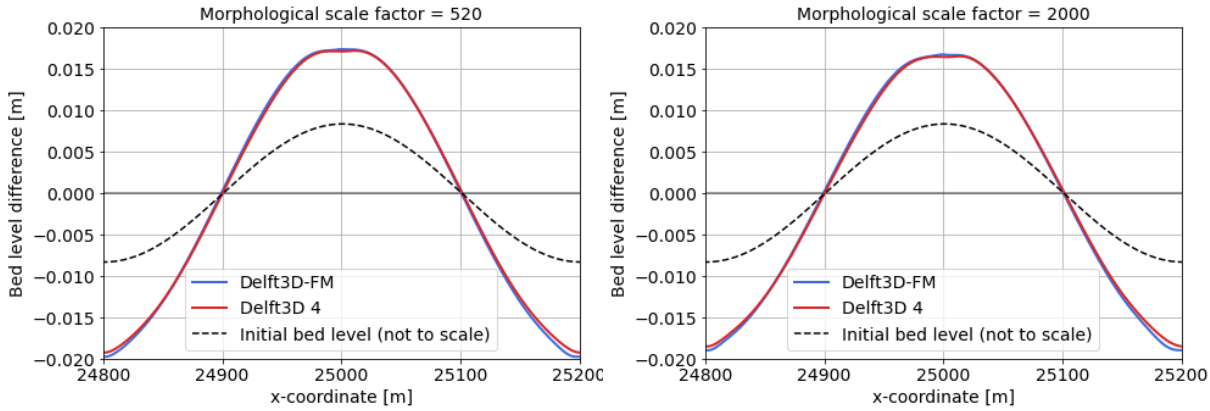

Figure A.7: Bed level change after a morphological period of 1040 days for a morphological scale factor of 520 (left) and after 1000 days with factor 2000 (right)

A.3 Results different wave length

The set-up of the base model used in Chapter 4 with a sand wave length of 400 m was also used to simulate the growth and migration of sand waves with different wavelengths. In this section the results for sand waves with a wave length of 160 m are included. For this wave length the difference in growth rate between the Delft3D-4 and the Delft3D FM model was observed to be larger. In the plots below the same hydrodynamic and morphological results are shown as those presented for the 400 m wave length case. In general very similar results were found between the two cases. In Figure A.8 the initial bed level of the simulation with a sand wave length of 160 m is shown. For other model set-up parameters reference is made to Chapter 4.

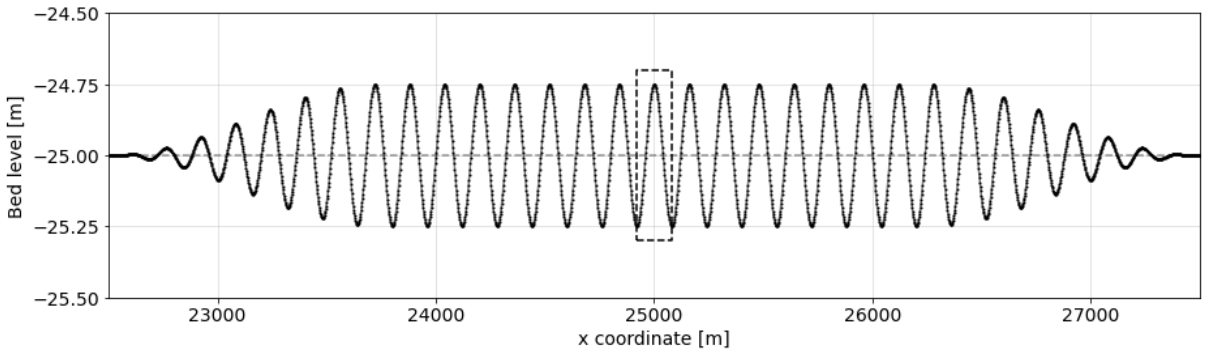

Figure A.8: Initial bed level with L = 160 m and A = 0.25 m. Box indicates location of Figure A.10

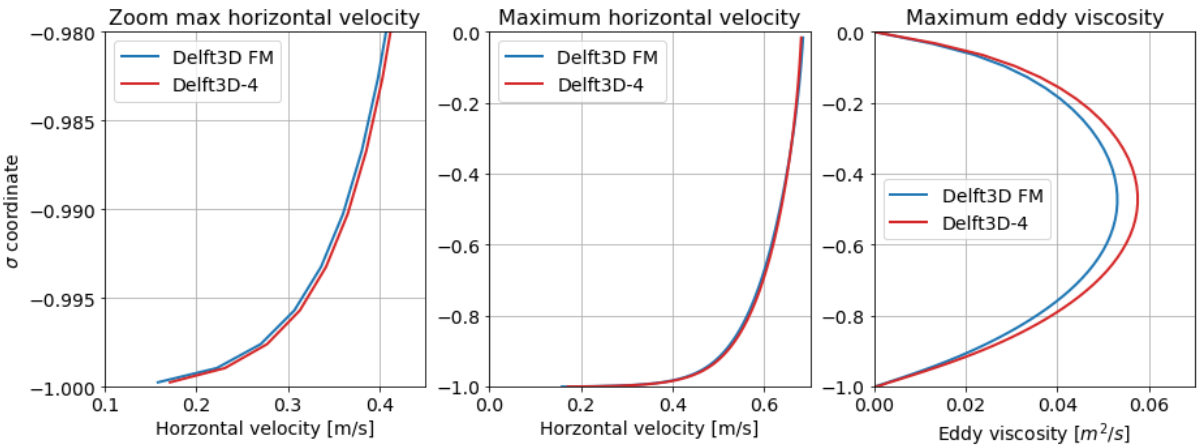

Figure A.9: Maximum horizontal velocity and eddy viscosity during flood at the crest of the sandwave at x = 25000 (middle of the domain), Case A: symmetrical S2 tide (L = 160 m)

The tide-averaged velocity field shows that the point of flow reversal lies closer to the bed for this shorter wave length. Furthermore, the tide-averaged return velocities higher up in the water column are found to be lower. These differences are clearly distinguishable in Figure A.11, where the tide-averaged flow velocity at the center of the flank is presented for both models. The point of tide-averaged flow reversal lies lower in the the Delft3D FM model relative to the Delft3D-4 model, as was seen in the original model.

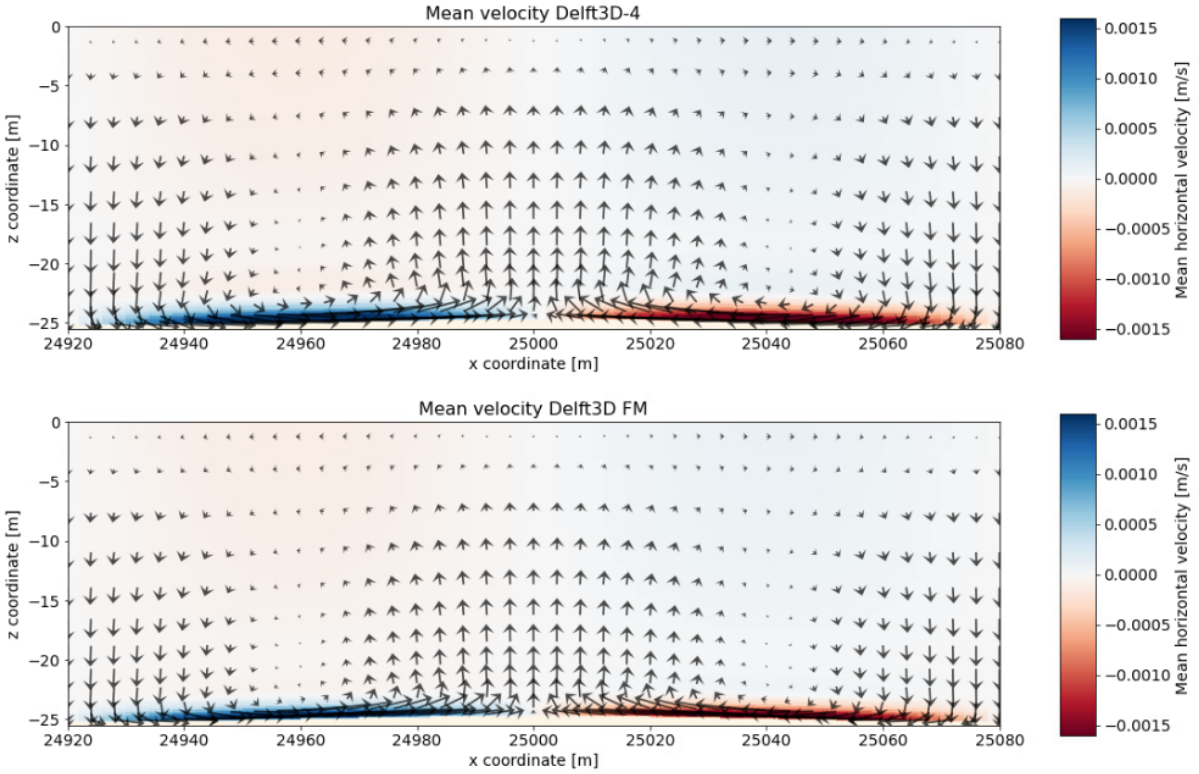

Figure A.10: Tide-averaged velocity, Case A: symmetrical S2 tide (L = 160 m). For location see Figure A.8. Vertical velocities not to scale

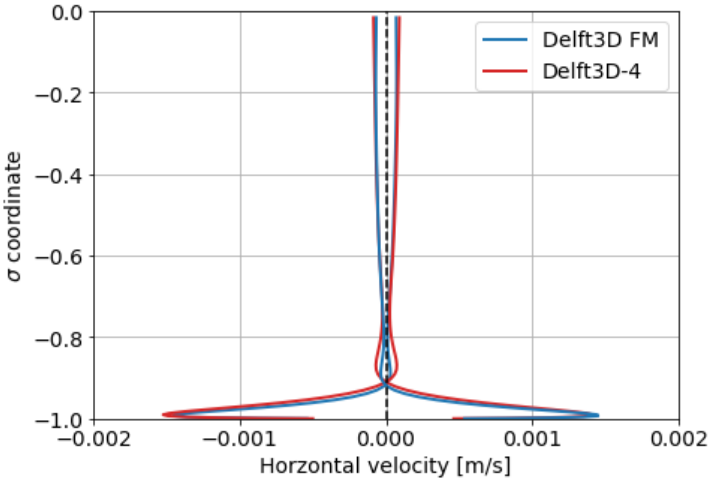

Figure A.11: Tide-averaged velocity at the middle of the sand wave flanks (x = 24960 m and x = 25040 m), Case A: symmetrical S2 tide, L = 160 m

The horizontal flow velocity at the bed, bed shear stress and instantaneous bed load transport are again higher for the Delft3D-4 model, relative to Delft3D FM. The same relations between these parameters are found in both models, as is clear from Figure A.12.

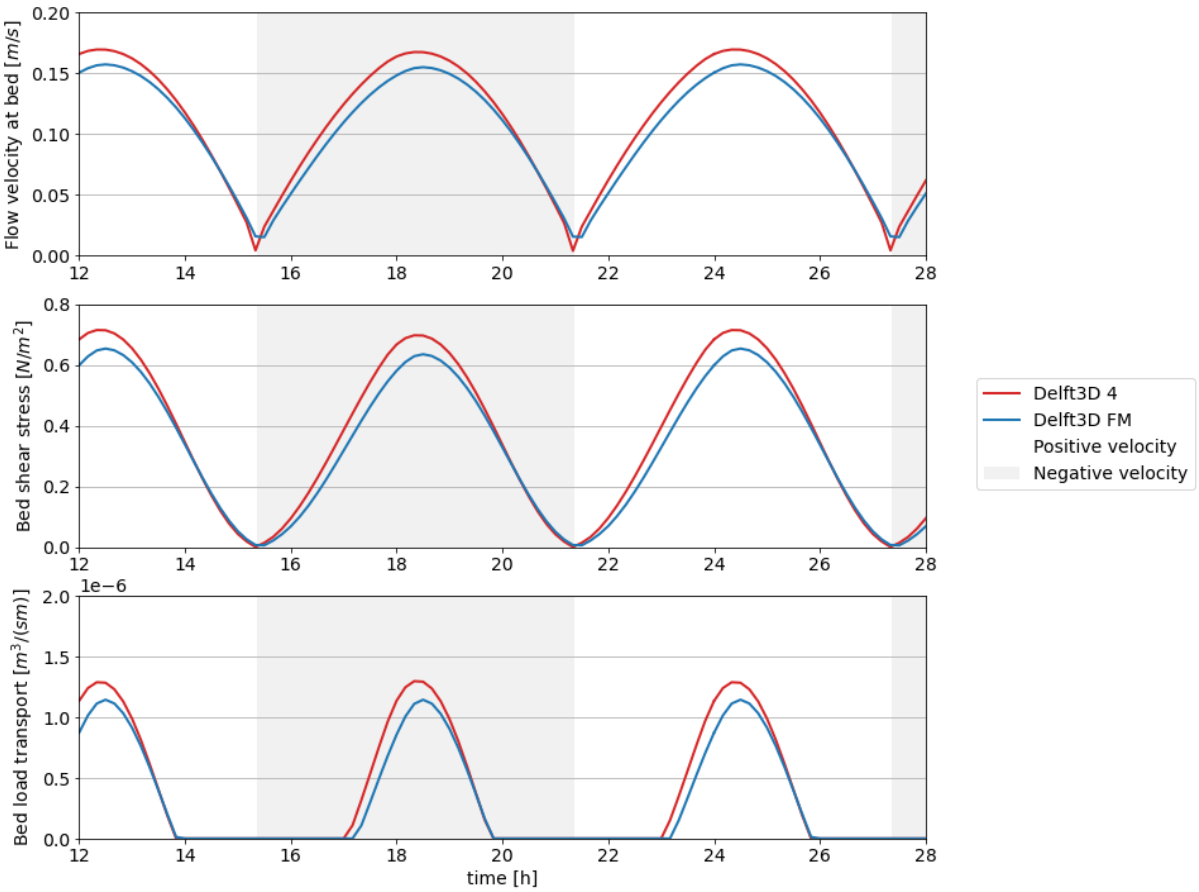

Figure A.12: Horizontal flow velocity at bed, bed shear stress and bed load transport over time at the middle of the left flank of the center sand wave (x = 24960 m)

In Figure A.13b the bed level change after 1 year of morphological change is shown. The differences between the models are in this case bigger than in the original model with a wave length of 400 m. The sand wave

growth rate in the Delft3D-4 model is smaller than in Delft3D FM, although both show a positive growth rate. The inequality of the growth rates is most likely caused by differences in the implementation of the bed slope related transport. A model in which this transport mode is neglected showed a reduced difference in growth rate and a higher growth rate for the Delft3D-4 model for this wave length. Both models show a dip in sand wave growth at the location of the crest. This could either cause a flattening of the crest or the development of two separate crests. A similar phenomenon was found in a study by Choy (2015). In this study the sand waves are observed to develop two crests during growth, which join again to form a single crest after some time.

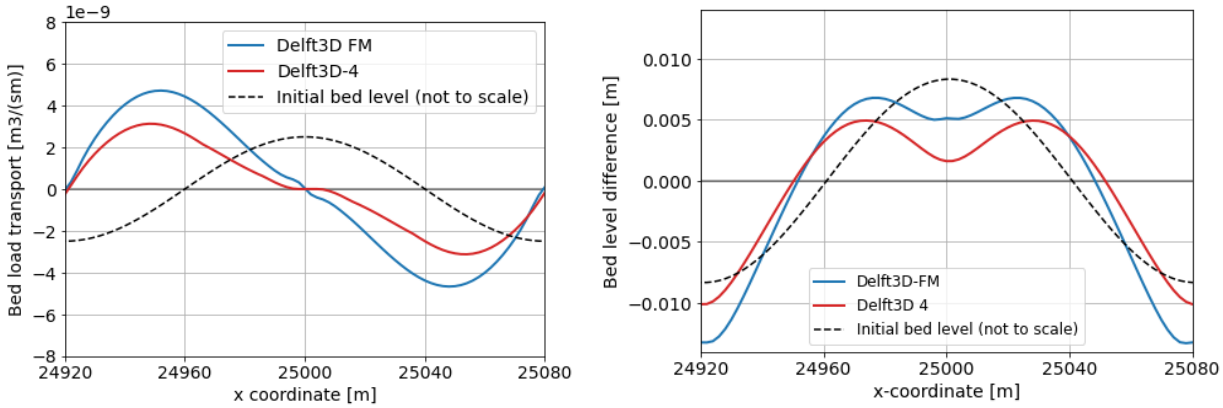

(a) Tide-averaged bed load transport, first tidal cycle, L = 160 m

(b) Bed level change after 1 morphological year for Case A: symmetrical S2 tide (L = 160 m)

Figure A.13: Average bed load transport and resulting bed level change for Case A: symmetrical S2 tide (L = 160 m)

B | HKZWF bathymetry smoothing

In this Appendix the reason for and the method of smoothening of the bathymetry used as the bed level in the simulation will be explained.

B.1 2DV model

For the bed level of the model a compounded 2010 bathymetry dataset is used. The dataset is filtered to extract large-scale bathymetry and megaripples (bed forms of smaller size). This filtered dataset is interpolated along the transects. After interpolation, wiggles with a height of around 0.1-0.2 m and horizontal scale of a few meters were found in the bathymetry. These disturbances are expected to be caused by measurement errors and/or incomplete filtering of the megaripples from the original measurements. The 2016 bathymetry, which has a higher measurement density, shows disturbances of a smaller size.
Due to the discretization of the Delft3D FM model the disturbances are smoothened during the simulation. Since the disturbances are either measurement errors or part of another bed form mode, the bathymetry is smoothened to filter out the wiggles. During this filtering the height of the sand wave should not (significantly) be reduced. To achieve this a simple filter was designed, which averages the bed level over an area with changing dimensions. At the gentler slopes of the bathymetry the area is increased up to a maximum of 60 m (30 in both directions). Closer to a steep slope the size of this area is reduced up to just the original data point on the steep slopes (in migration direction) of the bathymetry. The original bathymetry and smoothened bathymetry from the 2010 dataset are shown in Figure B.2 and Figure B.1. From the latter figure it is also clear that the filter does not significantly reduce the sand wave height. The 2016 bathymetry is also smoothened using the same filter for the comparison of model and measurement results.

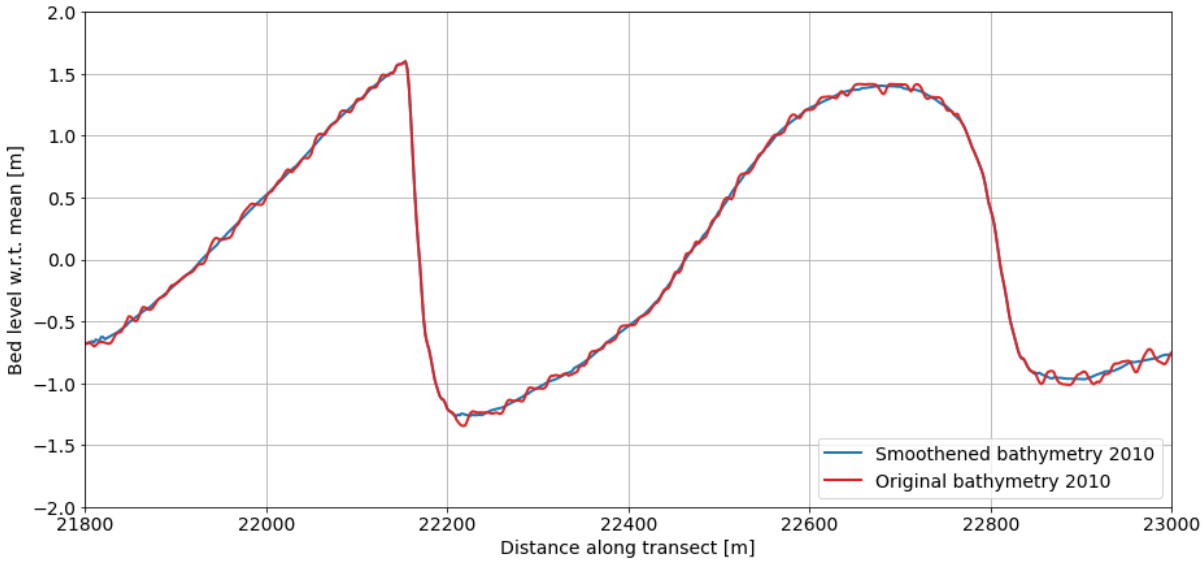

Figure B.1: Original and smoothened bathymetry East Transect HKZWF

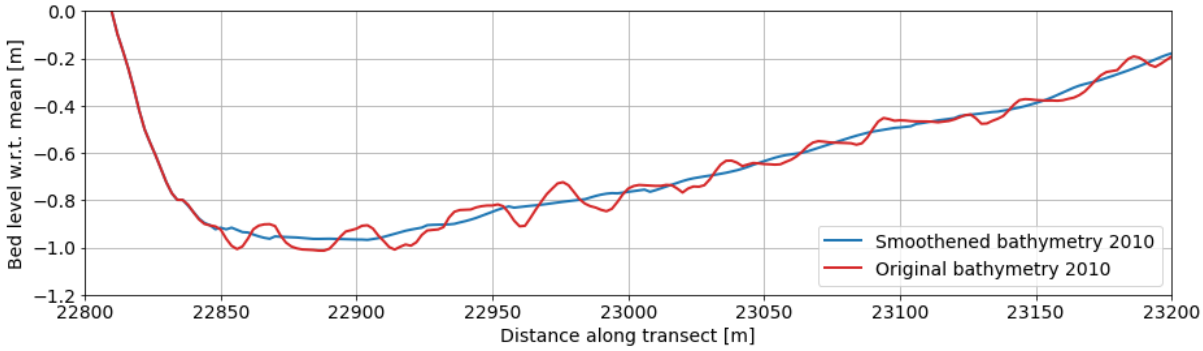

Figure B.2: Original and smoothened bathymetry East Transect HKZWF

B.2 3D model

To obtain the initial bed level of the 3D model the same filter is applied. The filter is first applied to the along crest direction and subsequently to the cross crest (sand wave migration) direction. Especially in the direction along the crests significant disturbances were found. Since the surveys are carried out in the direction approximately perpendicular to the sand wave crests, these errors most likely are caused by vertical referencing issues. These disturbances in along crest direction are shown in Figure B.4. In Figure B.3 the interpolated and smoothened bathymetry for the sand wave domain of the 3D HKZWF model are shown. This figure clearly shows that significant disturbances in along crest direction are indeed removed by the filter.

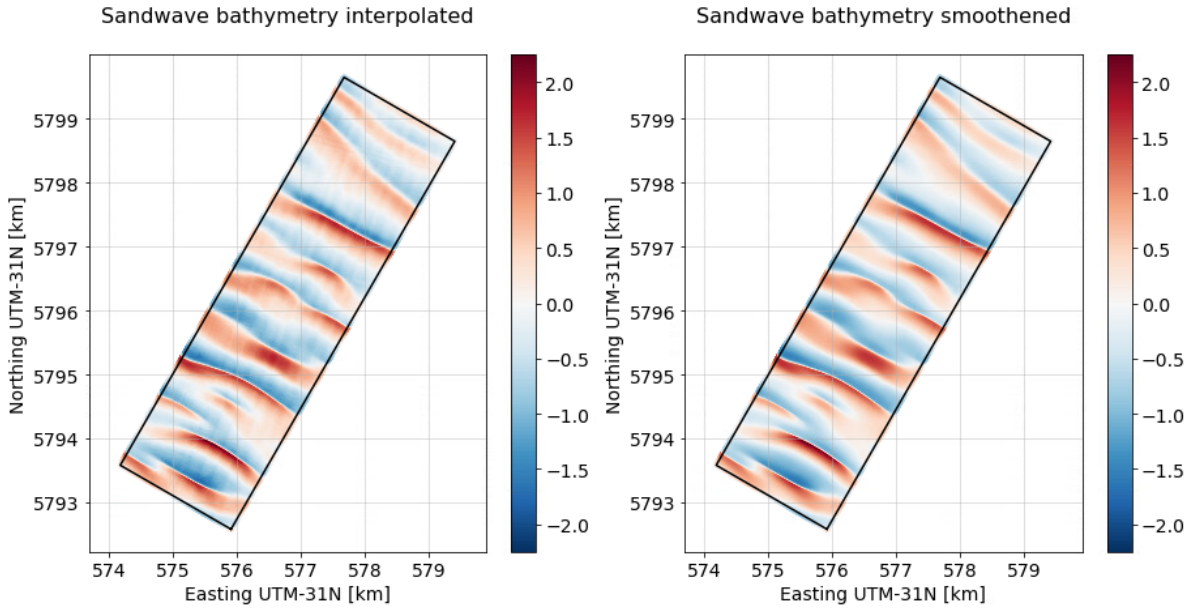

Figure B.3: Original and smoothened bathymetry 3D HKZWF model sand wave domain

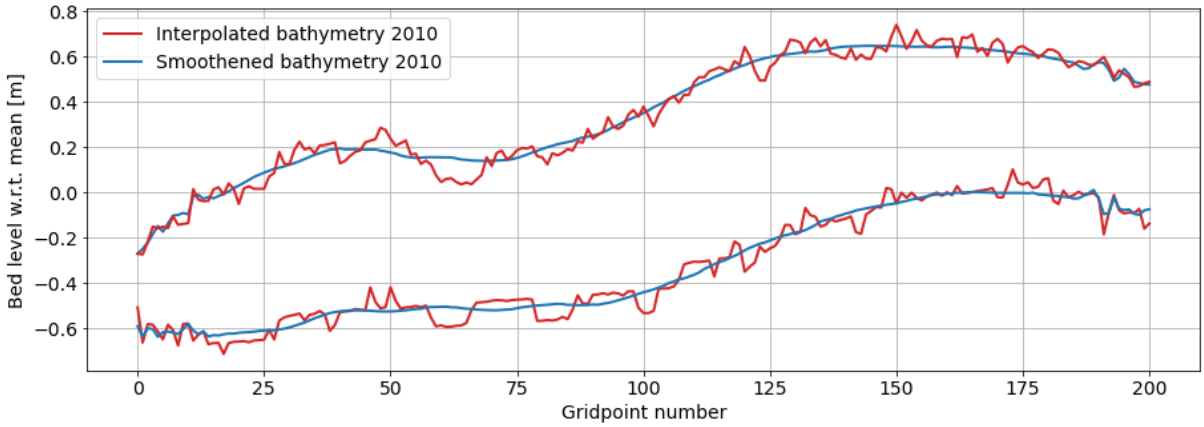

Figure B.4: Original and smoothened bathymetry 3D HKZWF model for two transects in along crest direction. Distance between the transects is 100 m

C | Additional results 2DV model HKZWF

Due to the extend of the results not everything could be included in the main report. In this Appendix the hydrodynamic and morphological results of the remaining parts of the 2DV East transect are shown. Subsequently the hydrodynamic and morphological results of the West 2DV transect are included.

C.1 Hydrodynamic results transect East

The figures in this section show the tide-averaged velocity patterns for the different tidal forcing cases tested in Chapter 5. The transect is split into four parts and the part that was already shown in the main report is also shown here for completeness. The definition of the cases and the respective forcing are repeated in Table C.1 and Table C.2.

Table C.1: Cases used in 2DV case study analysis transect East

Case	Tidal forcing	Residual current
I	M2	no
II	M2, S2	no
III	M2, S2, M4	no
IV	M2, S2, M4	yes
V	Full tidal signal	-

Table C.2: Forcing of the East transect Delft3D FM model at the far North and South boundary

Boundary	Variable	Constituent	Period (T) [min]	Amplitude (A)	Phase (ϕ) [deg]
South	Parallel velocity	M2	745	0.723 m/s	111
		S2	720	0.193 m/s	128
		M4	372.5	0.053 m/s	148
		U0	-	0.005 m/s	-
North	Water level	M2	745	0.573 m	138
		S2	720	0.148 m	174
		M4	372.5	0.198 m	205

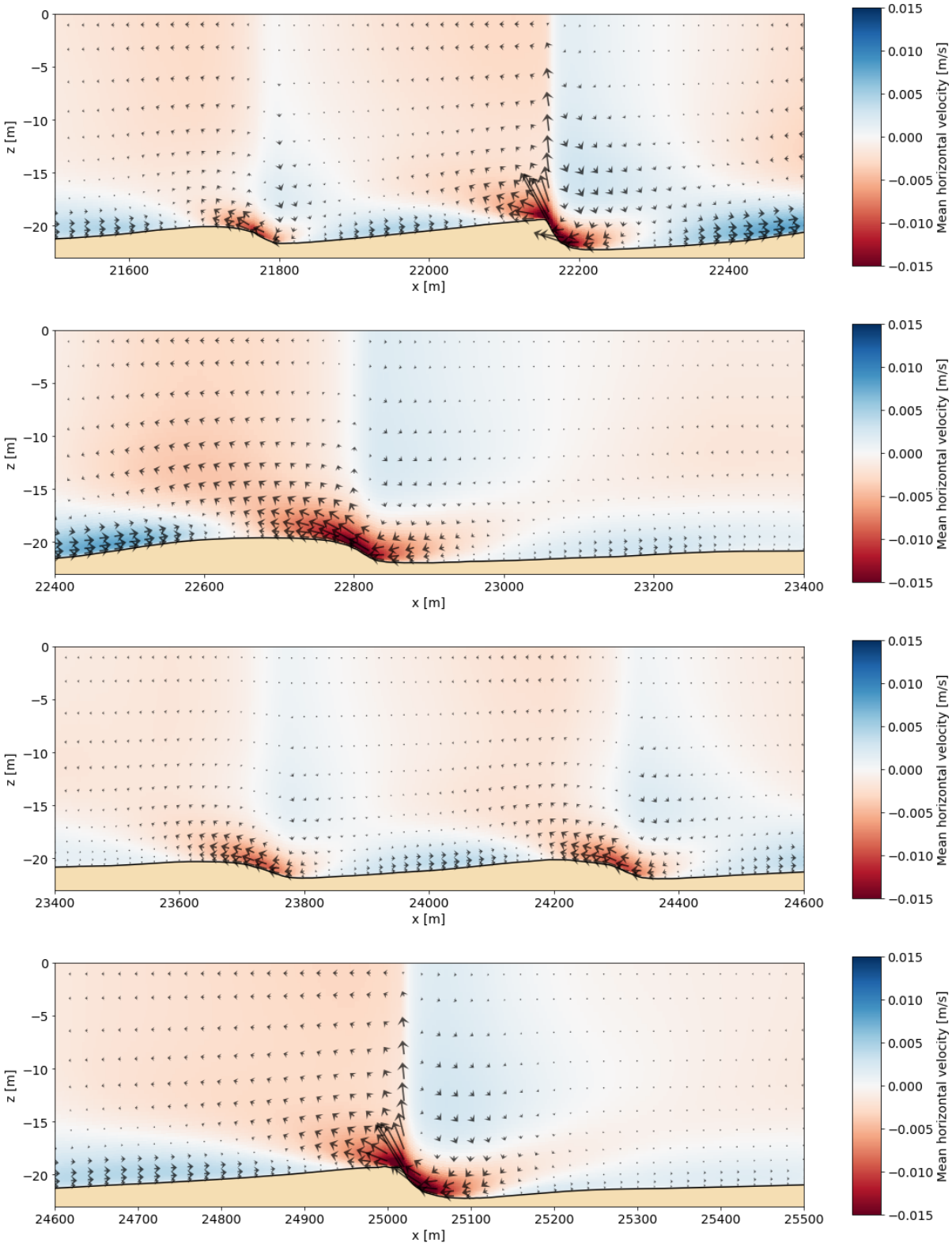

Figure C.1: Tide-averaged velocity field over the Eastern transect for M2 forcing (Case I). Colors indicate mean horizontal velocity, arrows combine direction and magnitude of the mean horizontal and (scaled) vertical velocity

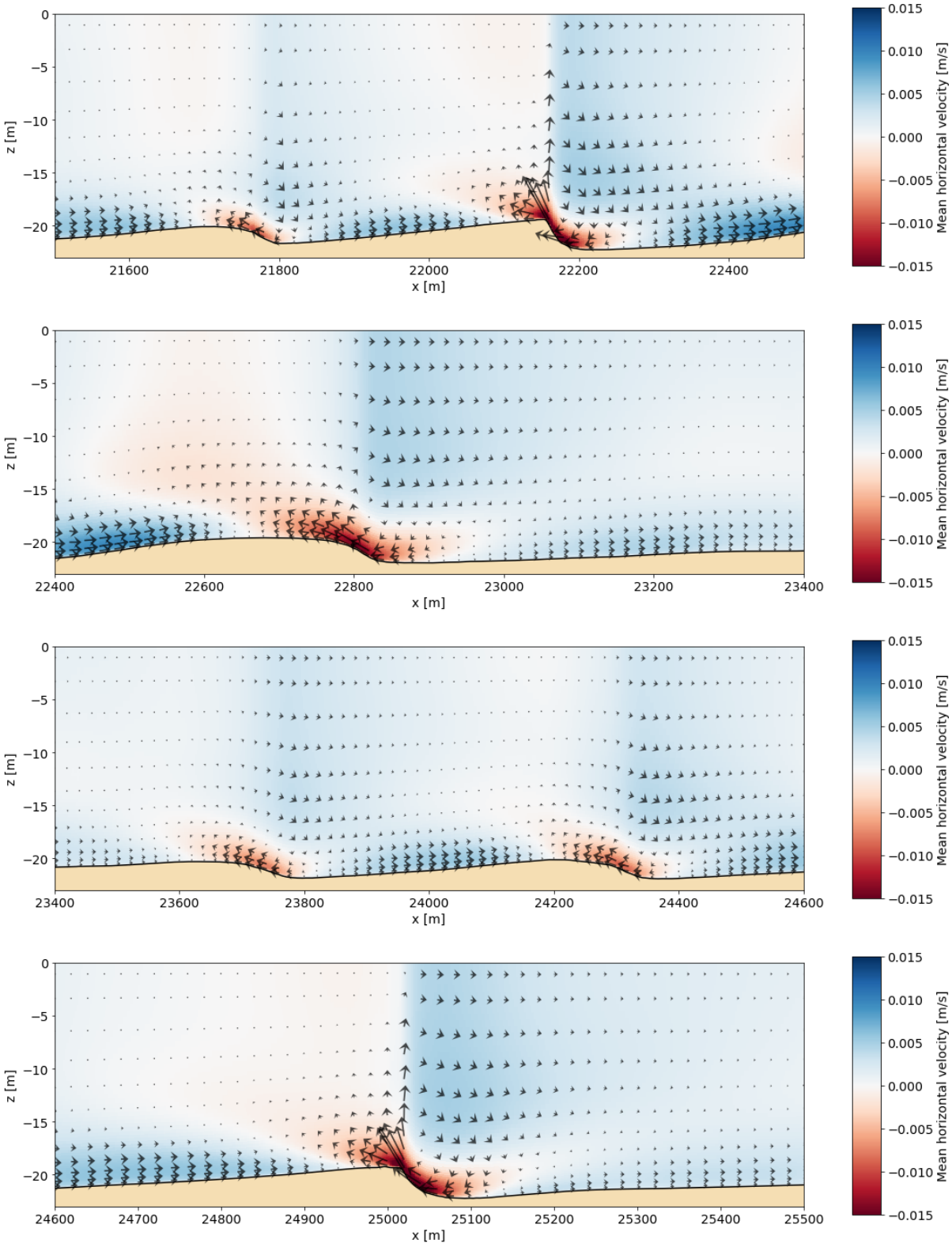

Figure C.2: Tide-averaged velocity field over the Eastern transect for M2 + S2 forcing (Case II). Colors indicate mean horizontal velocity, arrows combine direction and magnitude of the mean horizontal and (scaled) vertical velocity

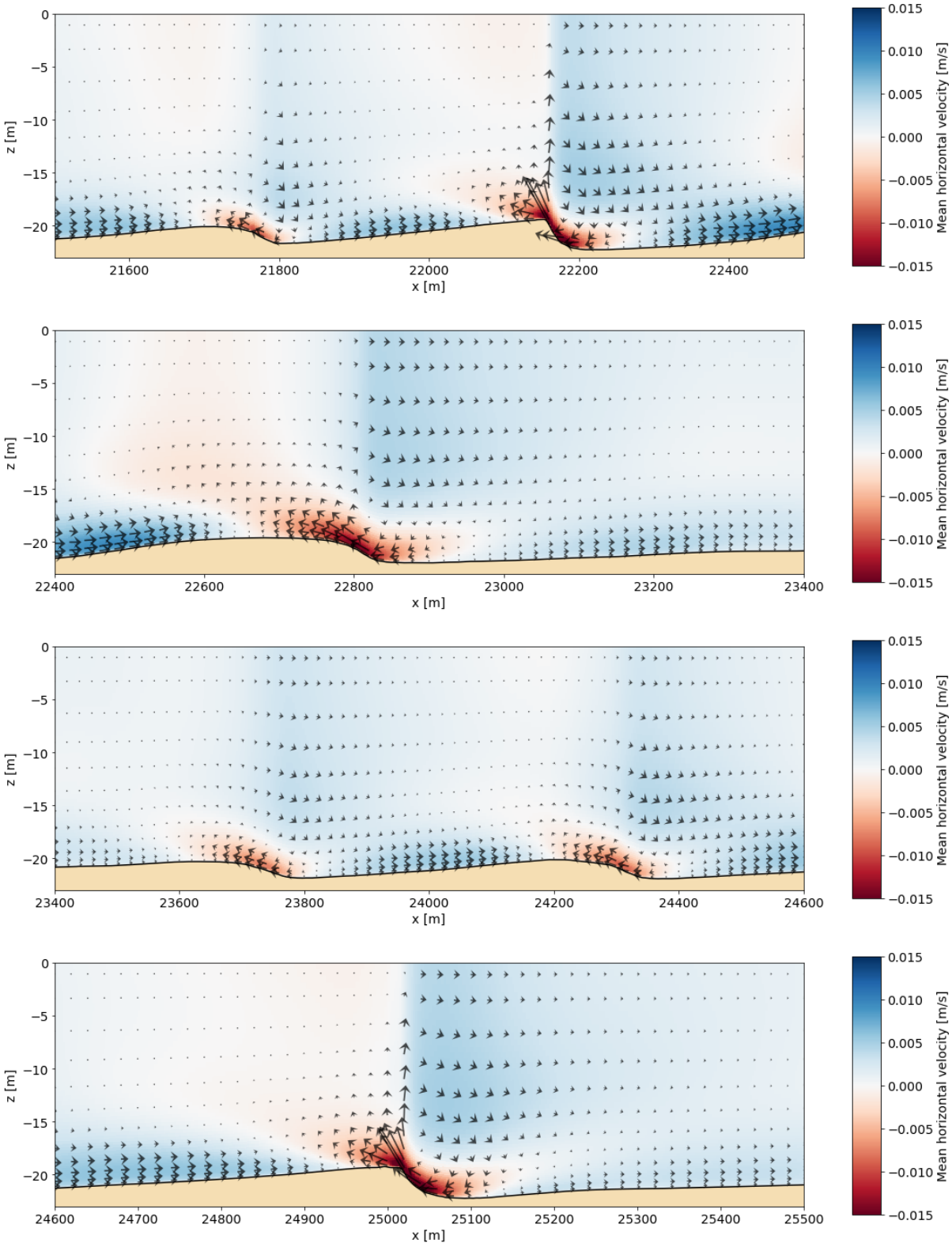

Figure C.3: Tide-averaged velocity field over the Eastern transect for M2 + S2 + M4 forcing (Case III). Colors indicate mean horizontal velocity, arrows combine direction and magnitude of the mean horizontal and (scaled) vertical velocity

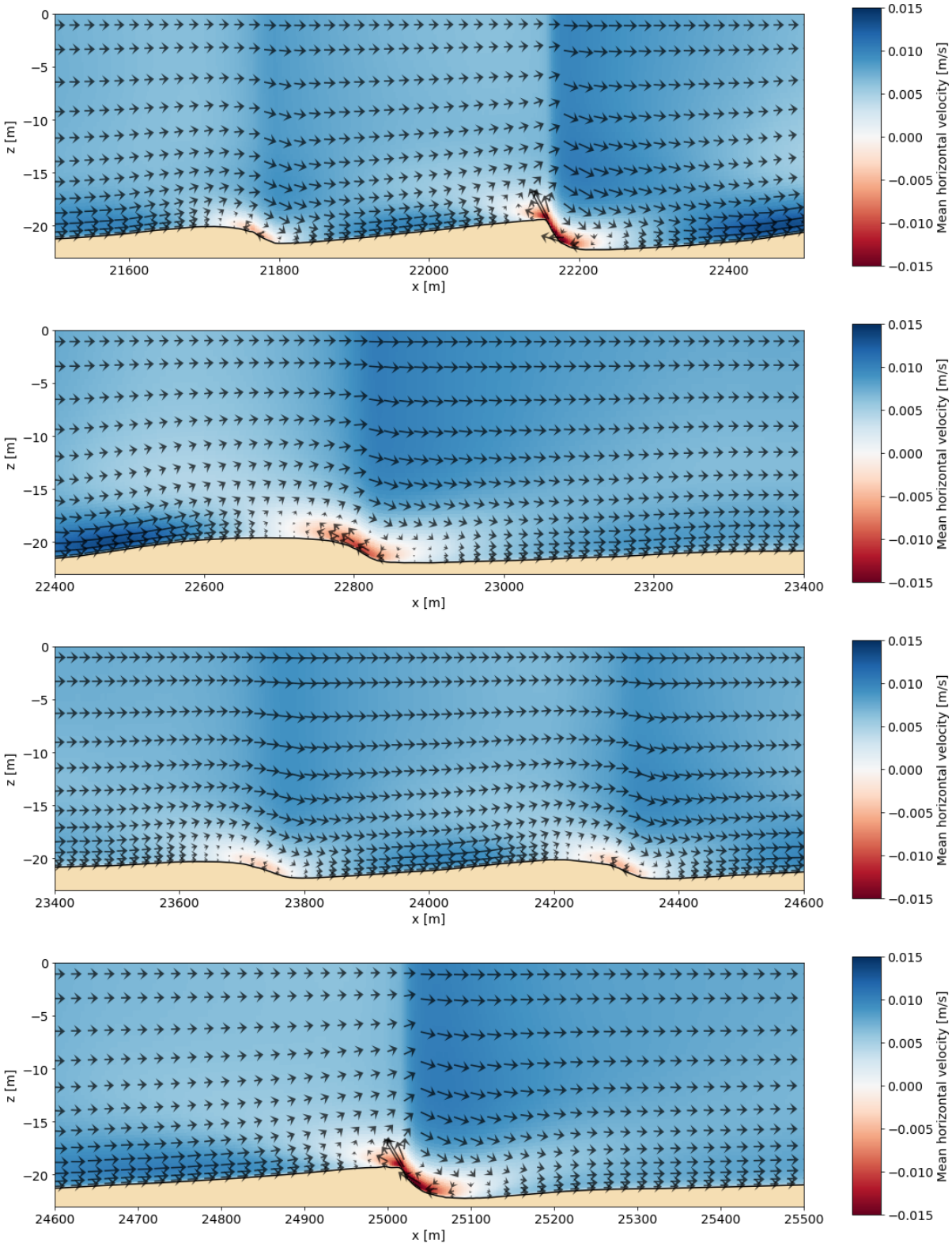

Figure C.4: Tide-averaged velocity field over the Eastern transect for M2 + S2 + M4 forcing including residual current (Case IV). Colors indicate mean horizontal velocity, arrows combine direction and magnitude of the mean horizontal and (scaled) vertical velocity

C.2 Morphological results transect East

In this section the morphological results are shown for all sand waves in the East transect for the different types of forcing used in the study. Due to the size of the differences the plots only show the lee side slope of the sand wave, where the differences between the models become apparent. The locations of the plots are clarified in Figure C.5.

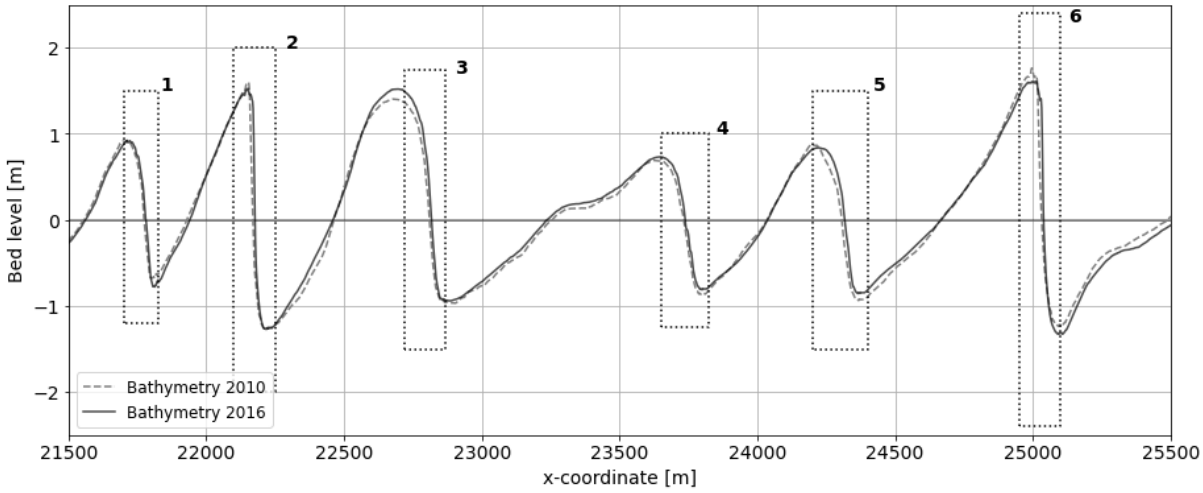

Figure C.5: Locations of plots showing morphological results, transect East

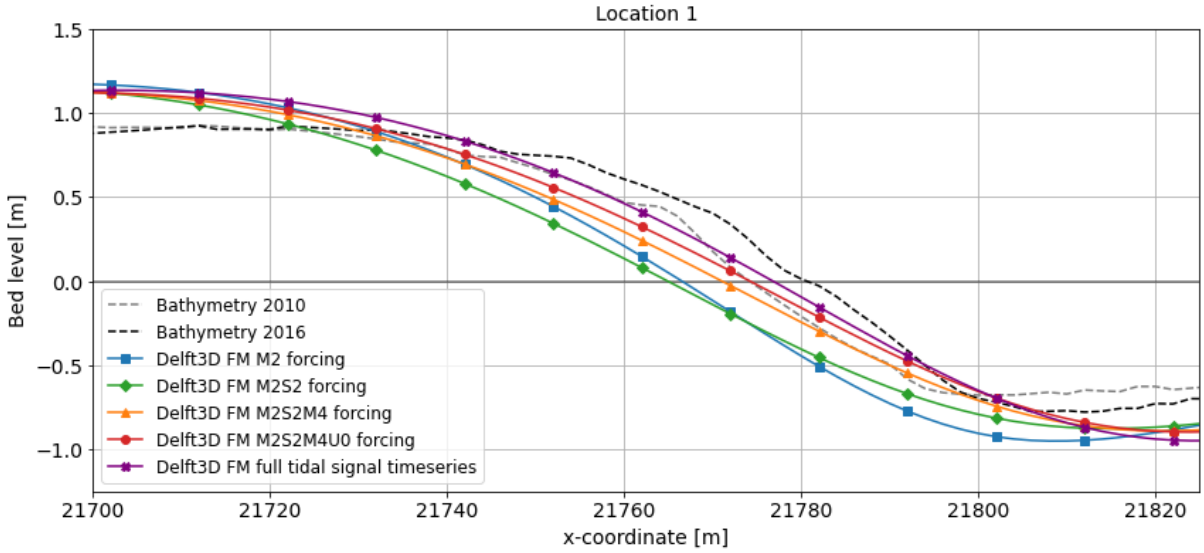

Figure C.6: Measured and computed bed level (after 6 years) for different forcing types, location 1, transect East

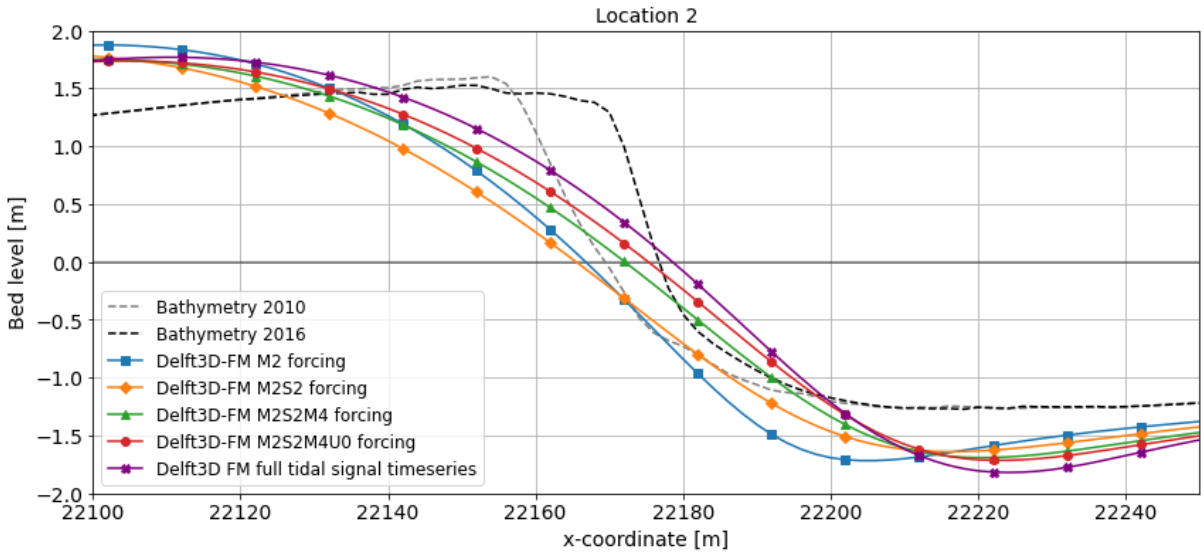

Figure C.7: Measured and computed bed level (after 6 years) for different forcing types, location 2, transect East

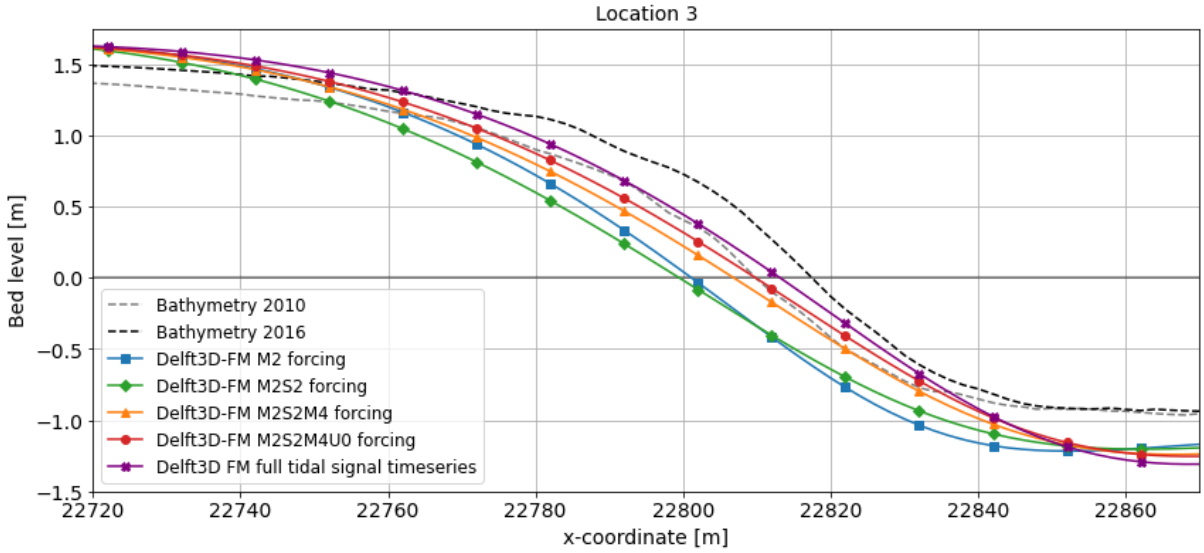

Figure C.8: Measured and computed bed level (after 6 years) for different forcing types, location 3, transect East

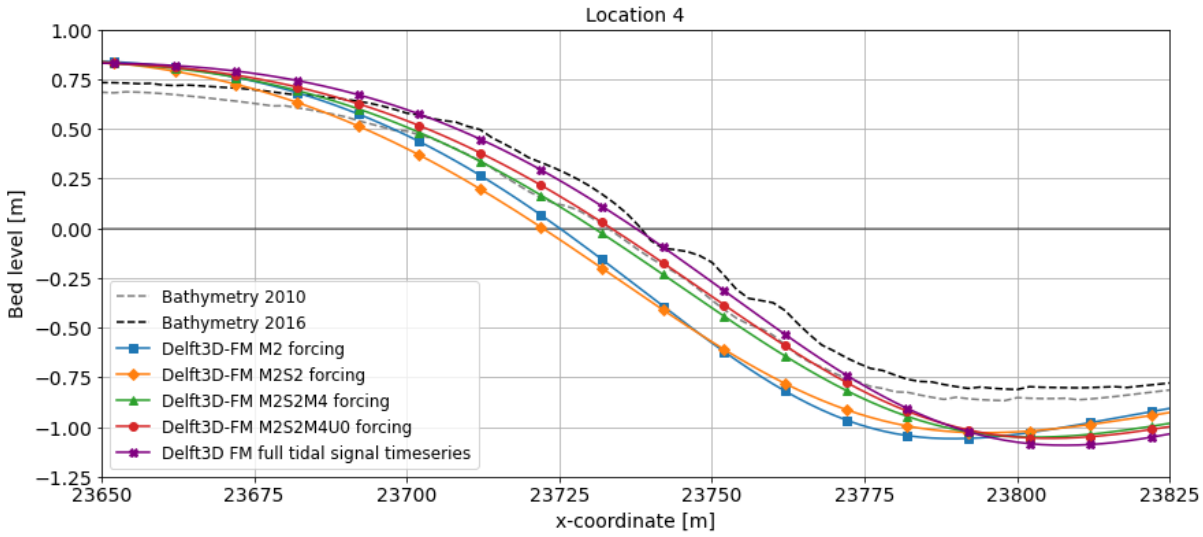

Figure C.9: Measured and computed bed level (after 6 years) for different forcing types, location 4, transect East

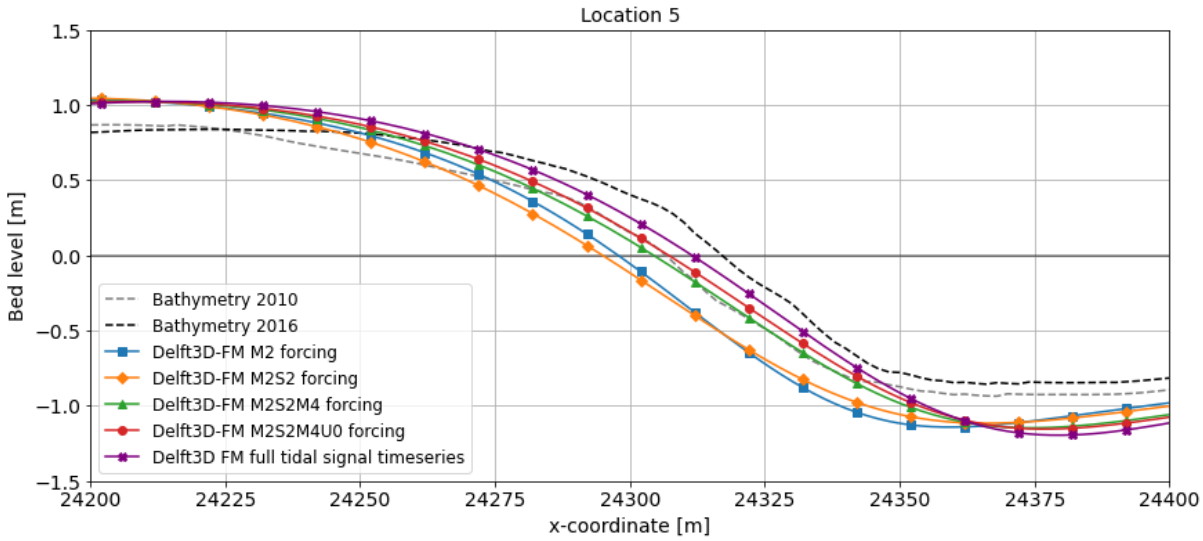

Figure C.10: Measured and computed bed level (after 6 years) for different forcing types, location 5, transect East

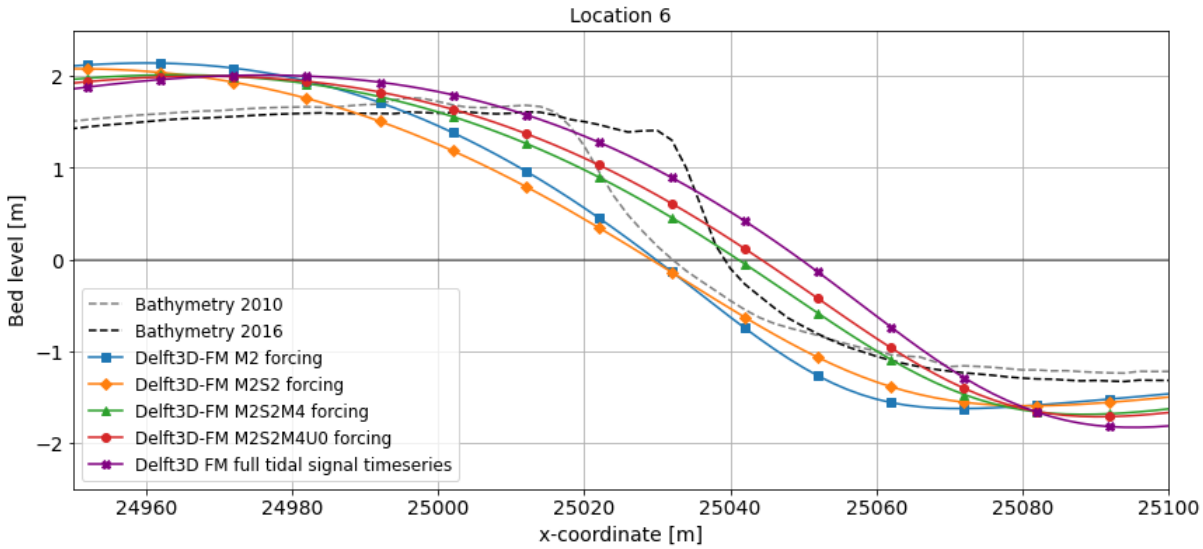

Figure C.11: Measured and computed bed level (after 6 years) for different forcing types, location 6, transect East

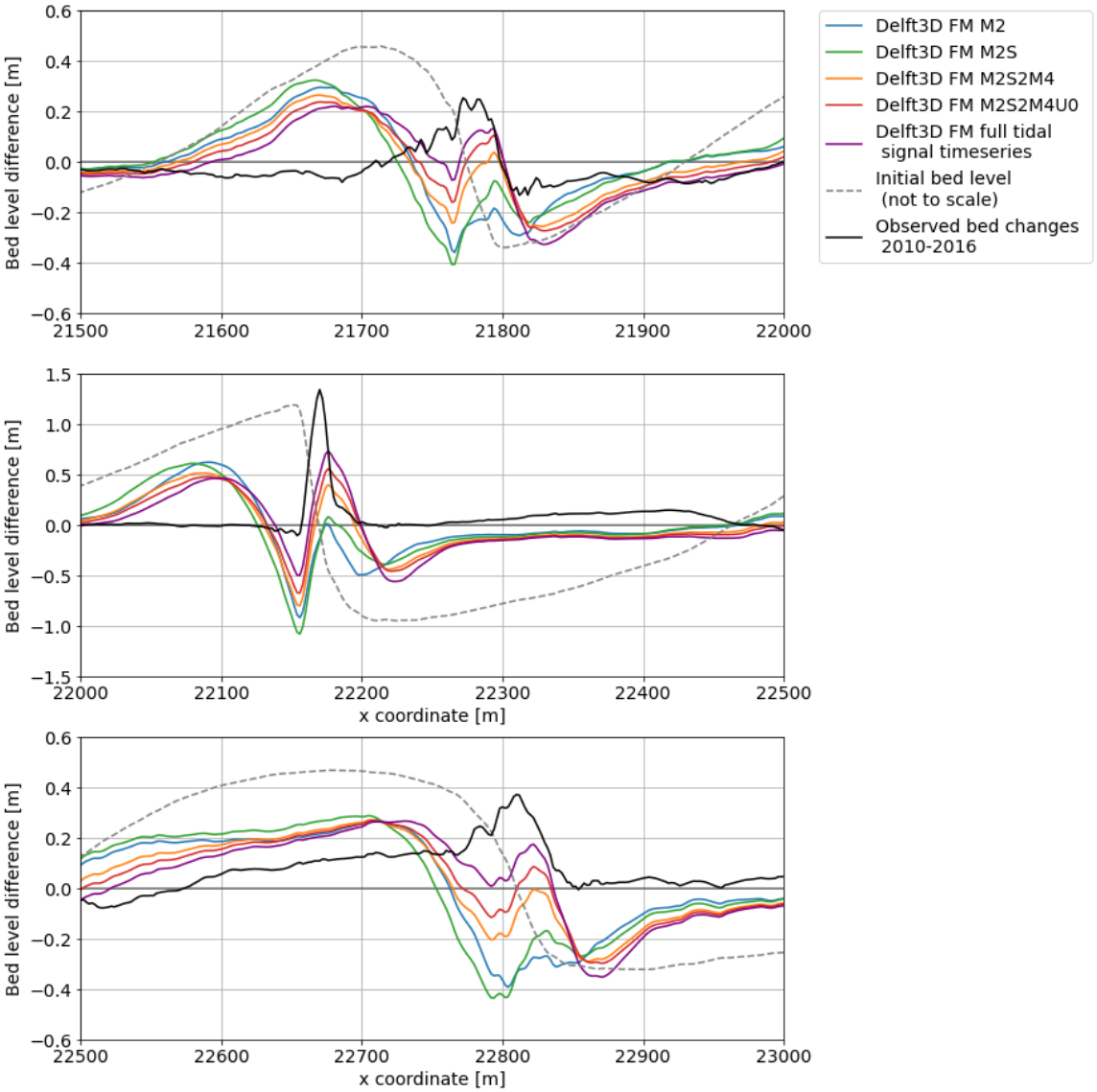

Figure C.12: Erosion and sedimentation over 6 years from measurements and Delft3D FM, all cases, transect East

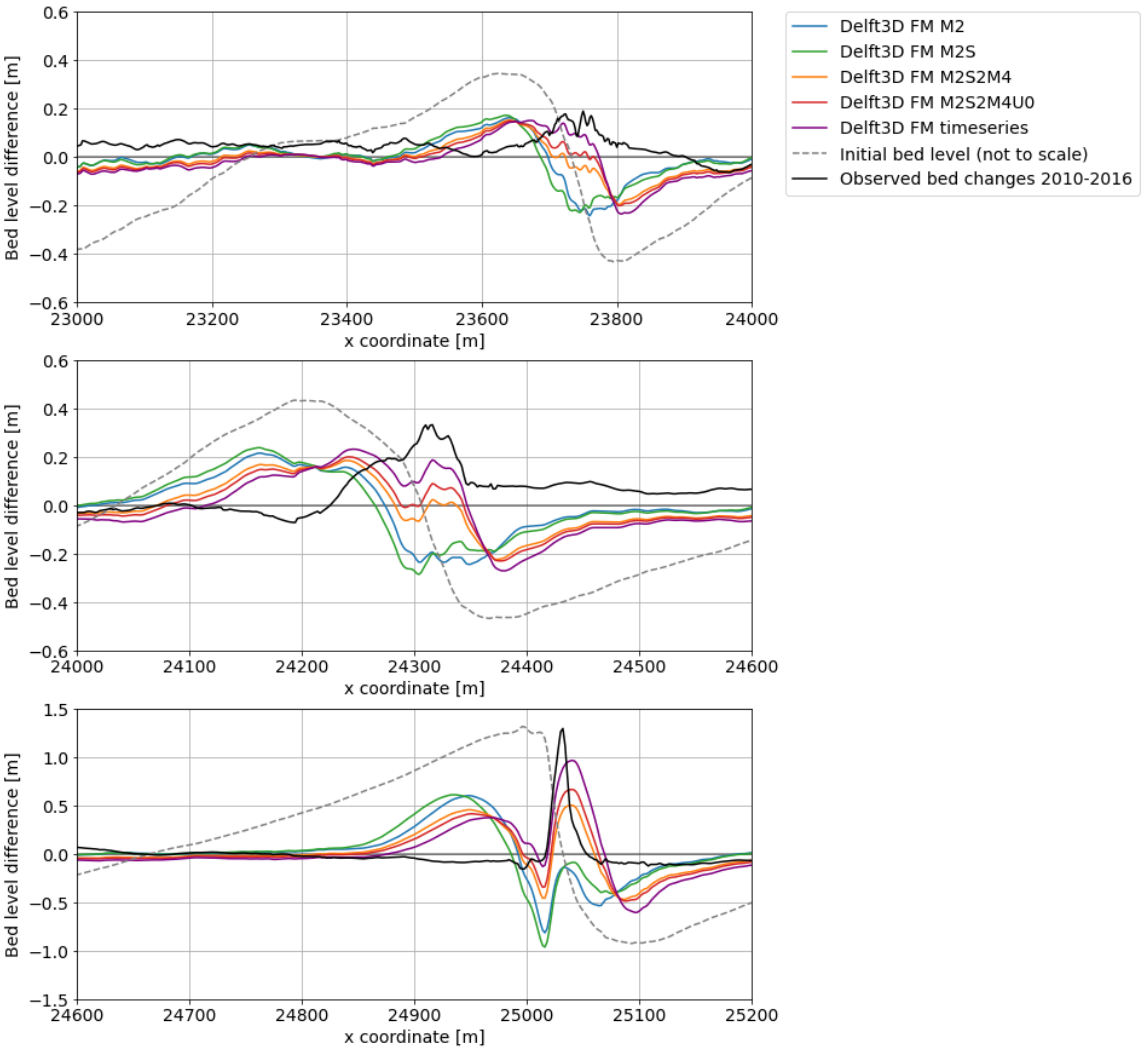

Figure C.13: Erosion and sedimentation over 6 years from measurements and Delft3D FM, all cases, transect East

C.3 Hydrodynamic results transect West

The figures in this section show the tide-averaged velocity patterns for the different tidal forcing cases tested in Chapter 5. The transect is split into four parts and the part that was already shown in the main report is also shown here for completeness. The definition of the cases and the respective forcing are repeated in Table C.3 and Table C.4.

Table C.3: Cases used in 2DV case study analysis transect West

Case	Tidal forcing	Residual current
I	M2	no
II	M2, S2	no
III	M2, S2, M4	no
IV	M2, S2, M4	yes
V	Full tidal signal	-

Table C.4: Forcing of the West transect Delft3D FM model at the far North and South boundary

Boundary	Variable	Constituent	Period (T) [min]	Amplitude (A)	Phase (ϕ) [deg]
South	Water level	M2	745	0.596 m	94
		S2	720	0.128 m	13
		M4	372.5	0.174 m	181
North	Parallel velocity	M2	745	0.672 m/s	128
		S2	720	0.169 m/s	145
		M4	372.5	0.047 m/s	226
		U0	-	0.011 m/s	-

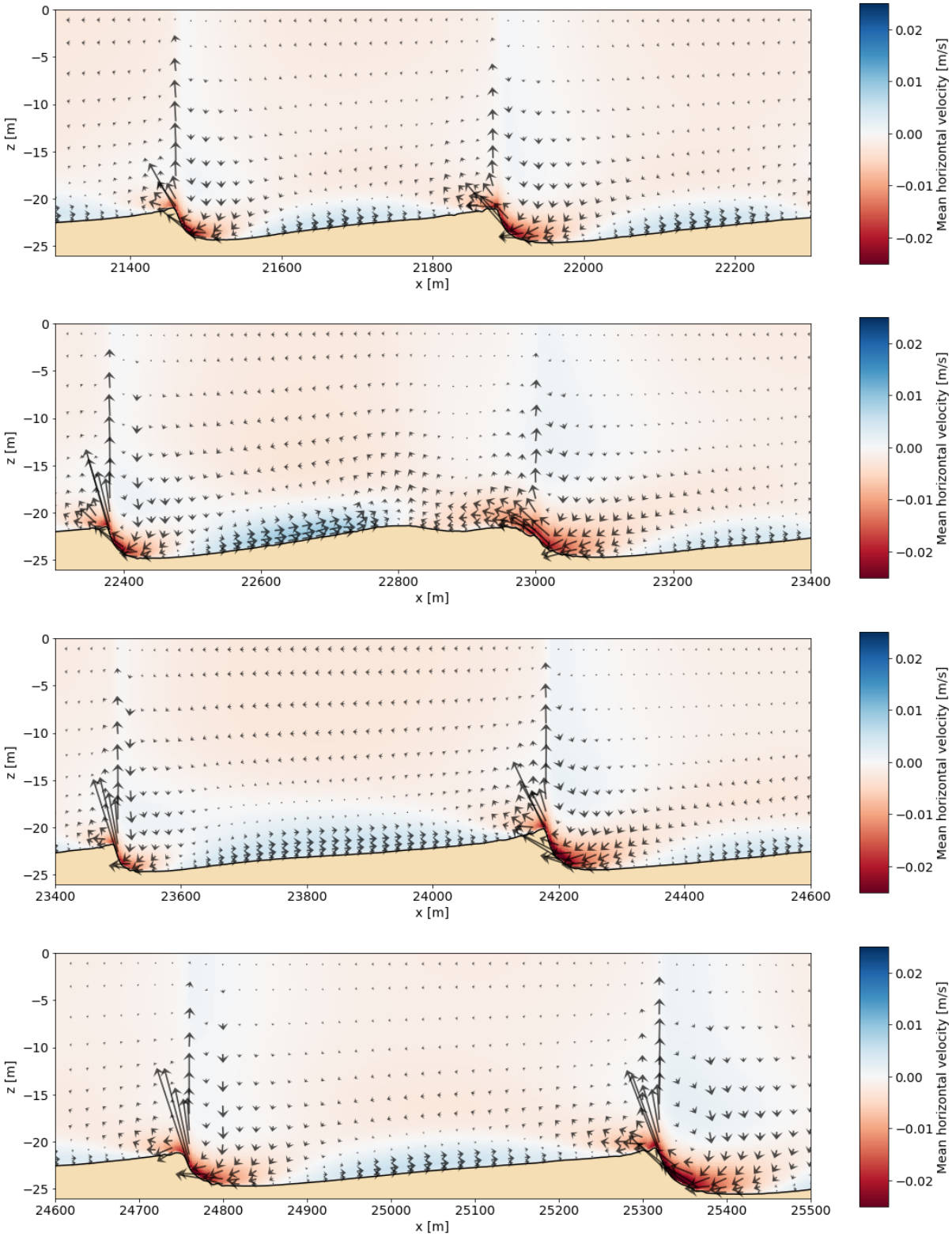

Figure C.14: Tide-averaged velocity field over the Western transect for M2 forcing (Case I). Colors indicate mean horizontal velocity, arrows combine direction and magnitude of the mean horizontal and (scaled) vertical velocity

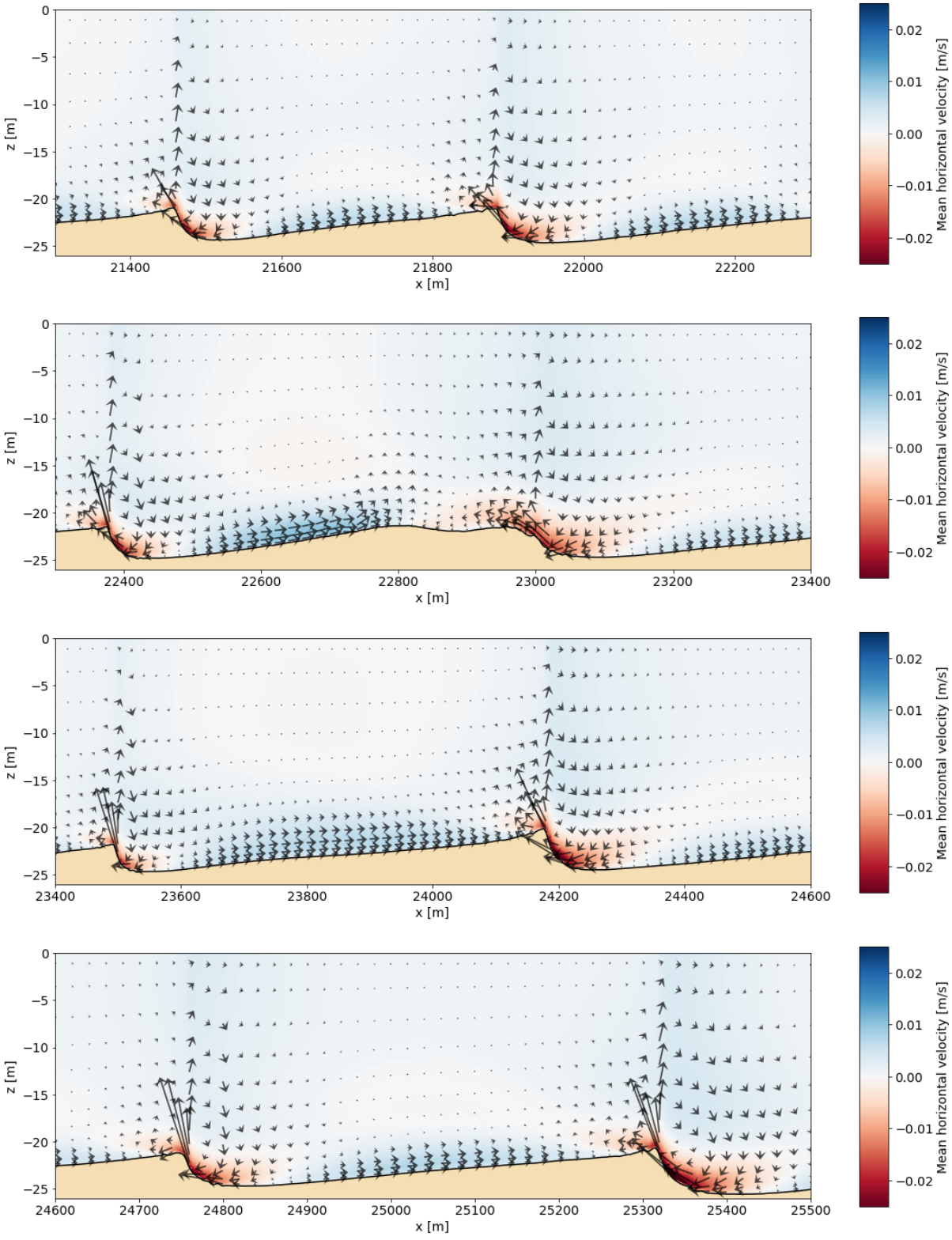

Figure C.15: Tide-averaged velocity field over the Western transect for M2 + S2 forcing (Case II). Colors indicate mean horizontal velocity, arrows combine direction and magnitude of the mean horizontal and (scaled) vertical velocity

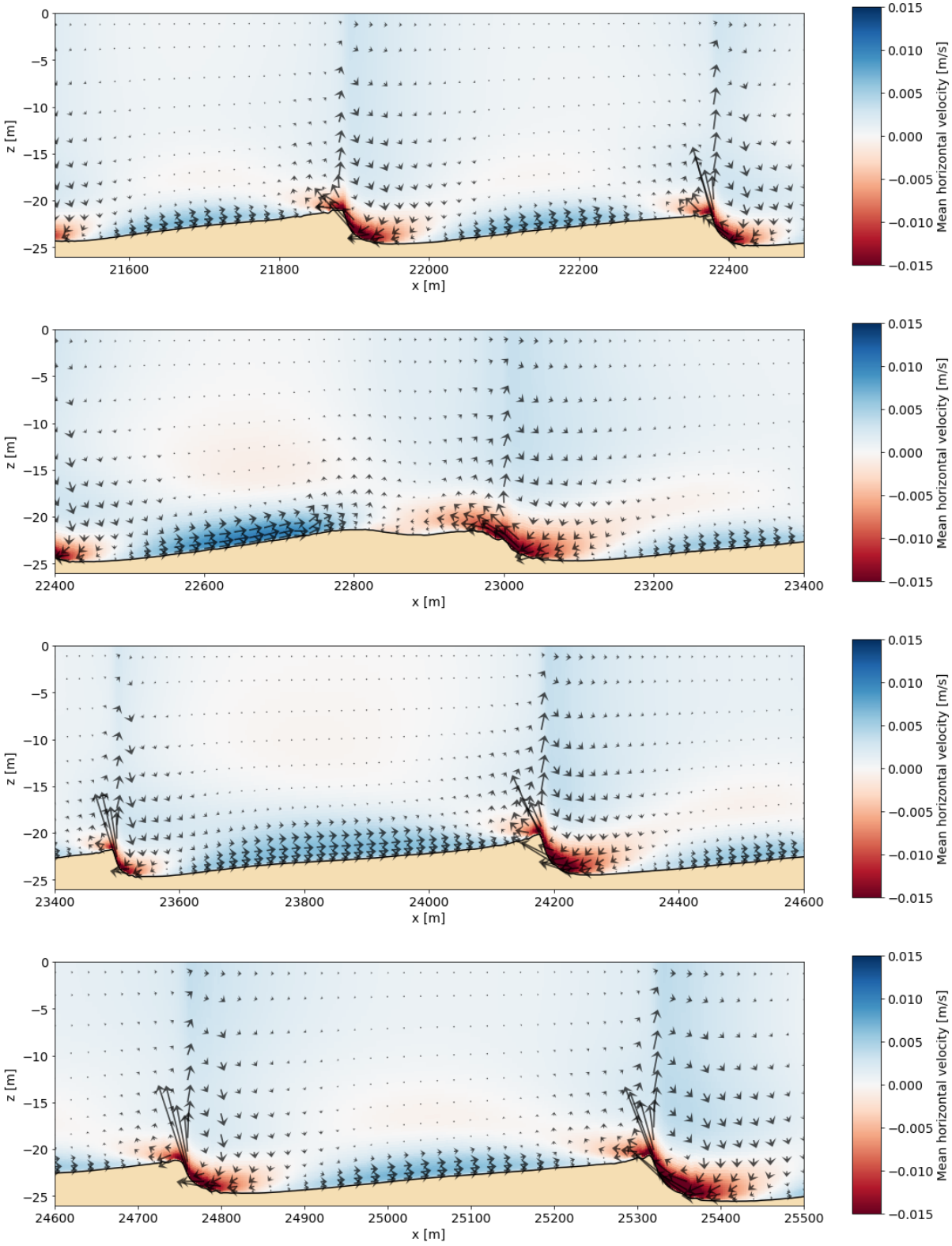

Figure C.16: Tide-averaged velocity field over the Western transect for M2 + S2 + M4 forcing (Case III). Colors indicate mean horizontal velocity, arrows combine direction and magnitude of the mean horizontal and (scaled) vertical velocity

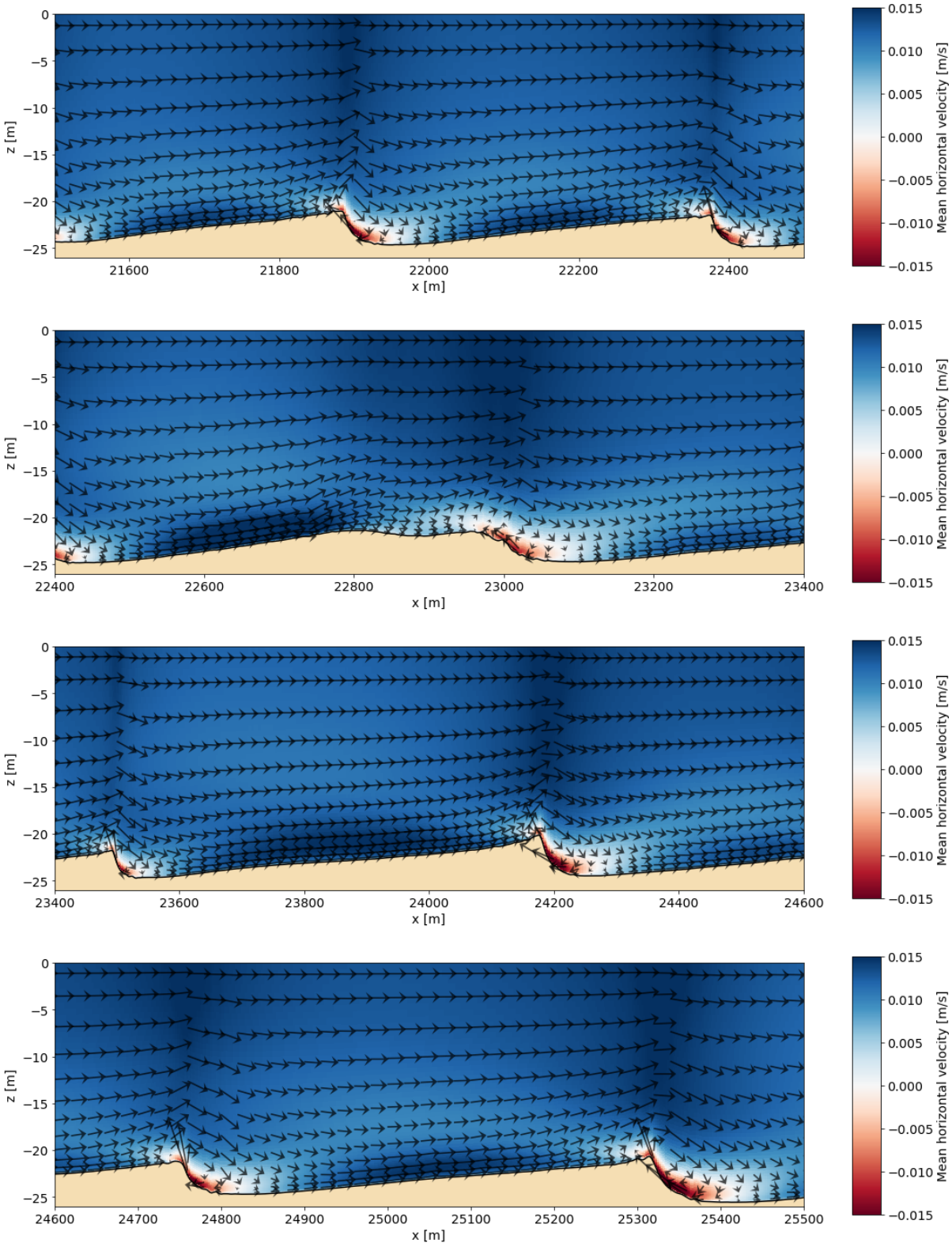

Figure C.17: Tide-averaged velocity field over the Western transect for M2 + S2 + M4 forcing including residual current (Case IV). Colors indicate mean horizontal velocity, arrows combine direction and magnitude of the mean horizontal and (scaled) vertical velocity

C.4 Morphological results transect West

In this section the morphological results are shown for all sand waves in the West transect for the different types of forcing used in the study. Due to the size of the differences the plots only show the lee side slope of the sand wave, where the differences between the models become apparent. The locations of the plots are clarified in Figure C.18.

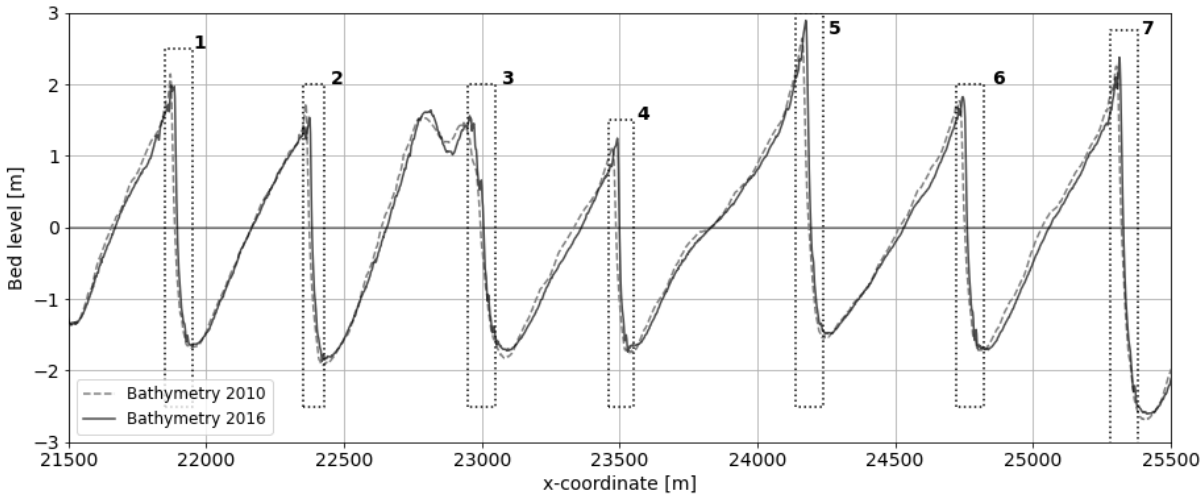

Figure C.18: Locations of plots showing morphological results transect West

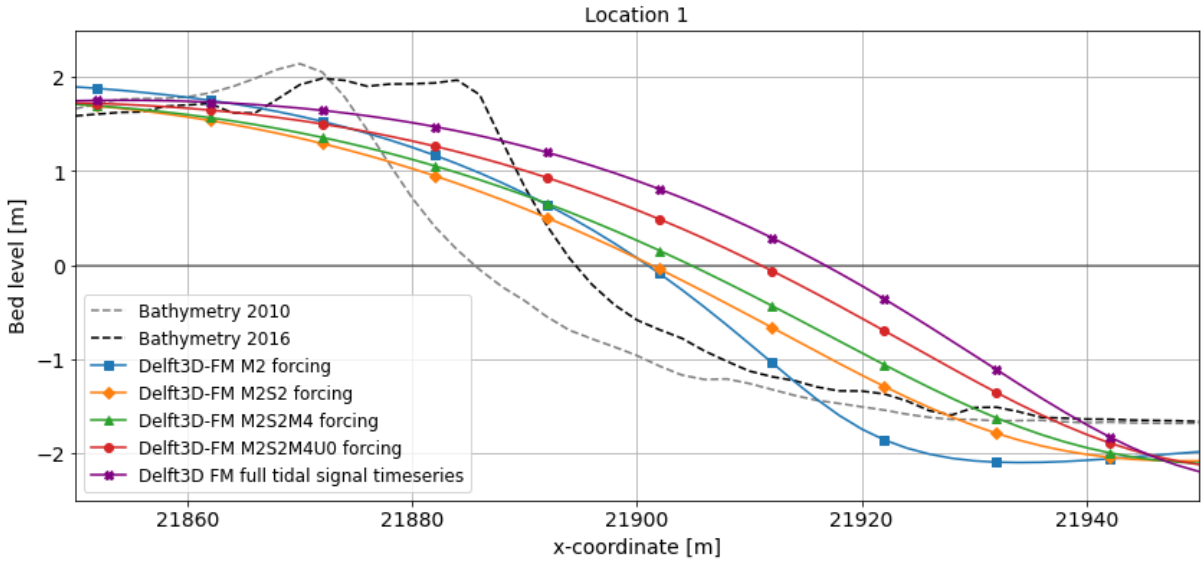

Figure C.19: Measured and computed bed level (after 6 years) for different forcing types, location 1, transect West

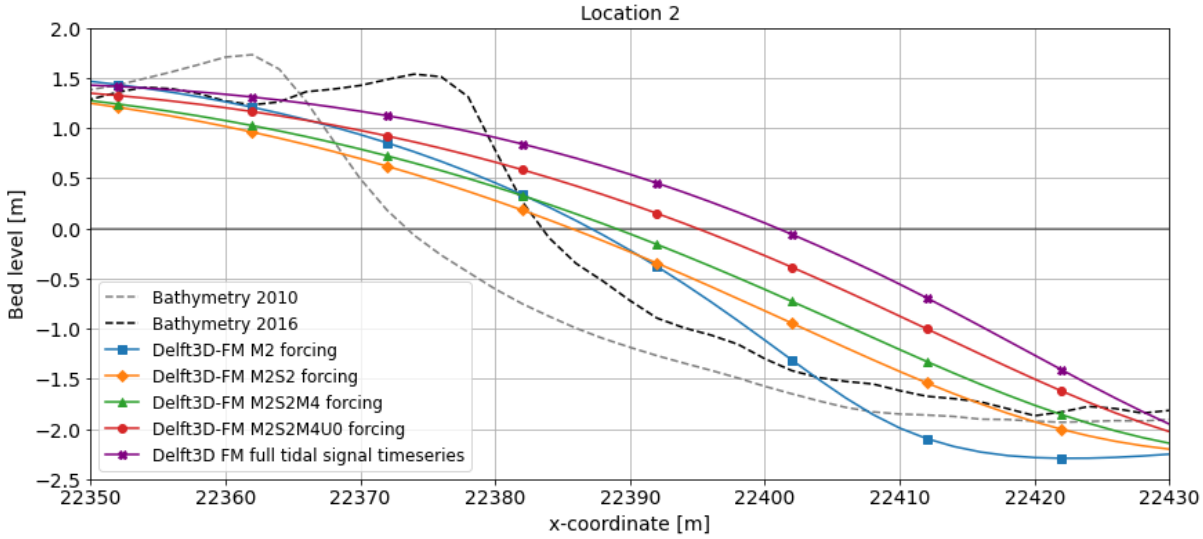

Figure C.20: Measured and computed bed level (after 6 years) for different forcing types, location 2, transect West

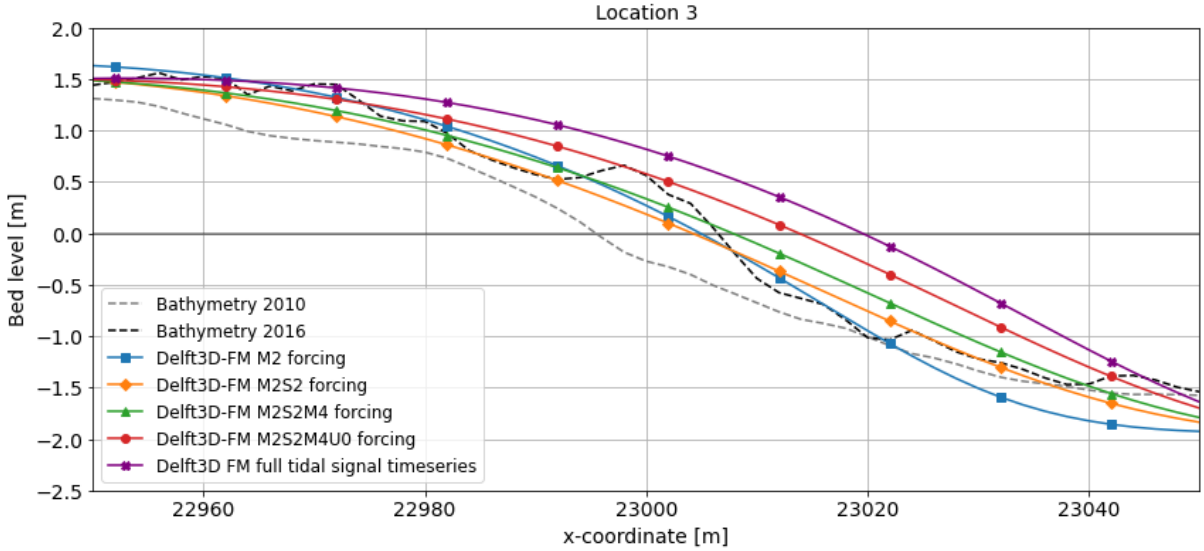

Figure C.21: Measured and computed bed level (after 6 years) for different forcing types, location 3, transect West

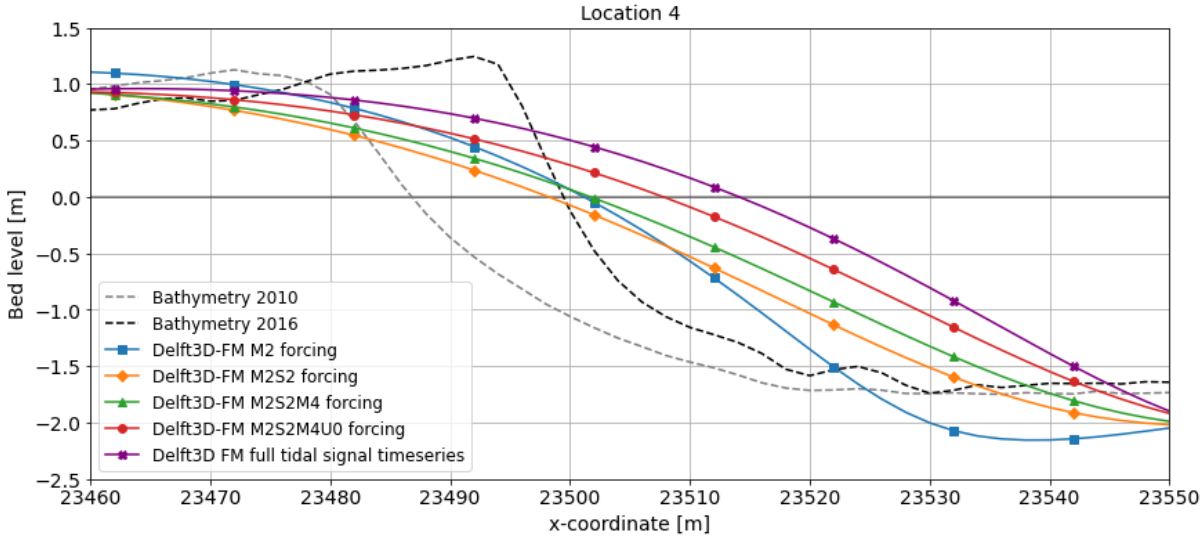

Figure C.22: Measured and computed bed level (after 6 years) for different forcing types, location 4, transect West

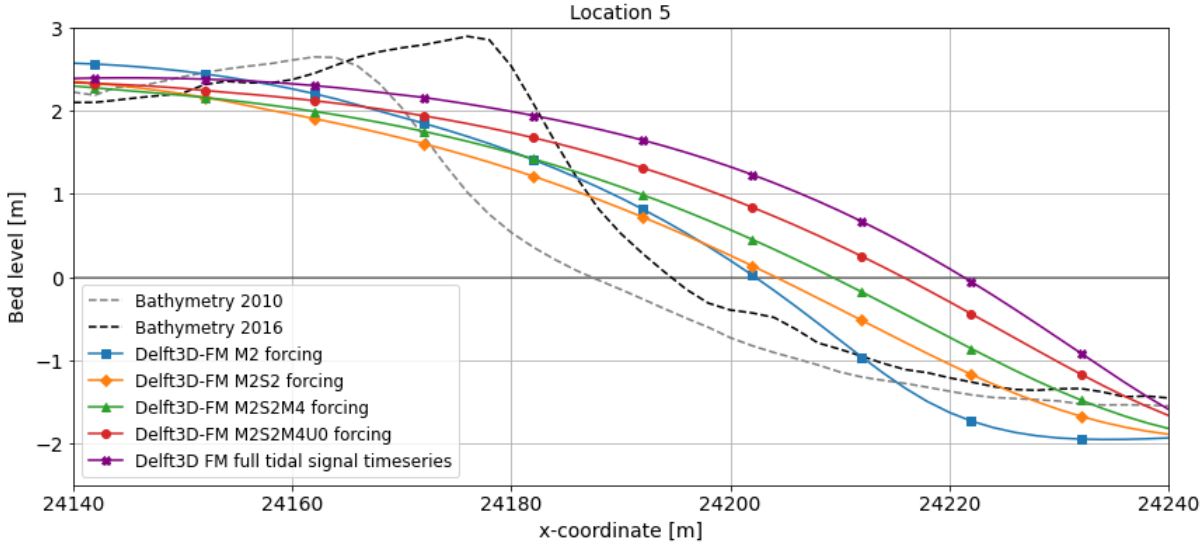

Figure C.23: Measured and computed bed level (after 6 years) for different forcing types, location 5, transect West

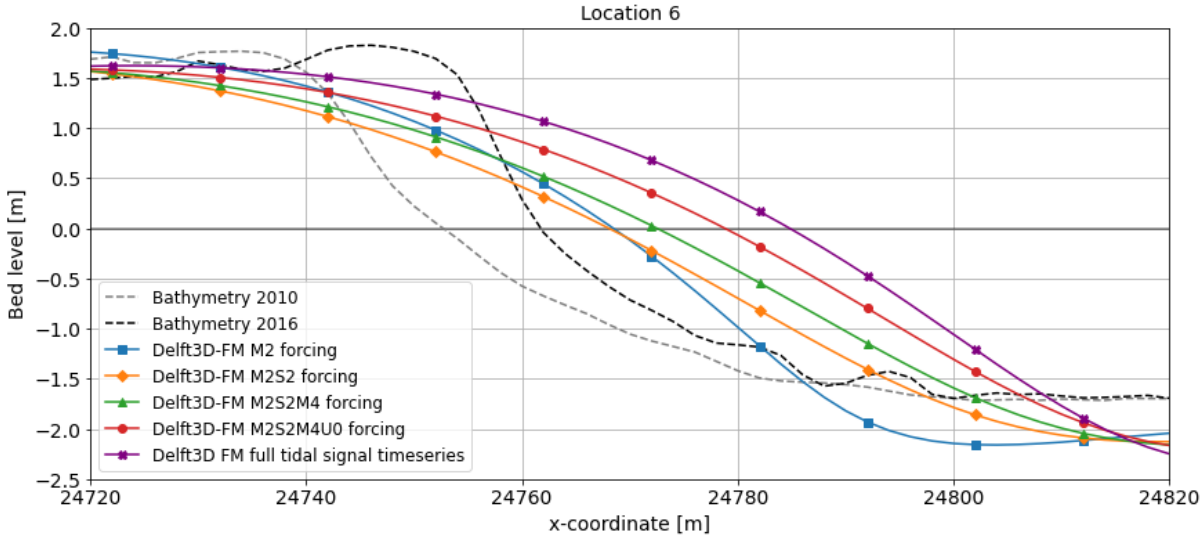

Figure C.24: Measured and computed bed level (after 6 years) for different forcing types, location 6, transect West

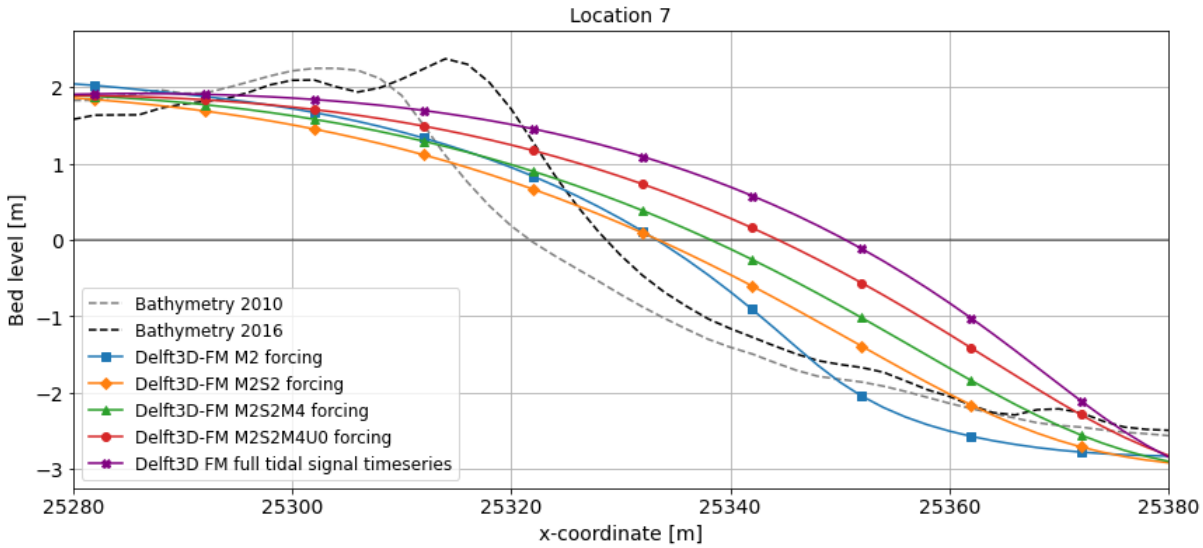

Figure C.25: Measured and computed bed level (after 6 years) for different forcing types, location 7, transect West

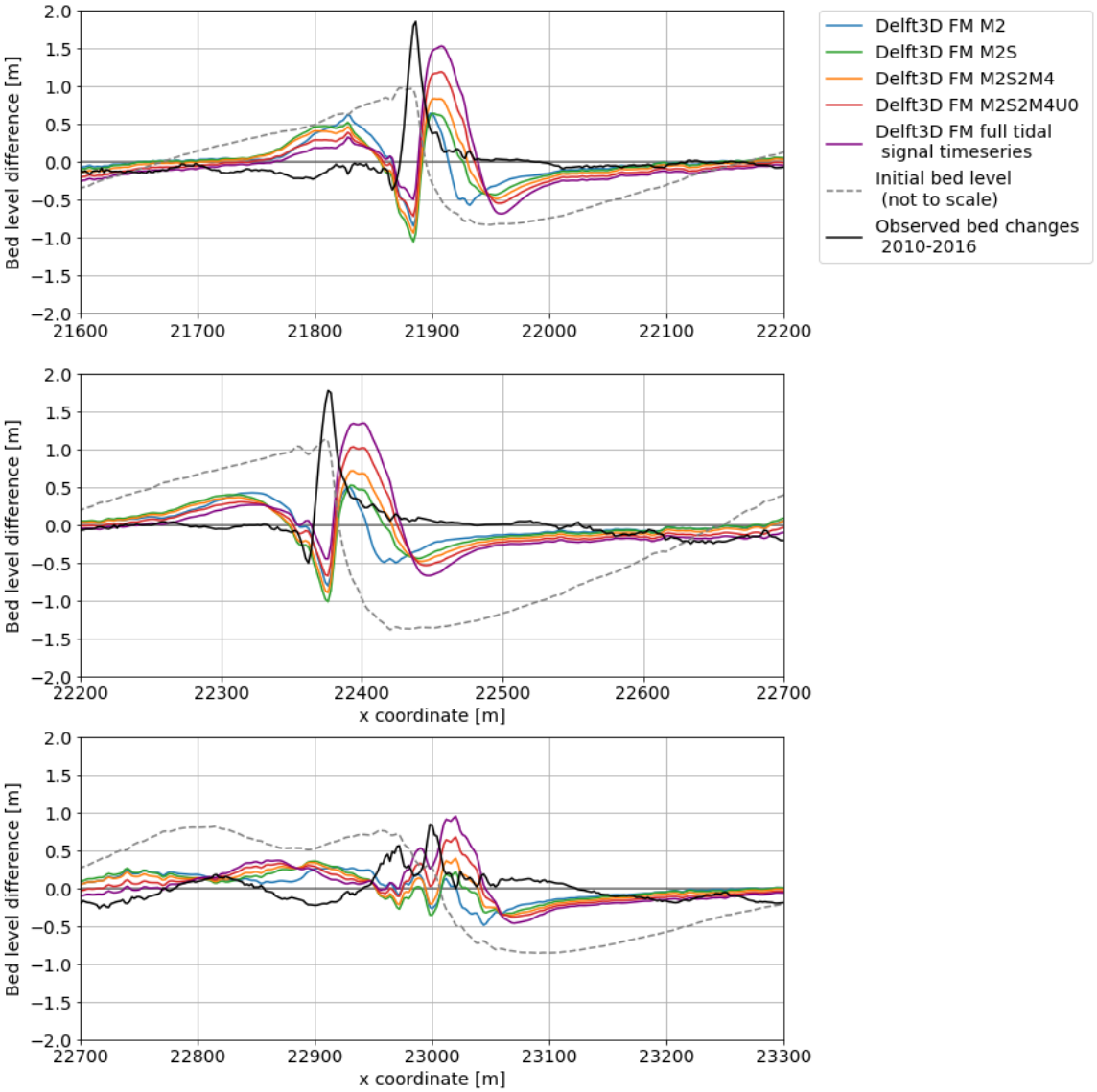

Figure C.26: Erosion and sedimentation over 6 years from measurements and Delft3D FM, all cases, transect West

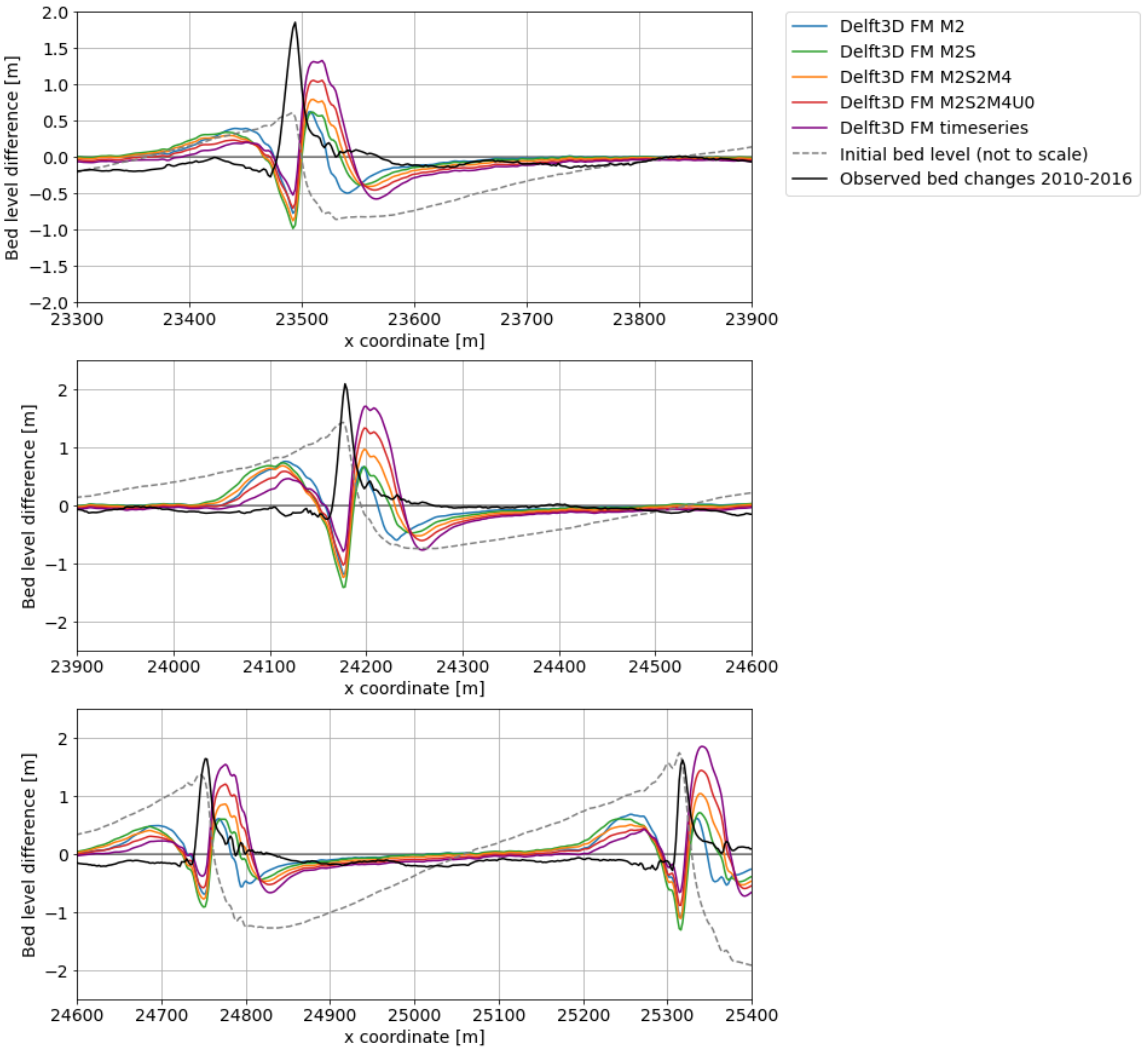

Figure C.27: Erosion and sedimentation over 6 years from measurements and Delft3D FM, all cases, transect West

D | Parallel model results

For the 3D simulations, the model was split up into partitions that run simultaneously and communicate. This is also known as running in parallel. To check the consistency of models which are run in parallel, the results of a 2DV parallel model are compared to the 2DV model results obtained by simulating as a whole (thus on a single core). The East transect Case IV model is simulated using 8 partitions (2 nodes and 4 cores). The results are shown in Figure D.1. The simulated bed level changes are nearly identical. This increases the confidence in the use of parallel models for sand wave applications. The 3D model itself could not be run as a whole for comparison since the computation times would in that case become unreasonably long. The computation time of the model decreased from the original 59 hours to 17 hours for a model run with 4 partitions. The new computation time is 3.5 times lower indicating an almost linear decrease in computation time. In case of a further increase of the number of partitions the relative gain becomes lower. The optimum number of partitions is dependent on the size of the model. When too many partitions are used the communication between the partitions will take too much time relative to the computations within the partitions. Since the 2DV model has a relatively low number of cells the computational gain diminishes already at a low number of partitions. The 3D model has over 200 times more cells, causing the optimum number of partitions to be much higher.

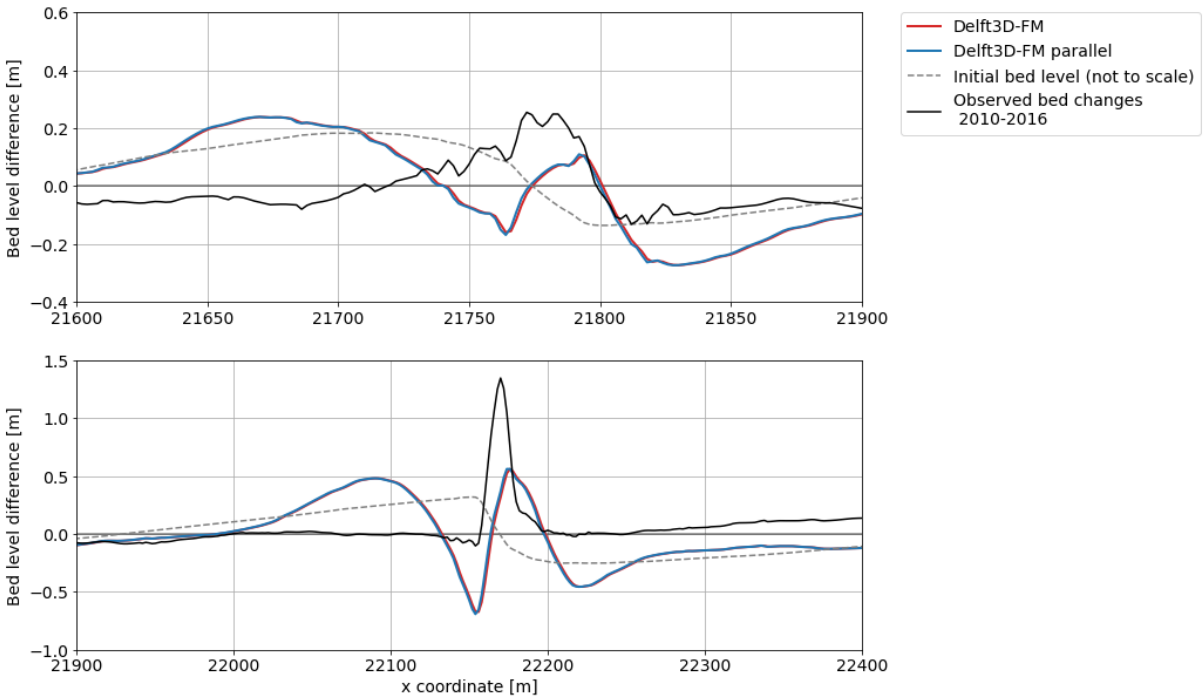

Figure D.1: Erosion and sedimentation patterns for the East transect Case IV model, run as a whole and run in parallel

E | Boundary condition extraction and validation

The boundary conditions for the 2DV and 3D case study models were extracted from the large scale DCSM model. This model has been validated with measurement data throughout the Dutch North Sea (Zijl et al. (2018) and Deltares (2016a)). The DCSM model is run for a period of one year starting from the end of 2012 to extract the boundary conditions for both models. In these model runs the tidal flows are simulated, but flows due to atmospheric pressures are not included.

E.1 2DV model

Extraction

The 2DV models have two open boundaries at the far South and far North end of the model. The South and North open boundaries are at a distance of 20 km from the start and end of the sand wave domain in the model respectively. In the DCSM model observation points are included for both transects at the locations of the open boundaries and at the locations of the start and end points of the sand wave domains. The observations at the locations of the open boundaries are used to construct boundary condition files. Two types of boundary conditions are used for the 2DV models: a time series containing the full tidal signal and harmonic boundary conditions containing one or several tidal constituents. For both boundary condition types the velocity parallel to the transect direction was used and perpendicular velocities were filtered out. Furthermore, since the bottom depth in the 2DV model differs from the bottom depth in the DCSM model, the velocities were scaled to preserve the local discharge. The time series for the full tidal signal model are extracted after a spin-up period of 3 days. For the harmonic boundary conditions the amplitude and phase of several tidal constituents are determined. This is done using the ttide python code, which is a conversion of the original t_tide Matlab code to python, converted by O'Flaherty-Sproul (2021). This code is able to extract the amplitudes and phases of constituents with known frequencies from a water level or velocity signal. Both the parallel velocity and the water level signal are processed using this code. The signal used has a length of one year and starts after a spin-up period of 3 days. The output of the code includes the estimated error of the phase and amplitude of the different tidal constituents. For the constituents and boundaries used in the 2DV models these variables, as well as the estimated phase and amplitude, are shown in Table E.1. The relative phases apply to the middle of the time series, which is 182 days later than the start of the DCSM model. The phases of the M4 and M2 constituents however do not change relative to each other.

Boundary	Variable	Constituent	Period (T) [min]	Amplitude (A)	Amplitude error	Phase (ϕ) [deg]	Phase error [deg]
East South	Parallel velocity	M2	745	0.723 m/s	0.0037 m/s	111	0.36
		S2	720	0.193 m/s	0.0043 m/s	128	1.42
		M4	372.5	0.053 m/s	0.0029 m/s	148	2.80
East North	Water level	M2	745	0.573 m	0.0057 m	138	0.64
		S2	720	0.148 m	0.0062 m	174	2.52
		M4	372.5	0.198 m	0.0065 m	205	2.93
West South	Water level	M2	745	0.596 m	0.0058 m	94	0.53
		S2	720	0.128 m	0.0059 m	123	2.59
		M4	372.5	0.174 m	0.0071 m	181	2.49
West North	Parallel velocity	M2	745	0.672 m/s	0.0042 m/s	128	0.34
		S2	720	0.169 m/s	0.0039 m/s	145	1.32
		M4	372.5	0.047 m/s	0.0023 m/s	226	2.79

Table E.1: Extracted variables and estimated errors for tidal constituents at East and West transect boundaries

Validation

Using the velocity and water level observations at the locations of the South and North edge of the sand wave domain the hydrodynamics in the 2DV model can be validated. Since the bed level is different between the 2DV models and the DCSM model at the validation points, the total water depth is shown instead of water level. This is done for all 2DV models. From the validation plots it is clear that with the addition of tidal constituents the representation of the tidal asymmetry in the flow velocity improves. For the East transect model the variation of the water level over the tidal cycle is somewhat overestimated. In the West transect model the tidal water level is better represented. In the full tidal signal model of the East transect a small wiggle in the tidal velocity can be seen. This is most probably caused by the simultaneous quick rising of the water level. The best match of hydrodynamics are found in the West transect M2S2M4U0 (Case IV) and full tidal signal (Case V) models.

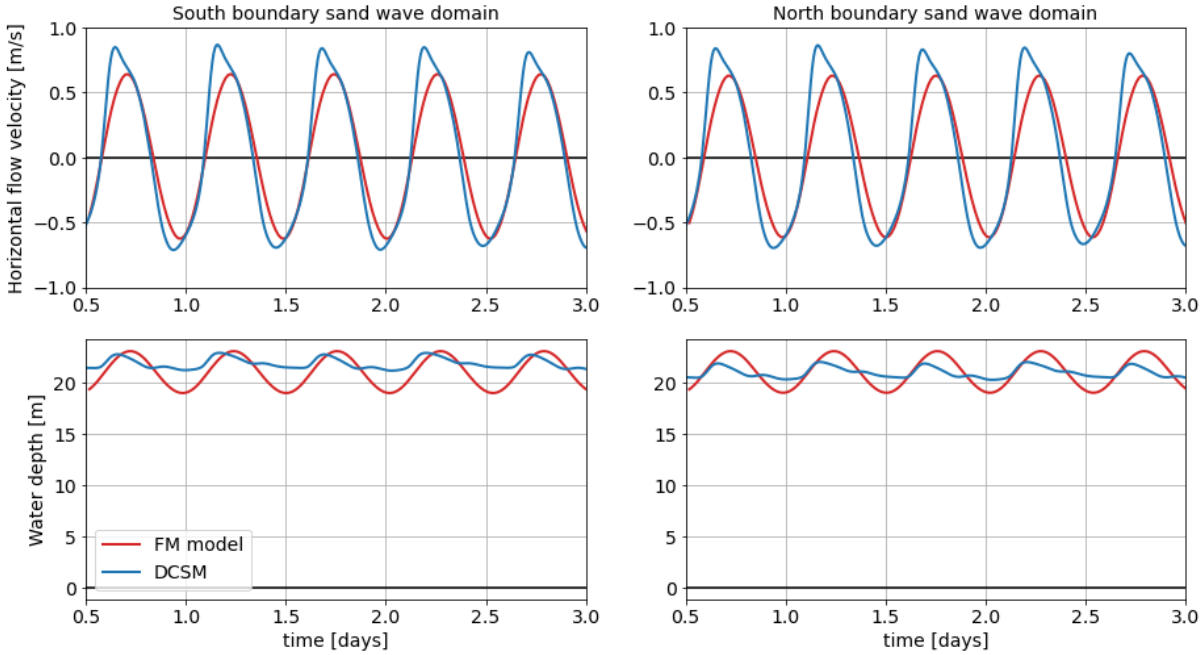

Figure E.1: Validation of flow velocity and water depth in the 2DV East transect M2 model (Case I) using observations from the DCSM model

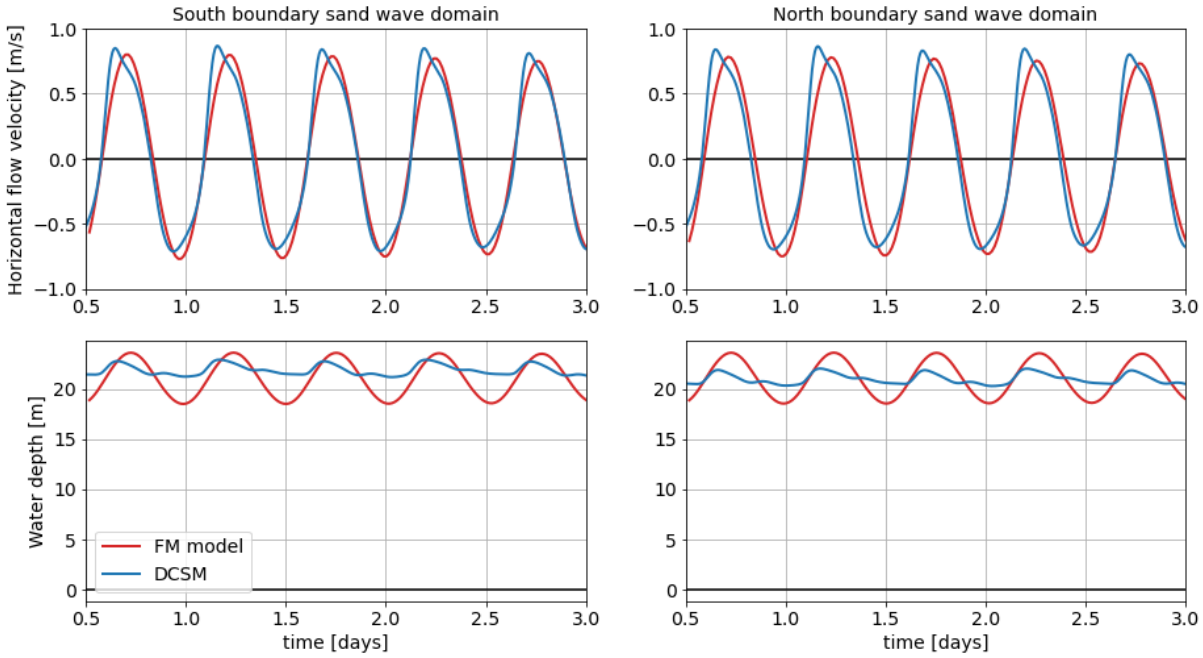

Figure E.2: Validation of flow velocity and water depth in the 2DV East transect M2 + S2 model (Case II) using observations from the DCSM model

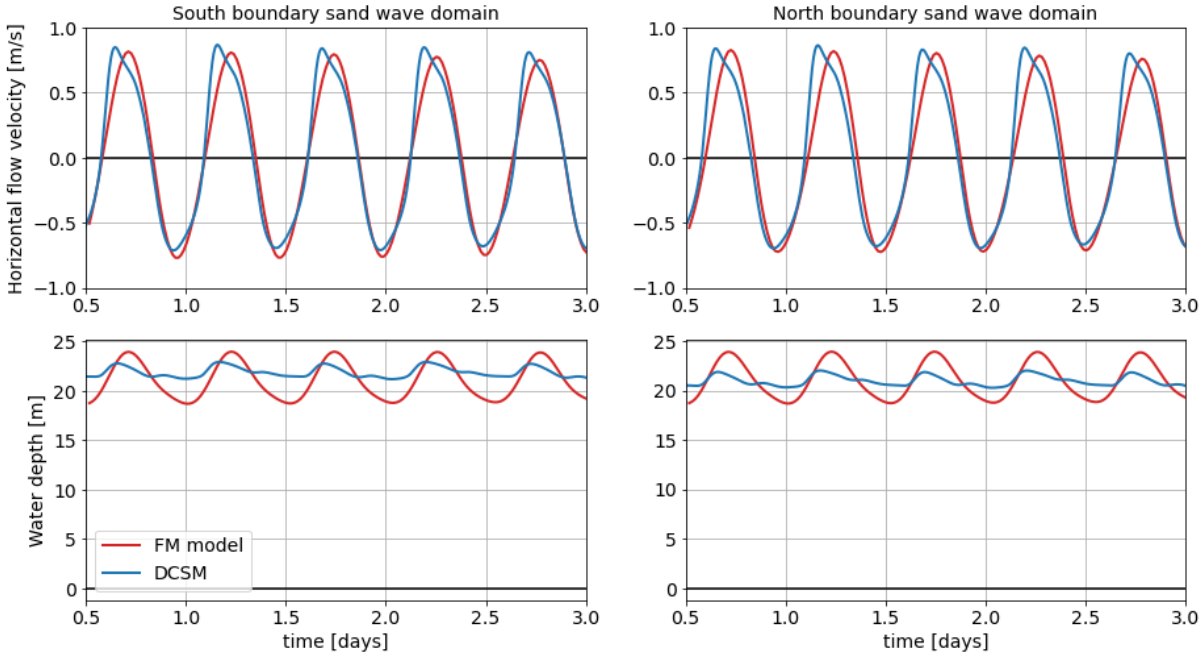

Figure E.3: Validation of flow velocity and water depth in the 2DV East transect M2 + S2 + M4 model (Case III) using observations from the DCSM model

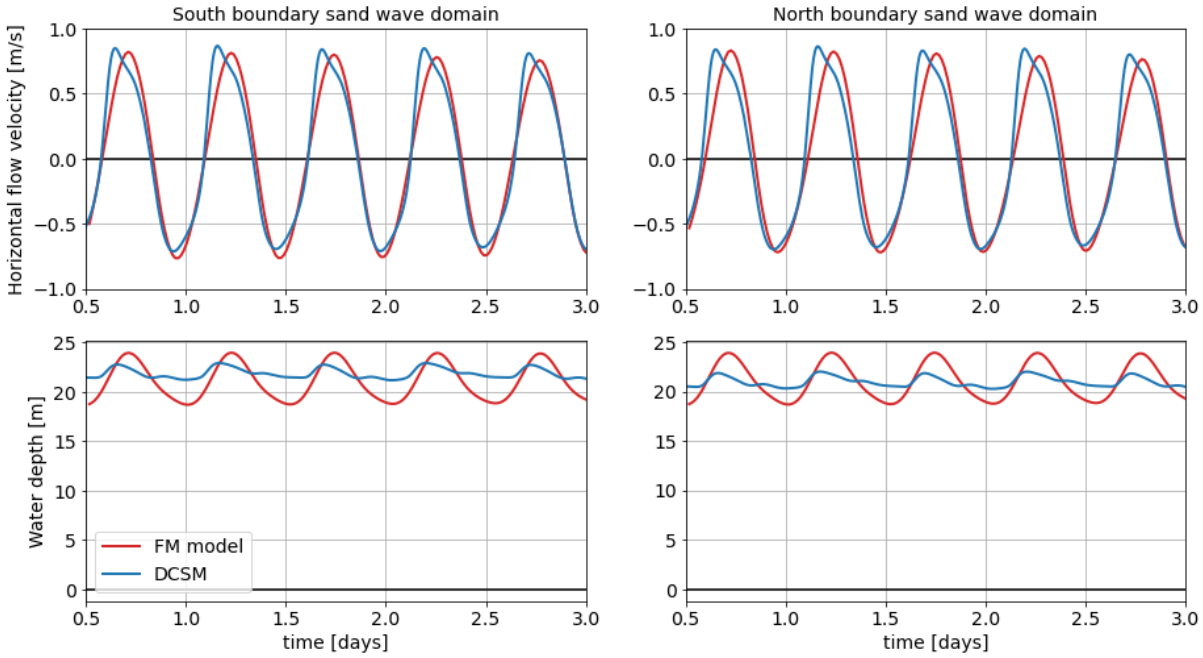

Figure E.4: Validation of flow velocity and water depth in the 2DV East transect M2 + S2 + M4 model including residual current (Case IV) using observations from the DCSM model

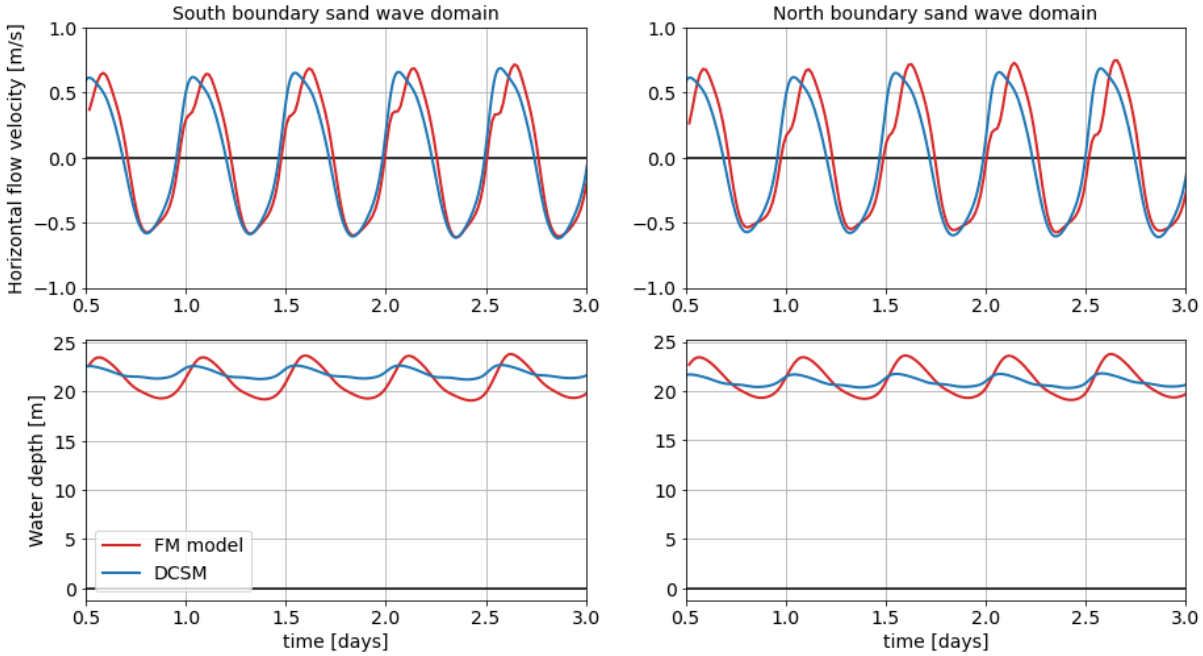

Figure E.5: Validation of flow velocity and water depth in the 2DV East transect full tidal signal model (Case V) using observations from the DCSM model

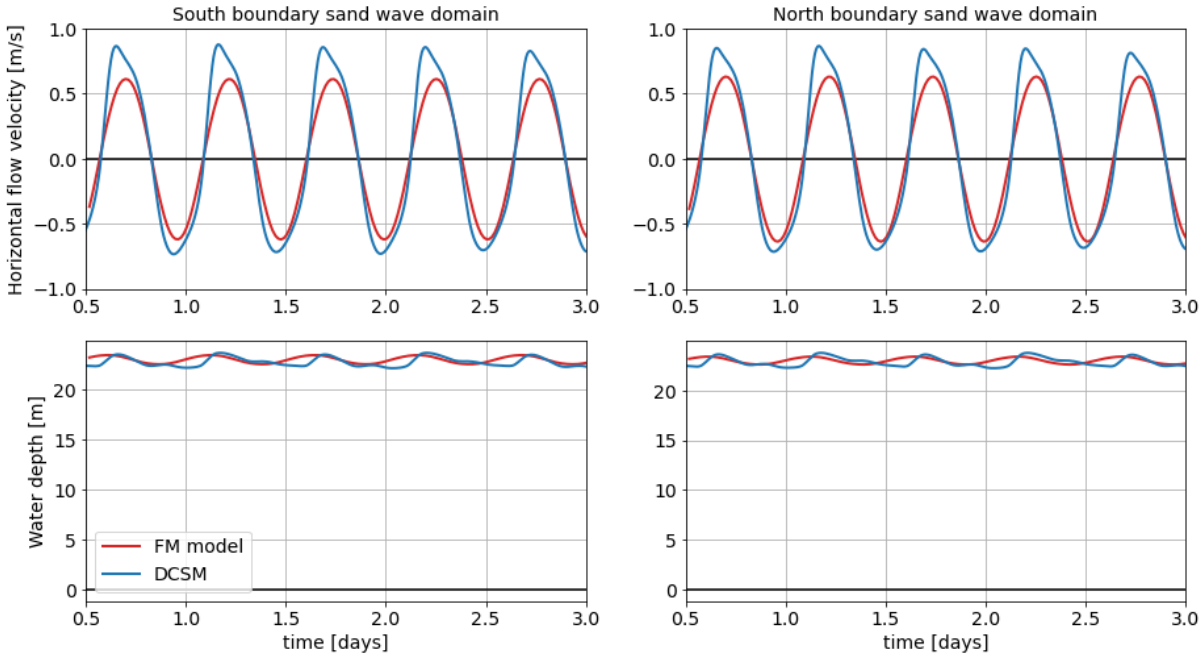

Figure E.6: Validation of flow velocity and water depth in the 2DV West transect M2 model (Case I) using observations from the DCSM model

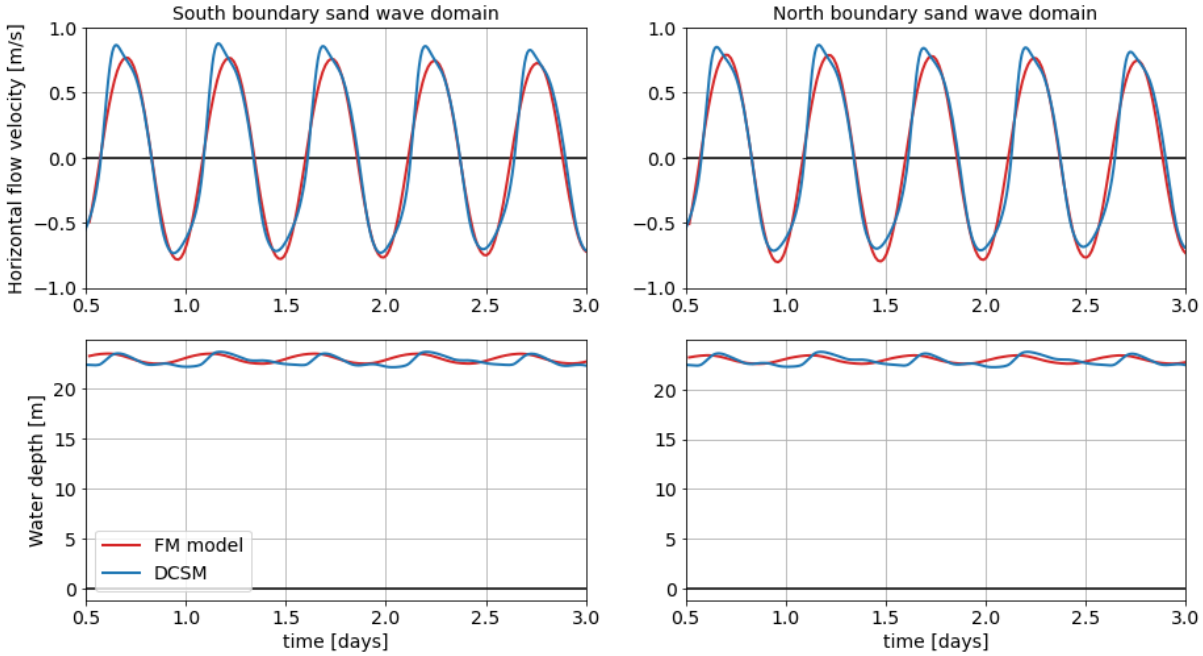

Figure E.7: Validation of flow velocity and water depth in the 2DV West transect M2 + S2 model (Case II) using observations from the DCSM model

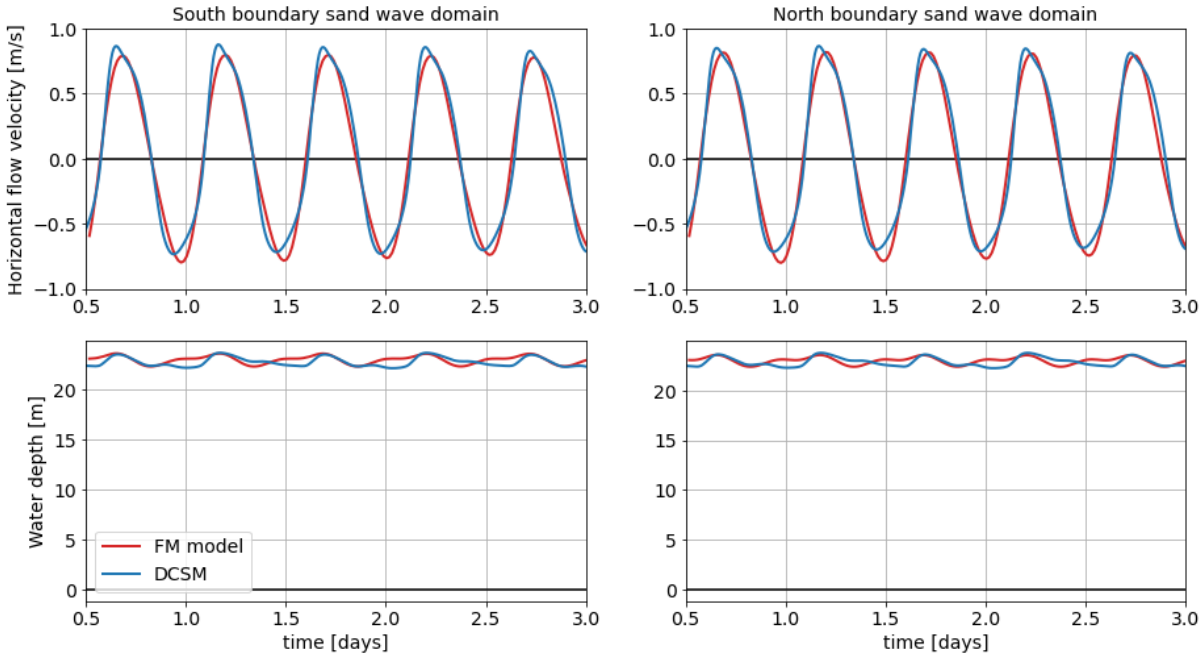

Figure E.8: Validation of flow velocity and water depth in the 2DV West transect M2 + S2 + M4 model (Case III) using observations from the DCSM model

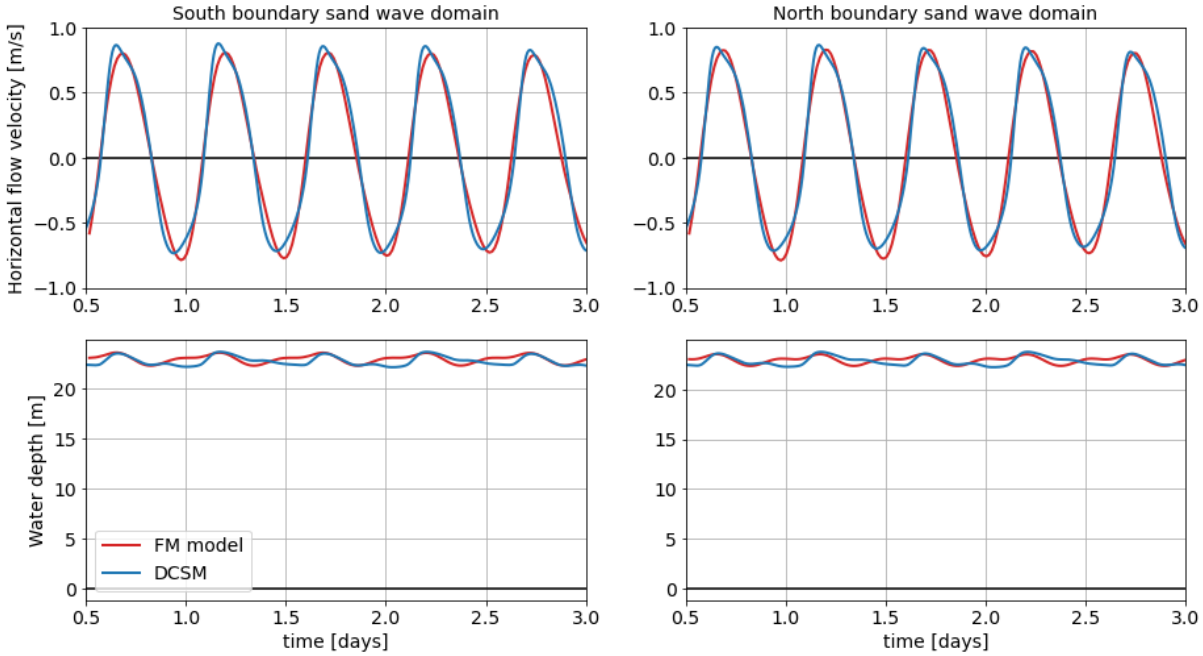

Figure E.9: Validation of flow velocity and water depth in the 2DV West transect M2 + S2 + M4 model including residual current (Case IV) using observations from the DCSM model

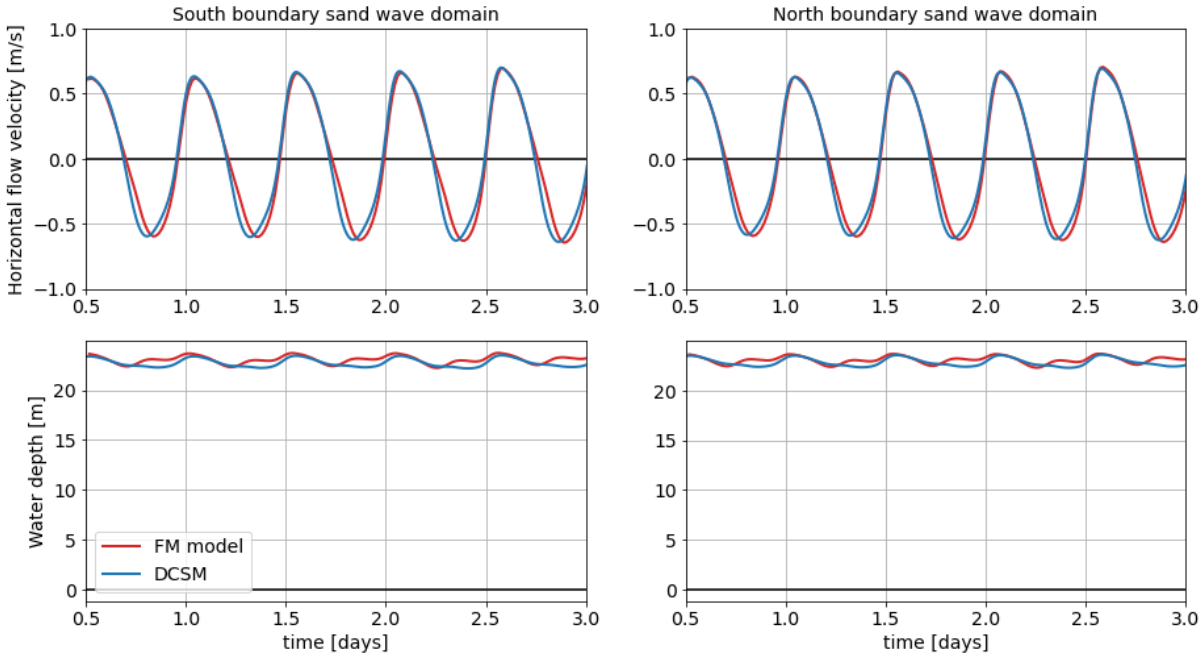

Figure E.10: Validation of flow velocity and water depth in the 2DV West transect full tidal signal model (Case V) using observations from the DCSM model

E.2 3D model

Extraction

For the boundary conditions of the 3D model again the large scale DCSM model is used. The model is run for 1 year, simulating the tidal flows in the Dutch North Sea. Along each boundary of the 3D model 9 observation points are added to the DCSM model, excluding the 4 corner points. This means that the distance between the observation points is larger at the East and West boundary. The flow is however approximately aligned with these boundaries. This means that the in- and outflow is limited and smaller changes in flow velocity are expected on the East and West side. From the extracted depth averaged flow velocity a logarithmic velocity profile over depth is created using the Chezy roughness in the model. The flow velocity at the boundary is defined at 6 depths, with increasing accuracy towards the bed. The water levels and flow velocities over depth in both horizontal directions for all 40 boundary points are combined in a boundary condition file. The flow velocity and water level are interpolated linearly in between the locations from the boundary file.

Validation

For validation the hydrodynamics are again compared to the DCSM model at the same locations as used in the 2DV validation. These points are located at the centre of the South and North boundary of the sand wave domain in the 3D model. The representation of the water level in the 3D model is almost identical to the water level in the DCSM model, making the lines indistinguishable in the plot.

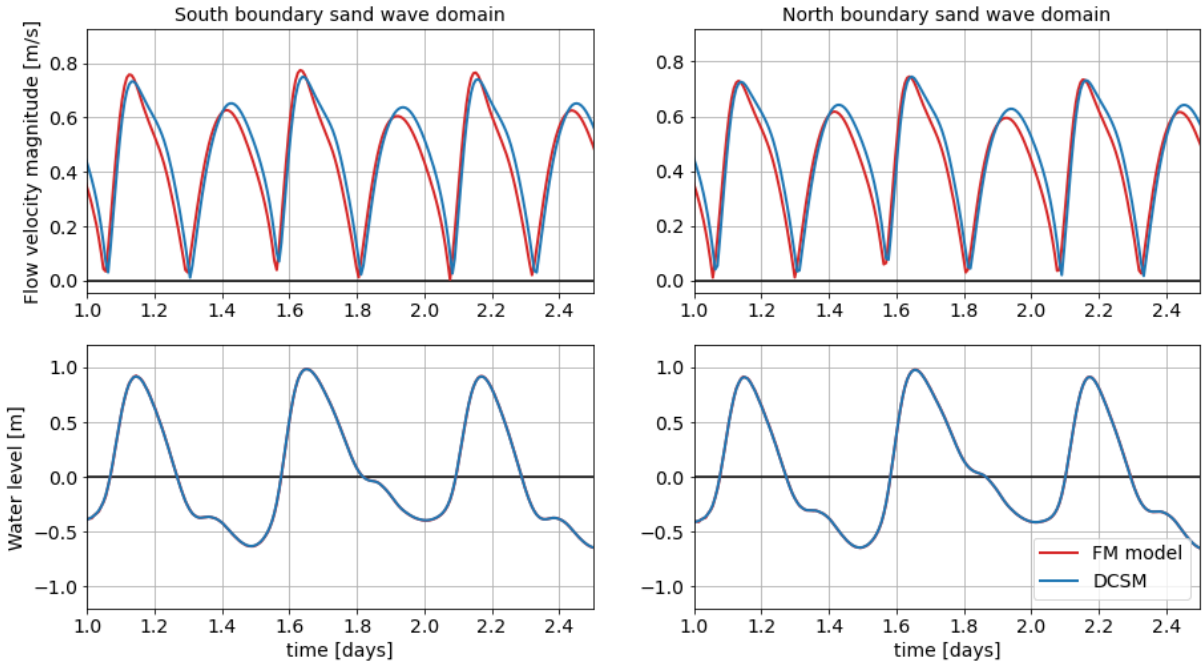

Figure E.11: Validation of flow velocity magnitude and water level in the 3D model at the centre of the South and North boundary of the sand wave domain using observations from the DCSM model

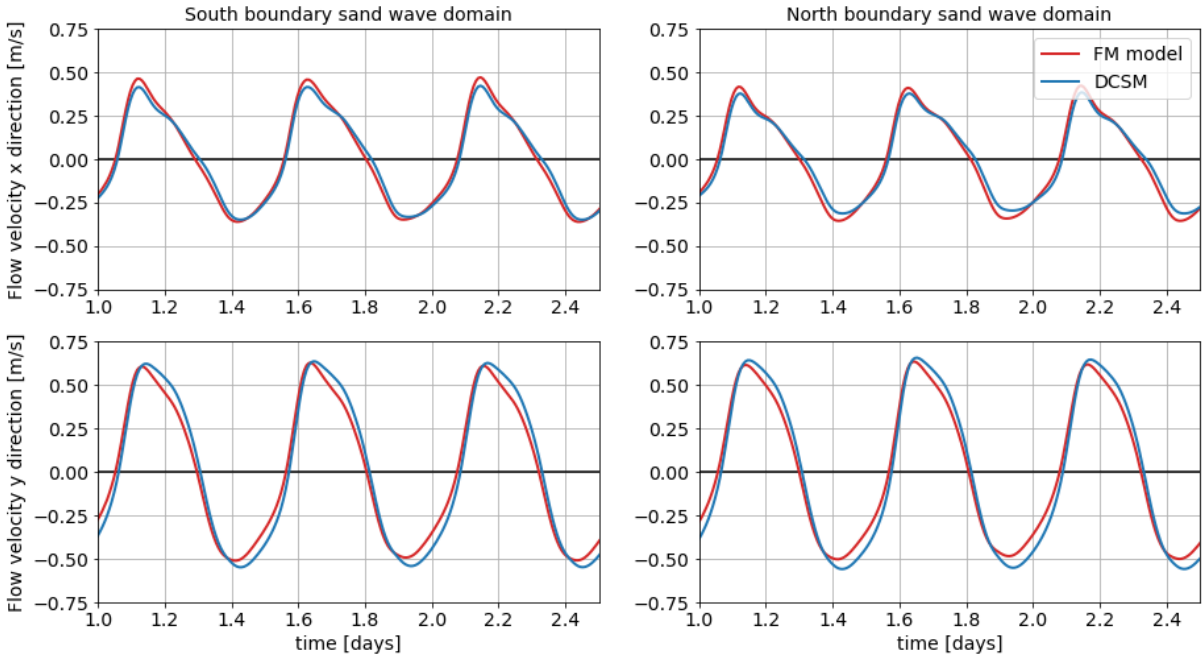

Figure E.12: Validation of flow velocity in both horizontal directions in the 3D model at the centre of the South and North boundary of the sand wave domain using observations from the DCSM model

F | 3D grid set-up, smoothness and orthogonality

The grid of the 3D model is mostly made up of rectangles. In the sand wave domain the rectangles are 2 by 10 m and from there sizes are doubled in one or two directions at a time. The sizes of the grid cells are shown in Table F.1. The connections between the grid cells of different sizes are created with triangular cells.

Table F.1: Grid cell sizes from sand wave domain to outer cells in the direction perpendicular to the sand wave crests (~South to North) and along the sand wave crests (~West to East)

Layer from sand wave domain	Perpendicular to crest [m]	Along crest [m]
-	2	10
I	4	10
II	8	10
III	16	20
IV	32	40
V	64	80
VI	128	160
VII	256	320
VIII	512	640
IX	1024	1280

Below some figures of the 3D grid as well as its smoothness and orthogonality are presented. Sporadically higher values for the smoothness and orthogonality parameters are observed indicating a less smooth or less orthogonal grid. Nearly all grid cells do comply with the guidelines for smoothness and orthogonality. The locations of these exceptions are always outside of the area of interest. Furthermore, they do not lie on the main flow direction relative to the sand wave area.

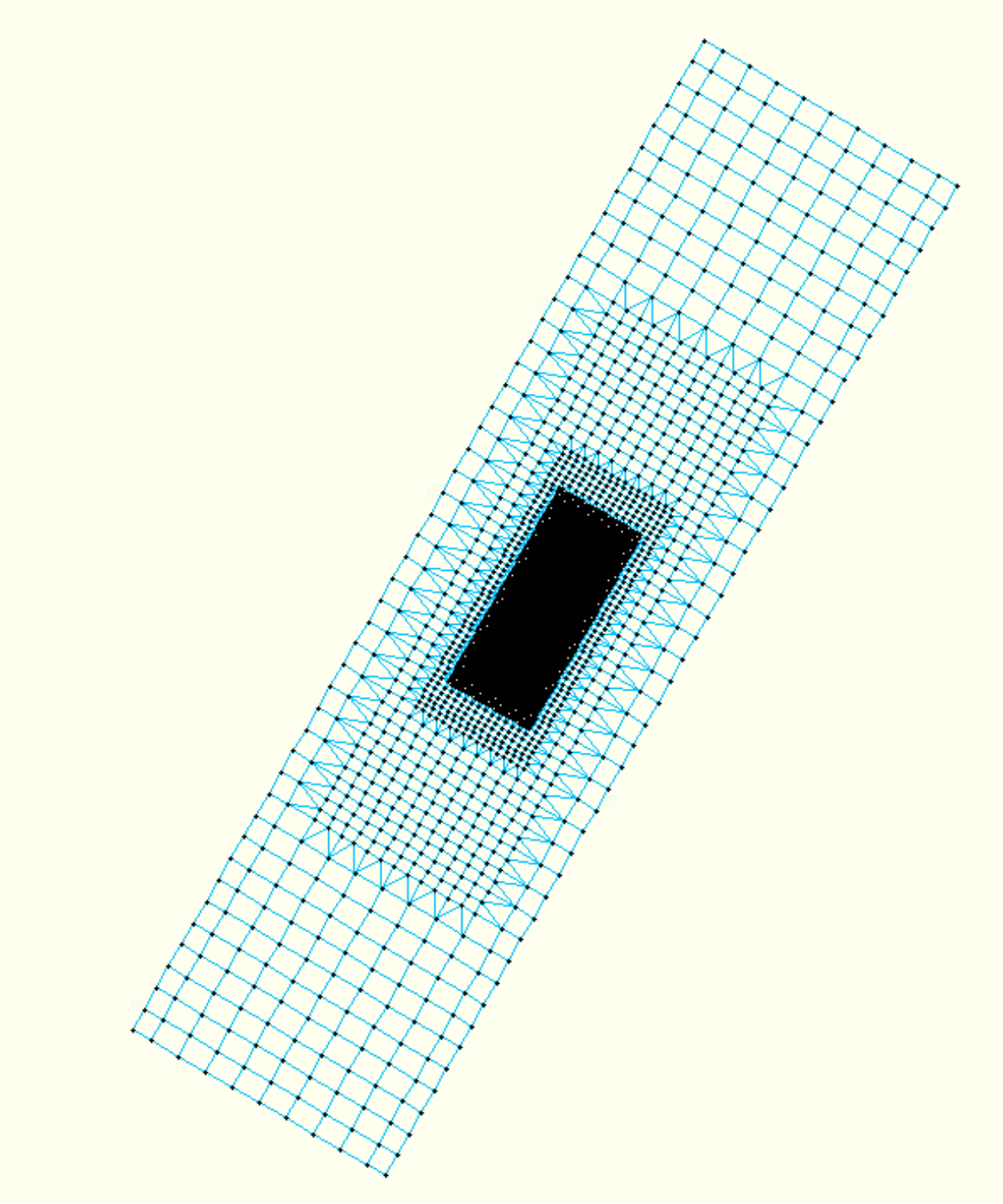

Figure F.1: Full 3D model grid

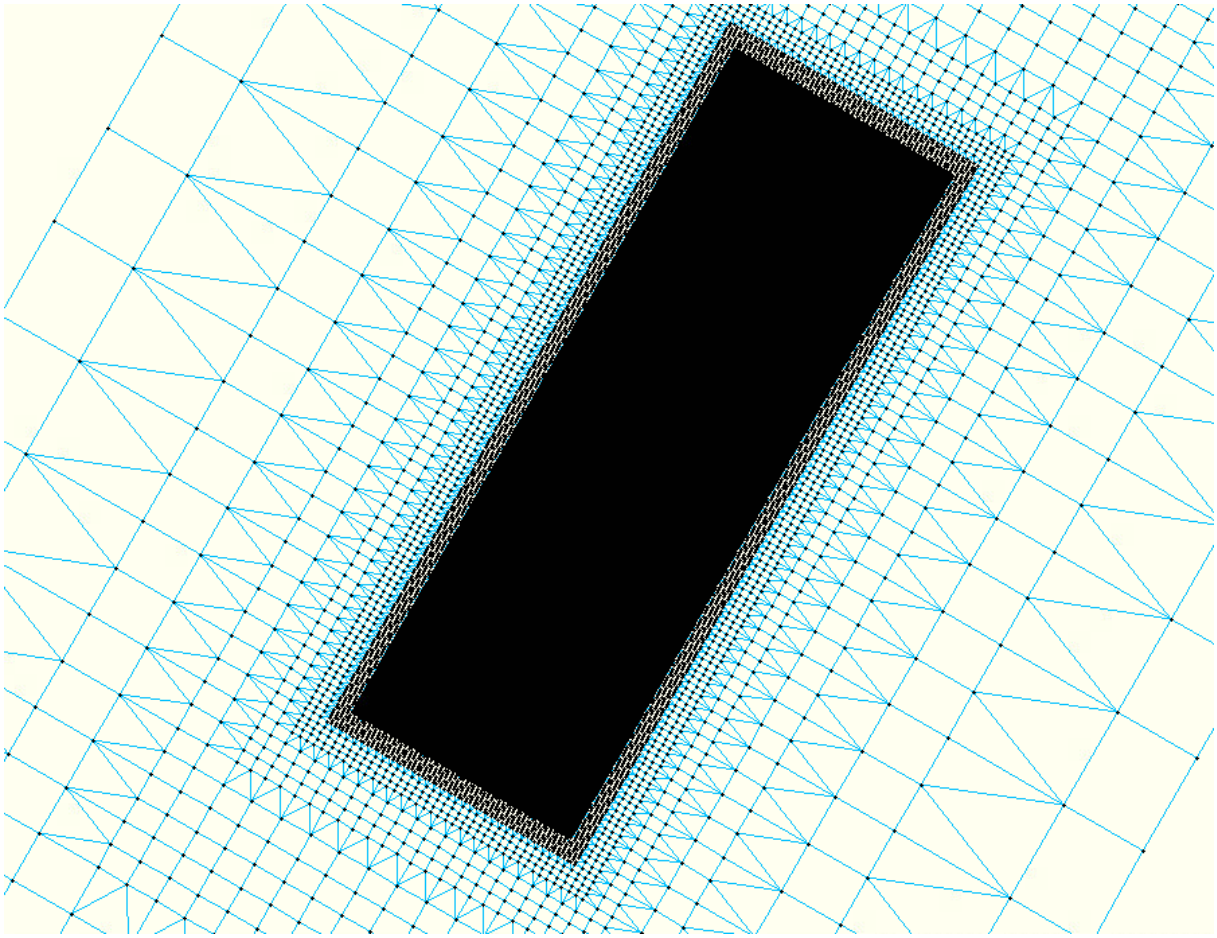

Figure F.2: Zoom of 3D model grid

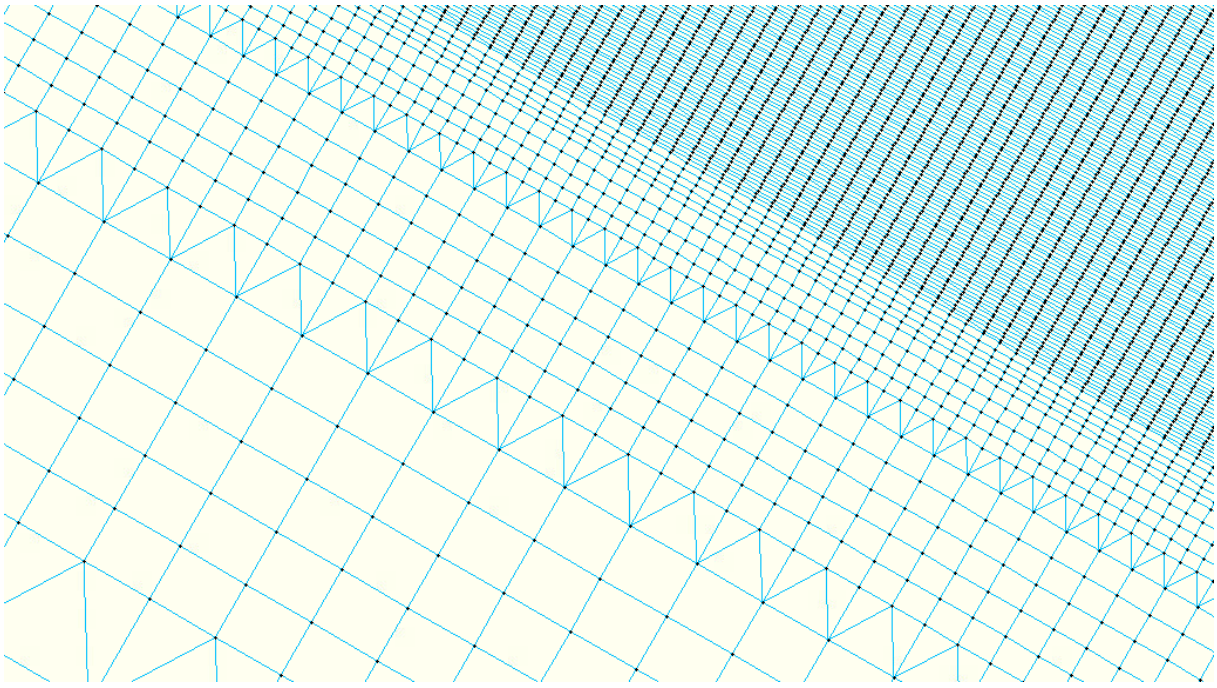

Figure F.3: Zoom of 3D model grid

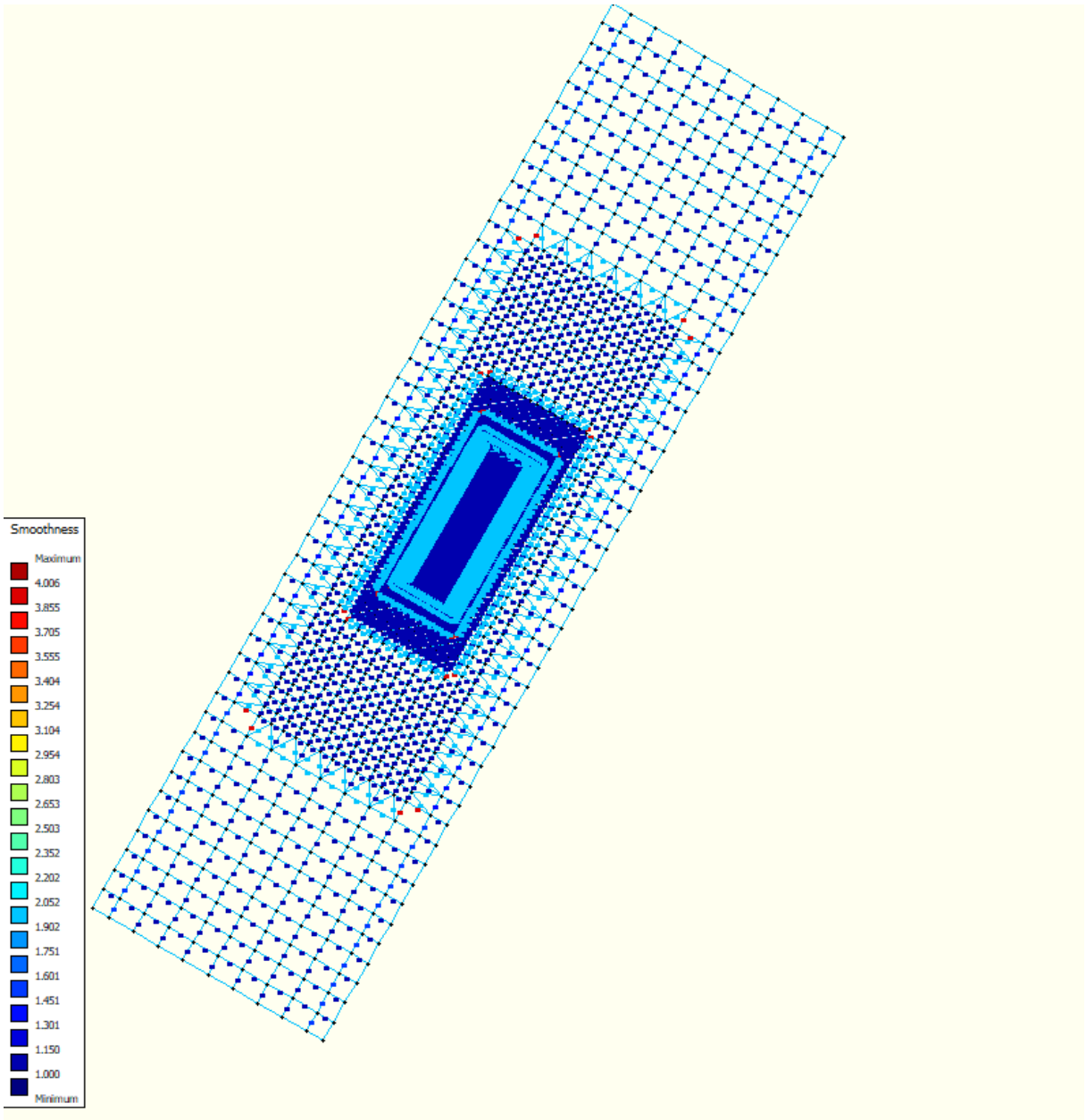

Figure F.4: Smoothness of 3D model grid

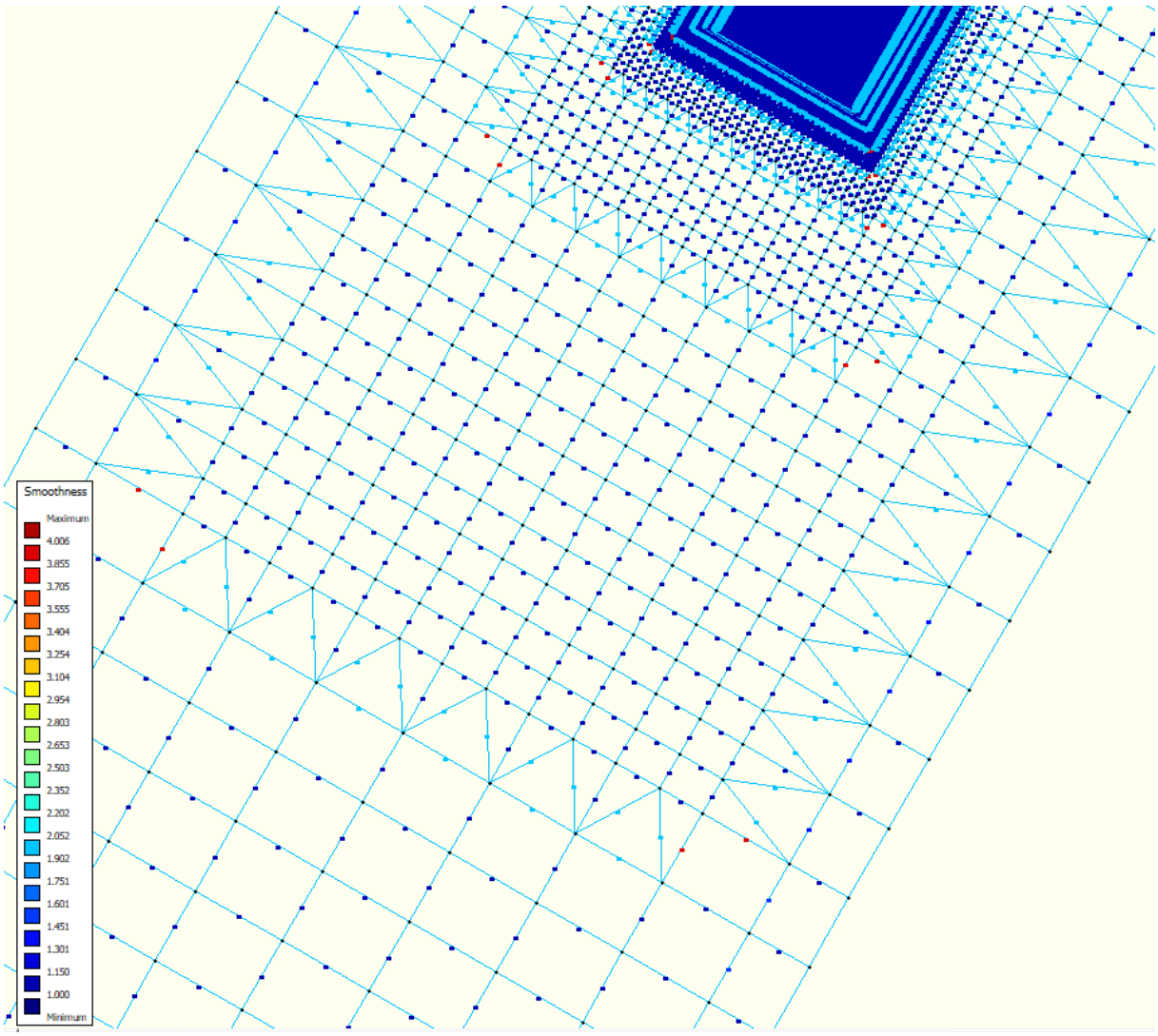

Figure F.5: Zoom of smoothness of 3D model grid

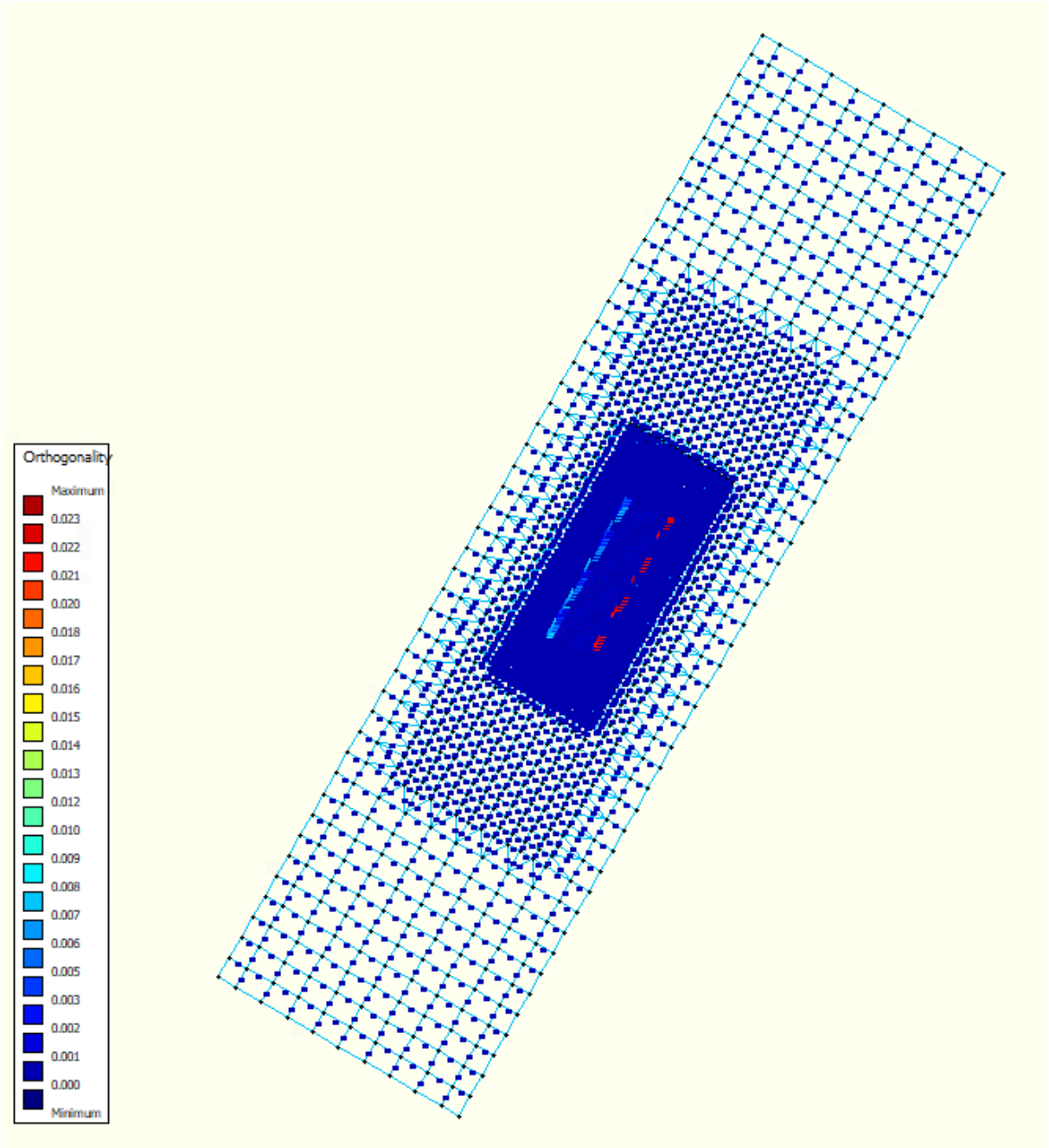

Figure F.6: Orthogonality of 3D model grid

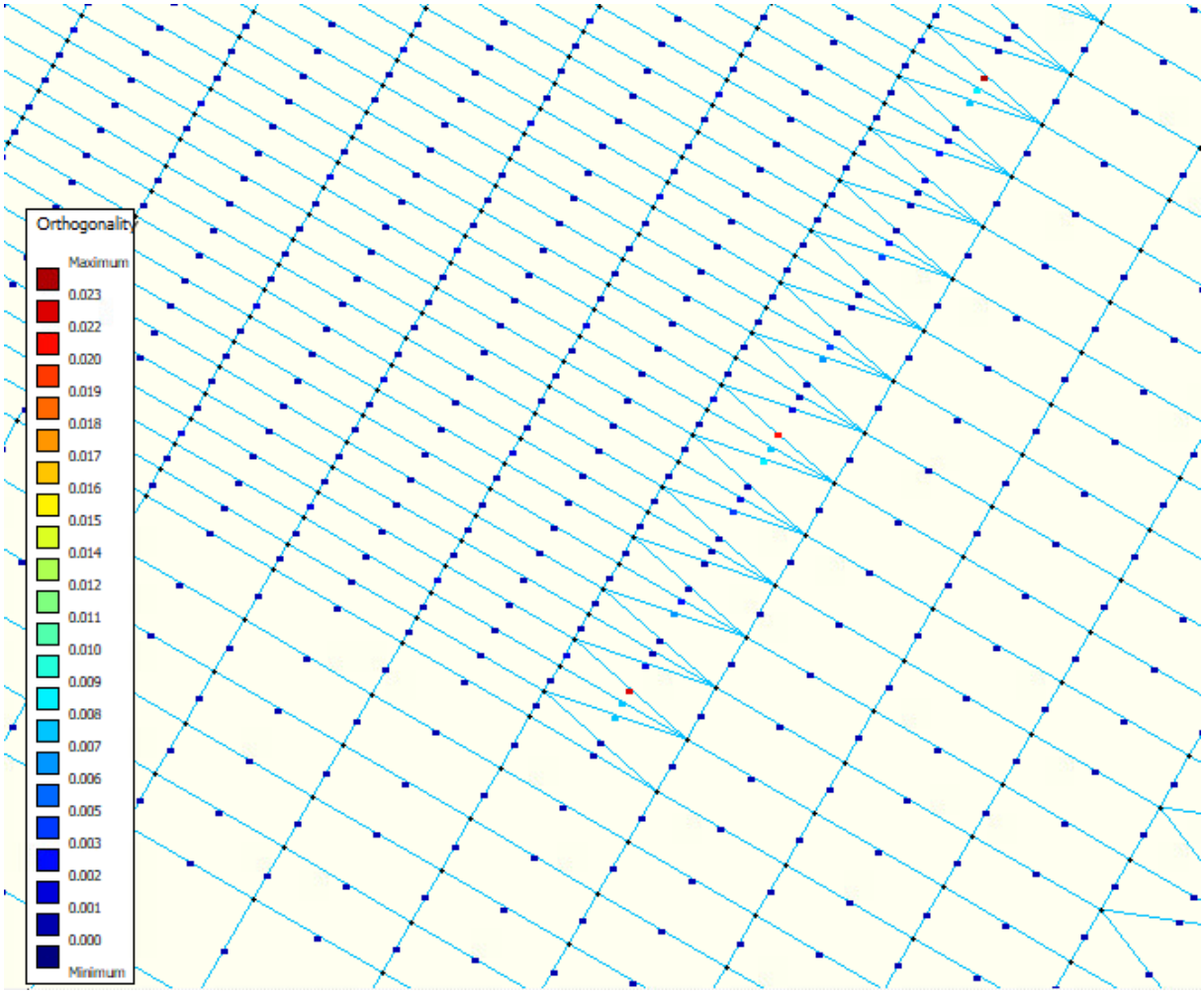

Figure F.7: Zoom of orthogonality of 3D model grid